

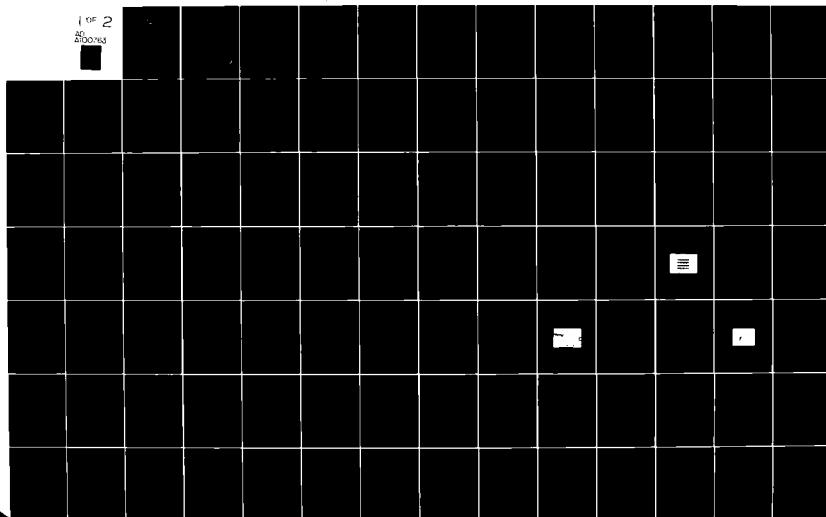
AD-A100 763

AIR FORCE INST OF TECH WRIGHT-PATTERSON AFB OH SCHOO--ETC F/G 6/5
THE DEVELOPMENT OF A TWO-DIMENSIONAL MULTIELECTRODE ARRAY FOR V--ETC(11)
DEC 80 G H FITZGERALD
AFIT/GE/BE/80D-21

UNCLASSIFIED

ML

1 of 2
AD A100763



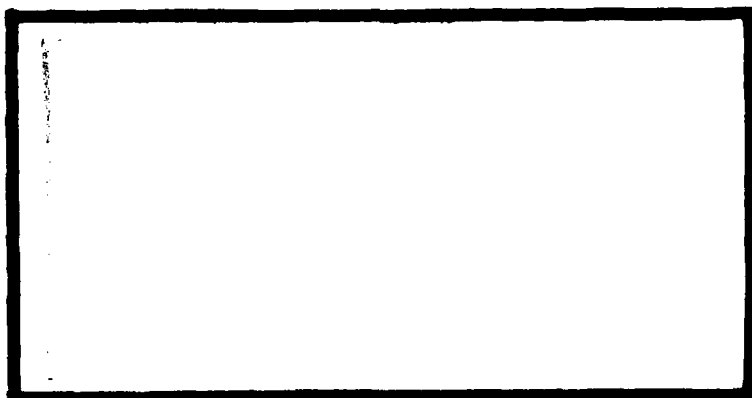
NDc

AD A100763



① 72
LEVEL 1

DTIC FILE COPY



DEPARTMENT OF THE AIR FORCE
AIR UNIVERSITY (ATC)
AIR FORCE INSTITUTE OF TECHNOLOGY

Wright-Patterson Air Force Base, Ohio

DISTRIBUTION STATEMENT A

Approved for public release
Distribution Unlimited

81 6

DTIC
ELECTE
JUL 1 1981

S 30 089 D
F

AFIT/GE/BE/80D-21

THE DEVELOPMENT OF A TWO-DIMENSIONAL
MULTIELECTRODE ARRAY FOR VISUAL PERCEPTION
RESEARCH IN THE MAMMALIAN BRAIN
THESIS

AFIT/GE/BE/80D-21

Gary H. Fitzgerald
Capt USAF

DTIC
ELECTE
S JUL 1 1981 D
F

Approved for public release; distribution unlimited

AFIT/GE/BE/80D-21 ✓

THE DEVELOPMENT OF A TWO-DIMENSIONAL MULTIELECTRODE ARRAY
FOR VISUAL PERCEPTION RESEARCH IN THE MAMMALIAN BRAIN

THESIS .

Presented to the Faculty of the School of Engineering
of the Air Force Institute of Technology
Air University
in Partial Fulfillment of the
Requirements for the Degree of
Master of Science

by

Gary H. Fitzgerald, B.S.

Capt USAF

Graduate Electrical Engineering

11 December 1980

Approved for public release; distribution unlimited.

Accession For	
THIS GRADE	<input checked="checked" type="checkbox"/>
FOR FAR	<input type="checkbox"/>
For the use of	<input type="checkbox"/>
Publication	
Distribution/	
Availability Codes	
Avail and/or	
Dist	Special
A	

Preface

This thesis develops a novel multielectrode array for neurological research and suggests a research method that may improve our knowledge of the human visual system. Motivation for such a project lies in two fundamental areas.

The first area concerns the development of visual pattern recognition devices. Years of pattern recognition research has resulted in marginal success. We can build commercially useful machines that read the printed page if the print is precisely controlled. But we have had little success with a device that can select objects from a complex visual scene. Such a machine could revolutionize military reconnaissance and weapons guidance. Of course, the human brain routinely accomplishes this task with seeming ease. If we could understand and emulate the algorithms used by the brain, the visual pattern recognition problem might be solved. Understanding the human visual perception mechanism is the second motivation for this thesis.

The human visual system is a complex and mysterious device. It can, with great ease, read the printed or handwritten word in a number of idiosyncratic forms. Even though much is known about the anatomy of the system, the algorithms used for human visual pattern perception remain unknown. Medical researchers feel that if we can properly identify the workings of the human visual system, we might better understand other functions of the human neurological system. Such knowledge could lead to solutions for many problems such as blindness.

This investigation is concerned with developing a multielectrode array that may help solve problems in these seemingly unrelated areas: pattern recognition and human neurology. The array is designed to obtain

fine grained data from the visual cortex of a living mammalian brain. The data should help identify the transfer functions used during the visual perception process. I do not expect any easy or quick solutions, but I believe that the multielectrode array will provide an important tool to increase the knowledge of human visual perception.

I gratefully acknowledge the advise and encouragement provided by Dr. Kabrisky, Maj. Borky, and Dr. Wolaver during this research. I am also indebted to Lt. Joseph Tatman for his design efforts on the multielectrode array. The use of the Air Force Avionics Laboratory's Integrated Circuit Facility was fundamental to this research project, and greatly appreciated.

Gary H. Fitzgerald

Contents

	Page
Preface	ii
List of Figures	vii
List of Tables	viii
Abstract	ix
I Introduction	1
Significance	1
Background	3
Present Knowledge of the Visual Perception System	3
Past Research With Recording Electrodes	5
Problem	9
Approach	10
Scope	11
Sequence of Presentation	12
II Biological Model and Theory of Operation	13
Introduction	13
The Neuron	14
Anatomy and Function of the Visual Pathway	18
Anatomy of the Visual Pathway	18
The Retinae	20
The Lateral Geniculate Body	22
The Visual Cortex	22
Cortical Interconnections	25
The Basic Computing Element	26
Physiological Research of the Visual System	28
Chemical Neuroresearch	28
Bioelectric Neuroresearch	30
Psychological Neuroresearch	32
Kabrisky's Theory of Visual Perception	37
A Method to Test Kabrisky's Theory	38
III Multielectrode Array Design and Fabrication	40
Introduction	40
Multielectrode Array Design	40
Overview	40
Interelectrode Spacing	42
Array Size	42
Contact Resistance	42
Multiplexing Requirements	44
The Insulation Layer	47

	Solution of the Three Fabrication Problems	47
	Multielectrode Array Fabrication	51
	Results of Electrical Tests	54
	Design Improvements	58
IV	Support Electronics	60
	Introduction	60
	System Descriptions	61
	Record Mode	61
	Playback Mode	65
	Drive Circuitry	65
V	In Vitro Multielectrode Array Evaluation	73
	Introduction	73
	Static Pinch-off Tests	74
	Test Set-up	74
	Test Procedure	74
	Test Results	75
	Crosstalk Tests	76
	Test Set-up	76
	Test Procedure	77
	Test Results	77
	Ambient Noise Tests	77
	Test Set-up	77
	Test Procedure	78
	Test Results	78
	Lifetime Tests	79
	Test Set-up	79
	Test Procedure	79
	Test Results	80
	Multiplexing Tests	82
	Test Set-up	82
	Test Procedure	83
	Test Results	83
	Electrode Impedance Tests	86
	Test Set-up	86
	Test Procedure	86
	Test Results	86
VI	In Vivo Multielectrode Array Evaluation	90
	Introduction	90
	Test Equipment Set-up	91
	Implant Protocol	94
	Baseline Test Procedures	95
	Data Acquisition Procedures	97
	Data Processing and Analysis	99

VII	Conclusions and Recommendations	107
	Introduction	107
	Conclusions	107
	Recommendations	109
	Bibliography	111
	Appendix A: Initial Fabrication Procedure	114
	Appendix B: Revised Process Schedule	118

List of Figures

<u>Figure</u>	<u>Page</u>
1 The Neuron	16
2 The Visual Pathways	19
3 Visual Field Arrangement	21
4 The Visual Cortex	24
5 The Basic Computing Elements	27
6 The Kanizsa Triangle Illusion	34
7 Mueller-Lyer's Illusion	36
8 The Multielectrode Array	41
9 Multielectrode Array Circuit Diagram	46
10 Lead Attachment to the Array	53
11 JFET Curve Tracer Characteristics	56
12 Record System Block Diagram	62
13 Timing and Voltage Level Diagram	64
14 Playback System Block Diagram	66
15 Drive Circuit and Array	67
16 JFET Switch Equivalent Circuit	71
17 Crosstalk in CVD Passivated Device	81
18 Electrode Impedance Test Set-up	87
19 Electrode Impedance	88
20 In Vivo Test Set-up	92
A-1 The Fabrication Process Sequence	120
A-2 Cross Section of the JFET Structure	124

List of Tables

<u>Table</u>	<u>Page</u>
1 Calculated Electrode Impedances	45

Abstract

A review of previous mammalian visual system neurological and psychological research is presented. Results of previous research motivated the development of a device that would record fine grained electroencephalic data from the surface of a living mammalian cortex.

A multiplexing multielectrode array has been developed and tested for this purpose. The device consists of a four by four array of electrodes and sixteen junction field effect transistors fabricated on a silicon substrate using integrated circuit manufacturing techniques. In vitro tests indicated the device is capable of detecting and multiplexing fine grained cortical signals. Technical problems with the passivation material precluded in vivo evaluation. A solution to this problem is presented and an in vivo test procedure recommended.

THE DEVELOPMENT OF A TWO-DIMENSIONAL MULTIELECTRODE ARRAY
FOR VISUAL PERCEPTION RESEARCH IN THE MAMMALIAN BRAIN

I. Introduction

Significance

Many years of neurological research have provided considerable information concerning the structure of the central nervous system. Yet little is known about the perceptual process of the mammalian brain. In particular, the methods used by the human brain to recognize handwriting and complex visual scenes are completely unknown. This thesis is significant because it develops an integrated circuit device that can access fine grained electroencephalic data from the visual cortex. These data may improve the understanding of the visual perception process. Three fundamental advantages would result from this improved understanding.

First, a machine may be developed that emulates the mammalian visual pattern recognition process. A machine that could identify specific objects in a complex visual scene has considerable military and civilian utility. Military reconnaissance is an application area of particular interest. Quality cameras, high altitude reconnaissance aircraft and reconnaissance satellites provide the equipment necessary for effective photographic intelligence gathering. But, in a scenario of high-speed mechanized conventional warfare, time required to process the miles of photographic film can render the intelligence information useless. Data from weather and earth resources satellites pose a similar problem for the civilian community. Computer models of the human visual system might solve this problem by providing an efficient, automatic pattern recognition system.

Increased knowledge of the visual perception process would improve understanding of brain function in general. The reason for such conjecture is the invariance of the cortical structure despite wide differences in types of data it processes (Ref 1:21). The outermost layer of the mammalian brain, called the cortex, processes visual, auditory and somesthetic information. The areas where these data are processed have been well mapped. Microscopic examination of the cortex shows that each processing area consists of six layers of nerve cells or neurons. The individual layers vary in thickness and the total cortical thickness also varies about 50 percent, but the basic six layered structure is invariant between processing areas. Connections between neurons are also invariant. Such invariance could be compared to the structure of a digital computer. The computer contains logic elements that produce specific responses to given inputs. For example, a binary adder's output is strictly a function of the input states. It does not matter that one set of inputs could model the function of an aircraft's flight dynamics while another set of inputs might represent the response of a highway system to changing traffic loads. Similarly, a processing area in the cortex produces a specific output based on its input data, no matter what the source of these data. Thus, increased knowledge of the visual pattern recognition process should enhance understanding of the function of other areas in the brain.

The third advantage of improved knowledge of the visual perception process concerns developing visual prosthetic devices for the blind. Until 1967, an individual with inoperative eyes or optic nerves was considered irreversibly blind. Research by Brindley (Ref 2), Donaldson (Ref 3),

and the Institute for Biomedical Engineering, University of Utah (1971) indicates that a prosthetic device can be developed to provide some sight to this class of blind individuals. Experiments on blind volunteers show that visual sensations are perceived when current pulses are applied to electrodes in contact with the visual area of the brain. Increased knowledge of the visual system could improve the quality of the prosthetic device. In addition, the multielectrode array developed by this thesis could be the prototype of a prosthetic device that would significantly improve the detail of the perceived image by increasing the number of cortical contact points per unit area as well as the total number of contact points.

Background

Present Knowledge of the Visual Perception System. Despite considerable neurological research, the methods used by the visual cortex for processing perceptual information remain unknown. The human visual system can, with reasonable ease, decipher ideosyncratic hand writing, identify a familiar face in a crowd, or pick out a specific object from a cluttered visual scene. These activities are known to be very difficult pattern recognition problems and designers have had little success in doing these things with very large computers. Much is known about the interconnections between the retinae and the primary visual cortex, but knowledge of the necessary, complex interactions between elements in the two dimensional visual field is very limited.

Anatomical research provides rather detailed interconnection diagrams of the retinae, optic nerve and the primary visual cortical area. The interested reader can refer to Figures 2, 3, and 4 for information concerning

these interconnections. It is known that the image impressed on the retina is homeomorphically mapped to the primary visual cortex so that relative positions of objects in the visual field are retained. Local cortical connections allow interaction through the thickness of the cortex, but connections between individual visual data elements are almost nonexistent. For this reason, it is believed that pattern recognition cannot occur in the primary visual cortex. This theory is supported by physiological research where points on the surface of the primary visual cortex are stimulated and the resulting response is observed. Such research shows that stimulation of the primary visual cortex yields a visual sensation of small points of light called phosphenes. The relative position of the phosphenes are retained and complex patterns are not perceived by the human subject. These results indicate that pattern recognition of complex visual data occur beyond the primary visual cortex.

Connections between the primary and secondary visual cortical areas are very complex and detailed, complete information concerning these interconnects is nonexistent. It is known, however, that each point on the primary visual cortex connects to many points on the secondary visual cortex. The complex interconnects allow, for the first time in the processing of visual information, interaction between elements in the two dimensional visual field. It is possible that pattern recognition begins either at the interconnects between the primary and secondary visual cortex or in the secondary visual cortex itself. When the secondary visual cortex is electrically stimulated, the subject reports seeing lines, or other more complex shapes. This result suggests that some pattern recognition has occurred.

In summary, present knowledge of the human visual system suggests that visual perception begins with the interconnections between the primary and secondary visual cortical areas. Extending the knowledge of this process requires additional research into these complex cortico-cortical connections. Two possible approaches to such research are suggested by previous successful neurological studies. The first approach is to develop a detailed anatomical wiring diagram of each neuron in the primary and secondary visual cortex. Total neural population in the primary visual cortex is about 10^8 (Ref 5:150). Since each neuron from the primary visual cortex connects to several neurons in the secondary visual cortex (a very conservative estimate is ten), there are at least 10^9 interconnections. If one could map one interconnection per second, the job would be completed in just over 30 years. Such a research approach does not appear promising. An alternate method is to map the data flow instead of the anatomical structure. This mapping could be accomplished by simultaneously recording electrical signals from the primary and secondary visual cortex so that a transfer function could be determined. Recording electrical signals requires a specialized electrode. The following paragraphs describe the past research with such electrodes.

Past Research With Recording Electrodes. Increasing the knowledge of cortico-cortical connections requires some form of electrode so that electroencephalic data can be recorded. Past researchers have used three major types of electrodes: the single cell microelectrode, non-invasive scalp electrodes, and the multielectrode array.

Single cell microelectrodes are generally made from tungsten or platinum alloy wires, or glass micropipette tubes which have been pulled to form

a tip diameter of about one micron. The microelectrode is inserted into the brain tissue so that the tip of the probe is inside a single nerve cell. Electrical signals from single nerve cells are recorded and analyzed by comparing cell activity with some form of input stimulus. Hubel and Weisel researched the anesthetized cat's visual cortex (Ref 6) with this type of microelectrode. They theorize that nerve cells are sensitive to specific line orientations within certain visual field areas but there is much controversy as to the validity of their results. One reason for the controversy is the assumption that the coordinated behavior of an aggregate of neurons (say, those of the primary visual cortex) can be determined by observing the activity of numerous neurons, one at a time, and assuming that the aggregate performance can be reliably inferred from their individual performances. One could compare this approach to that of determining a computer's function by observing the operation of numerous transistors, one at a time. To determine the function of the computer, many transistors must be observed simultaneously. The same is true for the primary visual cortex and its neurons. Some research has been accomplished that records the function of large groups of brain cells.

The scalp electrode electroencephalograms (EEGs) take advantage of the neuronal electrical activity by recording electrical activity of neuron groups produced on the surface of the scalp. The recordings can provide important medical diagnostic information but they appear to lack sufficient detail to determine how the brain processes information. Brain function research with scalp electrode EEGs can be compared to examining the operation of a large computer by recording electrical activity on the surface of its cabinets. Since the early 1960's, signal averaging has been used to increase the ability to detect more fine grained electrical signals from the

visual cortex with scalp electrodes. This experimental technique, called the visual evoked response (VER) method, allows closely spaced scalp electrodes to define where signals originate in the visual cortex. The VER experimenter records EEG signals while stimulating the visual system with a specific input. After numerous recordings are made, the EEGs are ensemble averaged as a function of time from stimulus onset. Since noise is uncorrelated and the evoked response is correlated, the averaging process reduces the noise level and increases the signal level. Thus, the resulting ensemble average represents an enhanced visual evoked response. Such research has identified locations of the VER on the cortical surface (Ref 7:17). Yet, VER research does not enhance our knowledge of the visual pattern perception process. It appears that investigation of the visual perception process requires electroencephalic data more fine grained than the VER, but more coarse than the individual cell microelectrode. The following paragraphs describe research in this area.

Historically, multielectrode arrays were fabricated from fine wire bundles. DeMott used wire bundles for auditory and visual evoked activity research (Ref 8). Simmons developed an auditory prosthetic device which consisted of a bundle of six fine wires (Ref 9).

These wire bundle arrays have several serious disadvantages. It is difficult to develop arrays which are reproducible in their mechanical and electrical properties and which maintain their mechanical and electrical stability during insertion. Electrical impedance depends on the surface area of the exposed tip, which for wire electrodes, depends on how reproducibly the insulation can be removed. Relative position of the fine wires is also very difficult to maintain. Finally, electrode termination to amplifiers and recording devices becomes increasingly difficult as array size increases.

In spite of these difficulties, DeMott developed and used a rather large wire bundle array to record electrical activity on the primary visual cortex of cats, racoons, and squirrel monkeys. The array consisted of 400 stainless steel wires spaced 0.25 mm apart, imbedded in plastic so that the array formed a flat contact surface of about 4 by 7 mm. Each wire was terminated to an RC coupled amplifier which was used to drive a neon bulb. The neon bulb's intensity represented the level of electrical activity for its respective electrode. His objective was to demonstrate that nothing worth recording existed on such a fine spatial scale. Instead, he discovered that the primary sensory areas of the cortex produced detailed electrical responses to visual stimulus. The electrical activity was distinguished by steep voltage gradients and excellent repeatability. It was largely independent of background cortical activity. Such results support the theory that fine grained electroencephalic data may be significant to determining how the cortex processes visual information. Unfortunately, the wire bundle arrays are difficult to fabricate and implant. However, the semiconductor industry routinely produces devices with reproducible electrical and physical properties. For this reason, photolithographic technology was considered for the solution to the multielectrode array fabrication problem.

Wise (Ref 10) developed the first biological multielectrode array using photolithographic techniques. He used gold conductors on silicon substrates and included a source follower FET amplifier for each electrode. This approach solved the mechanical and electrical problems associated with wire bundle arrays, but did not address the problem of terminating numerous wires to external recording equipment. Research by Tatman (Ref 11) solved this problem.

Tatman developed a novel matrix multielectrode array. This device time multiplexes the signals on each column of electrodes down to a single wire. Thus, an array of 400 electrodes requires only 40 connecting wires. This approach enables the researcher to record fine grained signals from a significant portion of the appropriate cortical surfaces.

Tatman's device consists of a matrix of gold electrodes spaced 0.25 mm apart on a silicon substrate. Each electrode is attached to a FET switch that is photolithographically fabricated on the same substrate. The output of each column of FETs is electrically terminated to an output lead and the gates of each row of FETs are likewise terminated to an input lead. By driving the FET switches with the proper logic circuits, each column lead signal consists of time multiplexed samples of the bioelectric data received by the electrodes. The Tatman multielectrode array constitutes the tool for the research in this thesis.

Problem

The problem to be solved is threefold. First, an operational multiplexing array and the necessary support equipment must be fabricated and tested. Second, the array must be used to obtain bioelectric data from the visual cortex of a mammalian subject. Third, the data must be analyzed to determine some operating characteristics of the sensory cortex. The ultimate goal is to define the transfer function(s) used by the visual cortex during the perception process. The following paragraphs describe the three elements of the problem.

A multiplexing multielectrode array that can access fine grained cortical bioelectric signals must be fabricated. This device must survive in a cerebral spinal fluid environment for several hours. Ideally, it should survive for months or years if the ultimate goal is to be accomplished

(see chapter three). Crosstalk and noise should be at least 10 db below the bioelectric signal levels so that high quality electroencephalic data are obtained and its multiplexing speed must exceed the Nyquist sampling rate for the highest bioelectric signal frequency so that aliasing does not occur. The device must also be sterilizable and sturdy enough to survive during the implant procedure.

The support electronics must control the multiplexing array so that the bioelectric signals from the cortex can be amplified and recorded. Additional support electronics must retrieve and digitize the multiplexed signals so that computer analysis can be accomplished.

The implant and resulting in vivo test procedure must allow access to the primary and secondary visual cortex of a living, unanesthetized mammalian brain. The subject should be of a species with good visual acuity. Visual stimulus equipment must be capable of developing repeatable, time synchronized stimuli to the subject. Great care must be taken to ensure humane treatment to the test animal (Ref 12).

Data analysis should determine if the bioelectric signals are capable of providing improved knowledge of the cortico-cortical connections in the visual cortex. The analysis should also identify any weakness in the acquisition and recording procedures, and help provide solutions to these problems. The ultimate objective of the data analysis procedure is to identify the transfer function(s) used by the mammalian brain during the visual perception process.

Approach

The approach to solving the problem identified in the previous paragraphs contains six major steps. The first four steps concern the

fabrication and testing of the multiplexing multielectrode array and the associated support electronics. Step five obtains bioelectric data from the test subject and the final step analyzes these data. The following paragraphs describe these procedures.

Fabrication of the multielectrode array requires that three major problems encountered by Tatman be solved. These problems are lack of ohmic contact with the metalized leads, leakage paths in the passivation layer, and cracks in the final passivation layer. Once these problems are solved, a revised process schedule must be developed and used to fabricate the multielectrode array. The support electronics must be designed and built. To insure the device and support electronics function properly, a series of in vitro tests must be conducted. These tests should determine FET pinch-off voltage, lifetime in a saline bath, crosstalk, ambient noise, multiplexing ability and frequency limit, and frequency response of the electrodes.

After the devices and support electronics are evaluated, a multielectrode array must be implanted on the visual cortex of a subject animal. The animal's visual system is stimulated and the resulting bioelectric signals are recorded. The animal must be unanesthetized during data acquisition so that brain function is essentially normal.

The recorded data are analyzed to determine data quality. Additional analysis must be accomplished to determine some characteristic of the visual cortex during the perception process.

Scope

In order to reduce the complexity of prototype support electronics, the initial multiplexing array is limited to a four by four. This array is sufficiently large to determine the feasibility of the approach and to identify any possible problem areas that warrant additional research.

The implant is limited to an acute process with no attempt to accomplish transcutaneous signal transfer. In future work, chronic implants may be desirable so that several days or weeks of visual data may be recorded.

Data analysis consists of evaluation necessary to determine operational quality of the multiplexing array and support electronics. In addition, limited data analysis should be accomplished to identify some fundamental characteristics of the visual perception system.

Sequence of Presentation

Chapter two discusses the biological aspects of the visual system and Kabrisky's theory concerning its operation. Chapter three presents the various requirements of the multielectrode array and the resulting design constraints. In addition, this chapter explains the fabrication process used to produce the multielectrode array. Chapter four shows the development of the support electronics and provides block diagrams of the resulting configurations. Chapter five explains the in vitro tests used to evaluate the multielectrode array and the support electronics. Chapter six discusses the proposed implant, data processing, and analysis procedures. Chapter seven lists the conclusions and recommendations of the thesis.

11. Biological Model and Theory of Operation

Introduction

Study of the mammalian visual perception process requires knowledge of the anatomical, physiological, and psychological aspects of the visual system. This chapter contains a description of these aspects. The approach is to present the information from a data processing viewpoint. As a result, the information contained in this chapter is not exhaustive, but is adequate to provide insight into the problem and goals of this thesis. The first five sections of this chapter discuss the results of past research into the anatomy and function of the mammalian visual perception system. The reader will note that the results of previous research strongly support Kabrisky's theory of visual perception which is explained in section six. The following paragraphs briefly describe the contents of this chapter.

The first section discusses the neuron's anatomy and function. The electrical data signals, called action potentials, and the chemical interconnections between neurons are described. In addition, this section presents information concerning the signal averaging characteristics of post synaptic potentials and how these potentials are recorded with small electrodes placed on the cortex.

The second section presents the anatomy and function of the mammalian visual system. Connections from the light sensors in the retinae to the primary visual cortex are described. This section also includes a functional description of the retina and lateral geniculate body.

The third section describes the visual cortex and includes information concerning its layered structure, the location of input and output neurons, and the structure of local cortical interconnections. It also theorizes about the connections between the primary and secondary visual cortex. This section culminates with a theoretical description of the basic computing element, how it may function, and its physical size.

The next section describes some physiological research. It discusses the results of chemical neuroresearch, describes a visual evoked response (VER) experiment, and provides information concerning past research with multielectrode arrays. In addition, it reviews the results of Hubel and Wiesel's single cell microelectrode research.

Psychological brain research is discussed. The visual system's response to optical illusions is compared to the response of a computer algorithm that models the visual perception mechanism. In addition, the spatial frequency sine wave grating response of the visual system is presented.

The next section presents Kabrisky's theory of the visual perception mechanism. It includes a description of the possible interconnects between the primary and secondary visual cortex and a transfer function that these interconnects might support. The final section presents a method to test Kabrisky's theory.

The Neuron

The neuron is the fundamental building block of the brain. Collections of this specialized cell perform the total function of the central nervous system. Data transmission as well as data analysis is solely a result of the neural activity. Although neurons occur in different forms, all

exhibit similar physical and functional characteristics. Figure 1 depicts these common physical characteristics.

The neuron is composed of three major parts: the soma, which is the main body of the neuron and contains the housekeeping components; a single axon, which extends from the soma and transmits data to the soma and dendrites of other neurons; and the dendrites, which are a group of arborized branches that gather and process data from surrounding neurons. The data acquisition and transmission functions are accomplished with two separate, but related activities. The first activity is the intraneural transmission of electrical pulses down the axon. The second activity is the chemical transmission of data from the axon of the transmitting neuron to the dendrites or soma of the receiving neurons.

Intraneural data transmission is initiated with ion exchanges between intracellular and extracellular fluids. Within each neuron, active ion "pumps" force positively charged sodium ions from the cell's intracellular fluid and potassium ions back into the cell. As a result, the ambient internal voltage level is about 70 millivolts more negative than the surrounding extracellular fluid. This potential difference is called a resting potential. The resting potential is maintained until some outside stimulus causes a depolarization or rise in the intracellular voltage. Should the intracellular voltage rise above some specified threshold voltage (about -60 millivolts in most neurons), complete depolarization will occur because the ionic permeability of the cell membrane will change and the cell will suddenly allow sodium ions to enter the intracellular space. The inrush of positive ions causes an action potential which is a positive voltage spike about 1 millisecond in duration and about 100 millivolts in

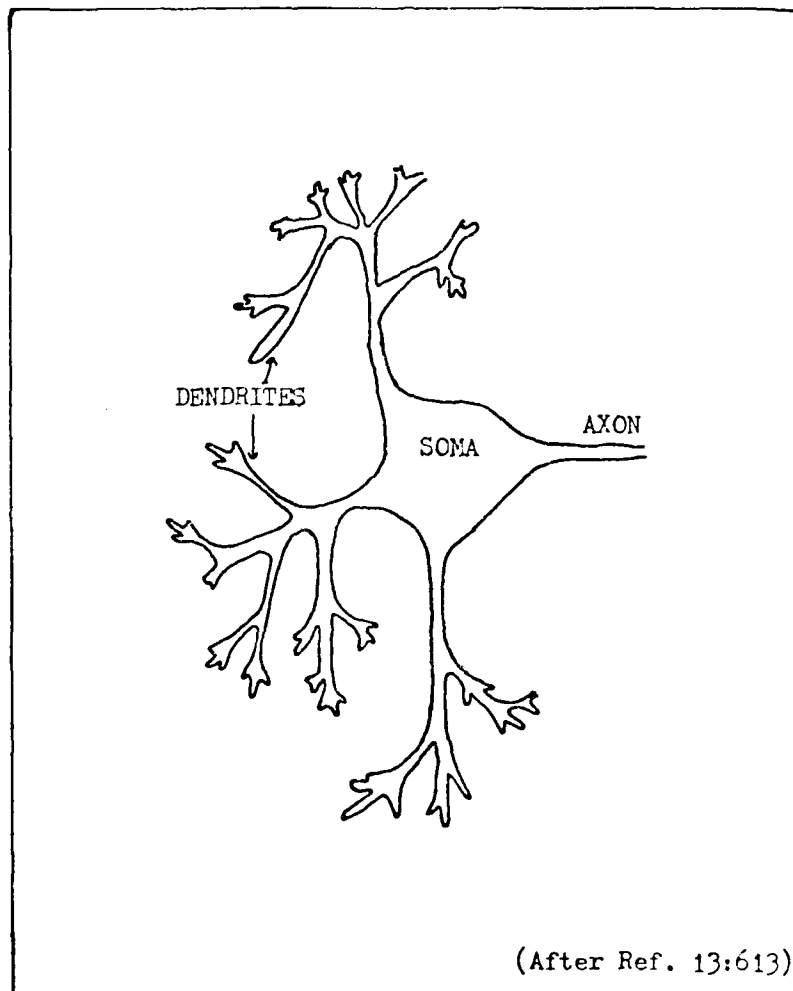


Fig. 1. The Neuron.

amplitude. The action potential is propagated throughout the neuron at a speed of up to 130 meters per second. After passage of the electrical impulse, the neuron will repolarize by removing the excess sodium ions and pumping in potassium ions. Repolarization can be done at rates sufficient to allow generation of several hundred action potentials each second. The action potentials are essentially invariant in amplitude and pulse width. Thus, pulse repetition rate is the modulating medium for electrical data transmission by the neuron. Once the action potential reaches the termination between its axon and the soma or dendrite of another neuron, a chemical data transmission process occurs.

Neurons transmit data to other nerve cells through a special inter-neuronal junction called a synapse. The axon terminates in a synaptic junction, which is a very narrow space between the axon of the transmitting neuron and the dendrite or soma of a target neuron. The electrical impulse in the axon causes the release of a chemical substance in the synapse called a neurotransmitter. About 30 different chemical substances are known or suspected to be transmitters in the brain (Ref 14:134). Some neurotransmitters tend to depolarize target neurons. The depolarizing effect enhances their excitability, which reduces the additional stimulation (electrical or chemical) required to elicit an action potential. These synaptic junctions are labeled excitatory and the depolarizing effect is called an excitatory post synaptic potential (EPSP). Other neurotransmitters tend to hyperpolarize or inhibit target cells. This effect is called an inhibitory post synaptic potential (IPSP).

Target neurons receive synaptic neurotransmitters from hundreds or thousands of other neurons and integrate the inhibitory and excitatory

post synaptic potentials to form a composite output signal. It is believed that the electric field produced by the summation of the EPSPs and IPSPs is received by small electrodes resting on the surface of the cortical tissue. Thus, an electrode would record data processing activity of the neurons beneath it.

Past research with multielectrode arrays indicate that the voltage potentials recorded from the cortical surface range from 200 to 500 microvolts in amplitude and from 1 to 40 Hertz in frequency. The electrode used for this research project measures 100 by 160 microns and will sit above a population of approximately 1600 neurons. A consequence of the results of the activity of these 1600 neurons will be recorded by each electrode. The visual cortex section in this chapter describes the cortical architecture which supports the theory that such recordings will enhance the knowledge of the visual perception process.

Anatomy and Function of the Visual Pathway

Anatomy of the Visual Pathway. Figure 2 illustrates the visual pathway from the retinae to the visual cortex. After visual data are generated in the retinae, they pass through the optic nerves to the optic chiasm. At the chiasm, the nerve fibers that serve the right half of the retina of each eye merge to form the right optic tract. The right optic tract synapses in the right lateral geniculate body and from here, the visual data pass through the visual pathway to the primary visual cortex (Ref 13:810). Since the lens of the eye inverts the image, the right primary visual cortex receives the inverted left half of the visual scene. This scene is mapped on the visual cortex so that relative position of the visual scene elements is maintained. If the data on the cortex were visible,

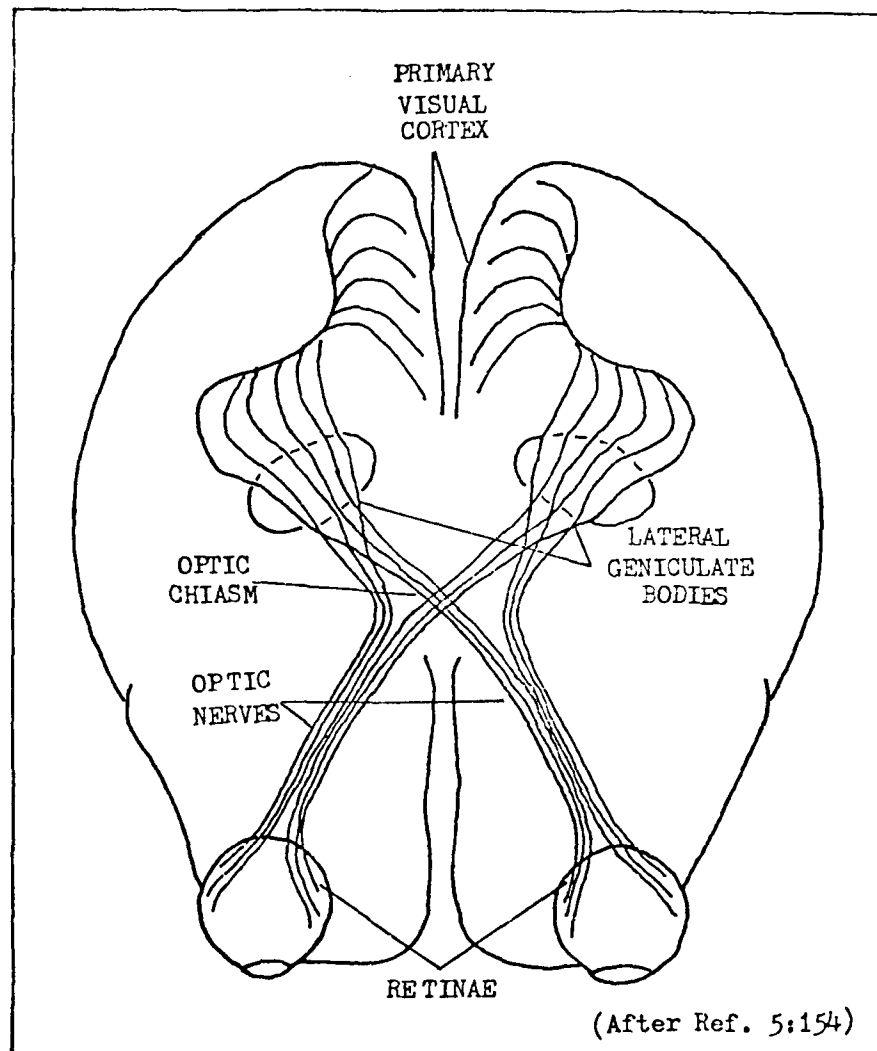


Fig 2. The visual pathways.

it would look like an upside down photograph of the visual scene that had been stretched in the center and compressed around the periphery. Figure 3 shows how the visual field is arranged as it passes down the visual data channels. The following paragraphs describe the function of the retinae and the lateral geniculate bodies.

The Retinae. The human retina contains light receptors called rods and cones. The central visual area is populated primarily with cones and the peripheral area with rods. The rods have a very low light intensity threshold and provide stimulation to optic nerve fibers for low light vision. They are not color sensitive. This is the reason why low level light conditions result in monochromatic vision. The cones have a much higher light intensity threshold and are responsible for color vision.

There are about 125 million rods and 5.5 million cones in each retina. Yet, only 900,000 optic nerve fibers lead from each retina to the brain. Thus an average of 140 rods and 6 cones must connect to each optic nerve. To accomplish this data reduction, the retina in the human eye has two fairly distinct regions: the foveal region where sharp visual images are obtained for about two degrees of the central visual field, and the peripheral area for the remainder of the visual field. Nearer the fovea, fewer and fewer rods and cones converge on each optic fiber. This causes a progressive increase in visual acuity toward the center of the retina. The central retina contains no rods at all, and each cone has a single dedicated optic nerve fiber. The far peripheral area has no cones and each optic nerve fiber serves over 600 rods. Thus, the peripheral optic nerve fibers receive data from a large area of the visual scene. This anatomical structure explains why the human peripheral vision has much

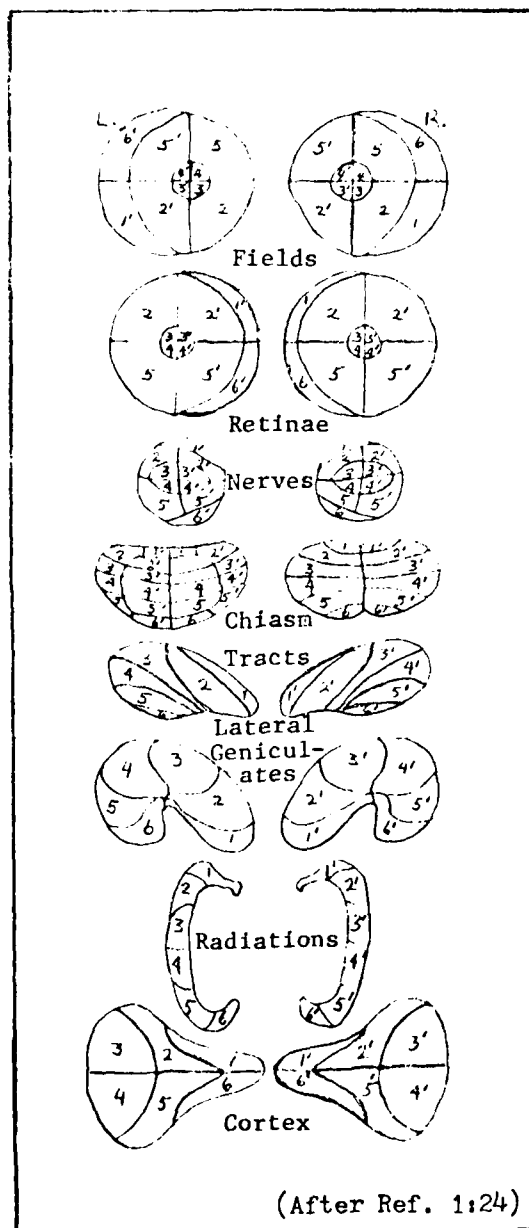


Fig. 3. Visual field arrangement.

less spatial resolution than the central vision (Ref 1:17).

Light stimulation of the rods and cones causes decomposition of a photochemical which in turn generates a voltage called the receptor potential. The receptor potential is carried down each rod and cone to a synapse where a post synaptic potential is impressed on a neuron. Thus, the post synaptic potential controls the action potential pulse rate of a nerve fiber in the optic nerve.

The Lateral Geniculate Body. The visual data generated by the retinae travel down the optic nerves to the chiasm and on to the lateral geniculate bodies. Layers one, four, and six of the six-layered lateral geniculate body receive signals from the nasal retina while layers two, three, and five receive signals from the temporal portion of the ipsilateral retina of the opposite eye. It is at this point that nerve fibers from superimposed retinal fields in the two eyes connect with co-located neurons. As a result, the geniculocalcarine fibers transmit visual fields from each eye through the optic radiations to closely related areas in the primary visual cortex.

The Visual Cortex

The cerebral cortex is the largest and most easily accessible part of the brain. Yet, we know little about its operation. Anatomical researchers have mapped some of the local interconnections and identified the structure and function of the various cortical areas. These cortical areas consist of a two millimeters thick, convoluted plate of neural tissue that covers the outer surface of the brain. Destruction or stimulation of certain areas of the cortex have provided some information about what these areas do. For example, the location of the visual cortex is well known.

The visual cortex is located on the posterior surface of the cerebral cortex. It consists of two areas called the primary visual cortex (Area 17 of Brodmann) and the secondary visual cortex (Area 18 of Brodmann). Figure 4 shows the location of these areas. The human primary visual cortex is about 26 square centimeters in surface area (Ref 1:29).

Dr. Wilder Penfield confirmed the location of the visual cortex in man during some unique physiological experiments. Dr. Penfield, a neurosurgeon, performed numerous brain operations in which he removed cortical tissue. These operations were an attempt to stop the occurrence of epileptic seizures. Before removing brain tissue of locally anesthetized patients, Dr. Penfield would electrically stimulate small areas of the cerebral cortex and observe the response of the alert patient. Electrical stimulation of the visual cortex caused the patient to see lights, colored forms, or black forms, moving or stationary, usually in the opposite visual field. It would also make the patient blind in that visual field. Dr. Penfield speculated that the primary visual cortex is a way-station through which afferent visual data pass to some central integrating area (Ref 16).

Microscopic examination shows each square millimeter of cortical tissue contains about 10^5 neurons (Ref 5:150). Thus, there are about 10^8 individual neurons in the human primary visual cortex. The neurons are arranged in layers about 50 to 100 cells thick. Six layers are generally recognized. These layers are sequentially numbered starting from the outer surface of the cortex to the innermost portion of the cortex where it interfaces with the white matter of the brain. Anatomical research indicates that layer IV of the visual cortex contains the terminal for

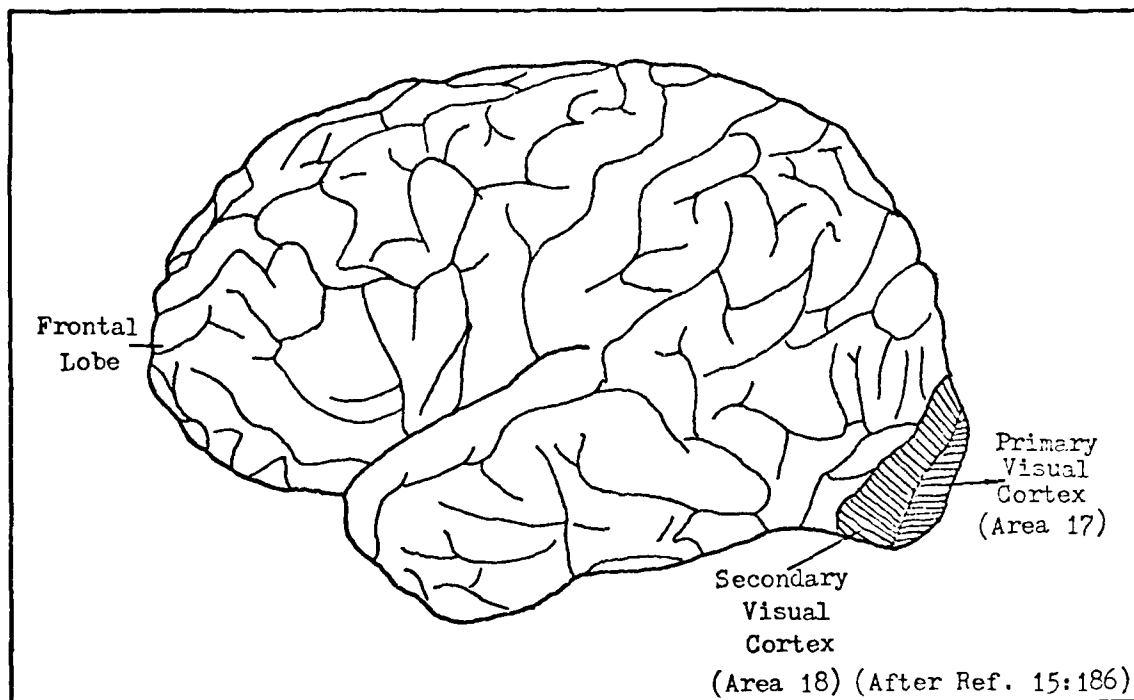


Fig. 4. The visual cortex.

afferent (incoming) visual data. Layers II and III provide connections with other areas of the cortex. The nerve cells from these layers are called association fibers because it is thought that visual information may be "associated" with other information via these nerve fibers. Layer V sends neural impulses to a portion of the brain called the superior colliculus, while layer VI sends visual data back to the lateral geniculate bodies. The reason for this feedback loop is unknown (Ref 17). Anatomical research of the cerebral cortex by Santiago Ramon y Cajal indicates that local cortico-cortical connections are primarily vertical. Thus, most data are transferred through the thickness of the cortex with lateral spread limited to a few millimeters.

Since the primary visual cortex maintains conformality of the visual scene, the limited horizontal cortico-cortical connections suggest that very little interaction of visual scene elements occurs here. In fact, since the cortical structure in general inhibits lateral data spread, the picture element interaction necessary for pattern recognition cannot occur within any cortical area. Thus, the pattern recognition process must occur when visual data are transmitted between visual cortical areas.

Cortical Interconnections. Little is known about the interconnections between the primary and secondary visual cortex. It is known, however, that the interconnections between these areas are very dense and many locations on Area 18 appear to be randomly enervated by a single location on Area 17 (Ref 1:51). Thus, the complex picture element interaction required for pattern recognition probably occurs in these interconnections. Kabrisky theorizes about the type of pattern recognition scheme that such interconnections would support. Section six of this chapter explains

his theory and how this thesis will help determine the validity of his theory.

The Basic Computing Element. The conformal arrangement of data on the cortical surface and the primarily vertical flow of data within the cortex suggest the existence of column-like computational components in the cortex. It has been suggested that these components can be considered as a collection of cell-like structures arranged perpendicular to the cortex and running through from top to bottom (Ref 1, 6, and 18). Figure 5 shows how these basic computing elements (BCEs) might be arranged. Each BCE would consist of many neurons and would process data received from one or more afferent nerve fibers. The results of its calculations would then leave the cortical area by one or more efferent nerve fibers. The finite lateral coupling of neurons and the few specific horizontal data pathways probably modify the data processing so that some cross-coupling (perhaps giving rise to lateral inhibition) between data channels occurs.

The size of the BCE can be estimated by observing the anatomical structure of the connections between the retinae and the visual cortex. The fovea dedicates one optic nerve cell for each light receptor. This one-to-one correspondence apparently continues through the lateral geniculate bodies and back to the primary visual cortex. The receptor cells in layer IV of the primary visual cortex occur at a rate of about 100,000 in 2.5 square centimeters. If each receptor cell serves a single BCE, one can postulate the size of a BCE to be about 0.05 millimeters in diameter, consisting of about 200 neurons. The Hubel and Wiesel data suggest that the BCE in the cat may be as large as 0.5 millimeters in diameter and contains about 25,000 neurons. Their results

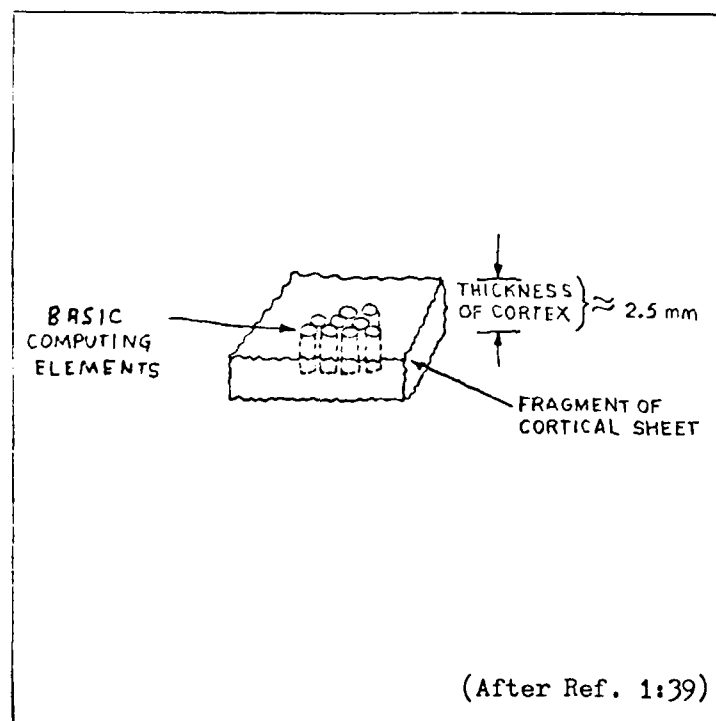


Fig. 5. The basic computing elements.

are discussed in the physiological research section of this chapter.

Physiological Research of the Visual System

Chemical and electrical physiological research provides considerable information about how the visual system transmits information from one location to another. This research has made possible an accurate mapping of the visual cortex into the blocks of neural tissue which may be the BCES described by Kabrisky. The following paragraphs describe the results of physiological research related to this thesis.

Chemical Neuroresearch. Neurotransmitters are not randomly distributed throughout the brain, but are localized in specific clusters. Techniques exist that can cause specific neurotransmitters to glow when exposed to ultraviolet light in the fluorescent microscope. Such studies have mapped portions of the cell structure originating in the brain stem and terminating in the hypothalamus, cerebellum, and forebrain (Ref 14).

A related study has provided interesting information concerning the primary visual cortex. The research method capitalizes on the fact that the brain cells depend primarily on glucose for metabolism. A chemical substance closely related to glucose, called 2-deoxyglucose, is actively taken up by the neurons, but the substance cannot be disposed of or metabolized. Thus the more active neurons will absorb more deoxyglucose than the less active neurons. When an animal is injected with radioactively tagged deoxyglucose and given a task that stimulates a particular mode of the visual process, the active neurons can be detected. To isolate the active neurons, the animal is sacrificed and its brain is sliced into thin sections. The sections are pressed against a photographic plate.

The radioactive isotope will expose the photographic plate in areas that contain more active neurons. The results of the experiment show the primary visual cortex consists of neural blocks about one millimeter square and two millimeters deep. Each neural block appears to serve a specific area of the visual scene (Ref 5).

Studies with the silver-degenerative method for mapping neuronal connections provide information concerning the right eye-left eye mapping onto the primary visual cortex (Ref 5). The silver-degenerative method is based on the phenomenon of axonal transport. If radioactively labeled amino acids are injected into an area of nervous tissue, the neuronal chemical transport system will move the tagged amino acids through the axon to the synaptic junction. When the neuron releases neurotransmitter substances into the synapse, some of the radioactively tagged amino acids are also released. The tagged amino acids proceed through to the next neuron in a similar manner. When a single eye of an animal was injected with tagged amino acids, some of the material escaped from the optic nerve and traveled through the synaptic junctions to the lateral geniculate body. Neurons in the geniculate body transported the material to specific locations on the primary visual area of the cerebral cortex. By coating tissue slices of the cortex with photographic emulsion and chemically developing the emulsion, location of the deposit sites for radioactive amino acids was seen. When viewing a slice of cortical tissue taken parallel to the surface of the brain, the photographed pattern was one of parallel stripes corresponding to terminals belonging to the injected eye. The gaps between stripes represent terminals belonging to the other eye. The width of the terminals in the macaque monkey is about 0.4 millimeters (Ref 5:159). Since the macaque

monkey's primary visual cortex is similar to the human, this research suggests that the terminals for each eye are about 0.4 millimeters in diameter.

Bioelectric Neuroresearch. Jeffreys and Axford's VER experiment provided some information about the location of the visual processing areas of the brain (Ref 7). The experiment consisted of stimulating various sections of 12 human subjects' visual field with a pattern of isolated squares while recording the electroencephalogram (EEG) with a horizontal transverse row of seven to nine scalp electrodes. The EEG signals were digitized and sampled by a computer every 4.7 milliseconds for a period of 300 milliseconds after stimulus onset. The first two components of the visual evoked potentials (VEPs), designated C.I. (latency 65-80 milliseconds) and C.II. (latency 90-110 milliseconds) were influenced by the retinal location of the stimulus. The results of the experiment are described below.

1. Corresponding peaks (C.I. and C.II.) of the VEPs to stimulation of the upper and lower half-fields were inverted in polarity.
2. For the left and right half-field VEPs the transverse distribution of C.I. but not of C.II. showed a polarity reversal across the lateral midline of the brain.

These results indicate that C.I. and C.II. have spatially separate sources. Based on known anatomy of the primary visual cortex, it appears that C.I., but not C.II. originates from the primary visual cortex. One could postulate that data transmission from the retina to the primary visual cortex requires 65 milliseconds while transmission from the primary to secondary visual cortex requires 25 milliseconds. These results support the idea that the primary visual cortex is a way station

through which afferent visual data pass to some central integrating area.

Research by DeMott with multielectrode arrays provide additional information about the visual system (Ref 8). He placed a 4 by 7 millimeters squared array of 400 electrodes spaced 0.25 millimeters apart on the primary visual cortex of a raccoon. The animal's visual system was stimulated with a flash of light subtending about three degrees of the central visual field. He sampled the data 300 times per second.

The bioelectric activity consisted of highly detailed patterns in a specific pattern which repeated quite reliably when the same stimulus was repeated. Although a diffuse response was occasionally seen in less than 10 milliseconds, the first distinguishable pattern activity usually appeared about 80 milliseconds after stimulus onset. The responses consisted of a "quickly changing" pattern that lasted 30 to 50 milliseconds followed by a "slow pattern" which occupied about 200 to 300 milliseconds. A 3 db reduction in stimulus intensity increased the latency of the fast pattern from 70 to 170 milliseconds. Recordings from the secondary visual cortex showed no response to the stimulus.

DeMott's test results suggest that the primary visual cortex responds quite well to uniform light stimulus, but the secondary visual cortex does not. One would expect such results if the secondary visual cortex's response depended on specific patterns for stimulation. Thus, the hypothesis that the secondary visual cortex accomplishes some pattern recognition is supported.

DeMott also experimented with multielectrode arrays with 1.5 millimeter electrode spacing. The bioelectric patterns were not observed.

He states that the maximum interelectrode distance that would reveal even crude outlines of this activity is about 0.5 millimeters. Such results support the previously discussed chemical neuroresearch which indicated the BCE size to be about 0.4 millimeters.

Research by Hubel and Wiesel consisted of inserting tungsten microelectrodes into a single neuron. This process allowed them to record action potentials from only one neuron at a time. When electrical activity of neighboring neurons was compared, they found that neurons in a plane perpendicular to the surface of the cerebral cortex responded to stimuli that originated from the same or adjacent visual areas, while neurons in a plane parallel to the cortical surface responded to stimuli from different visual areas. The horizontal spacing between neurons responding to different visual areas was about 0.5 millimeters. They theorize that most data transmission in the primary visual cortex occurs in the vertical plane, and that the BCE size is about 0.5 millimeters. This theory and the results of their research fit well with research by Cajal (Ref 5) and DeMott (Ref 8).

Psychological Neuroresearch

The psychologist's black box approach to examining the human visual system provides some clues that may help to establish the mechanism of human visual perception. Two areas of particular interest are the analysis of visual illusions and spatial-frequency stimulus research. The following paragraphs describe the results of research in these two areas.

The perceptual psychologists have extensively studied human response to various visual illusions for more than a hundred years (Ref 19). As a result, the responses of the human visual system to certain stimuli are

well known. One would expect that an accurate computer model of the human visual system would react similarly to such stimuli. A primary objective of this research is to develop a mathematical model that, when excited with a visual illusory image, will retain or enhance the illusion.

Consider, for example, the Kanizsa triangle illusion (Fig 6). One perceives a whiter-than-white triangle made up of lines that are not there. Since some theorize that the human visual system may process visual information via two-dimensional Fourier transforms (Ref 21), it seems logical to process the Kanizsa triangle in such a manner to determine if the illusion is retained. Dr. A. P. Ginsburg conducted such an experiment. The following paragraph briefly describes the procedure and results.

A two-dimensional discrete Fourier transform of the original picture was made. Since previous studies have shown that the high frequency components of such a transform can be removed without destroying a human's ability to recognize objects, the magnitude of the spatial frequencies were attenuated according to known high spatial frequency characteristics of the human visual system. An inverse Fourier transform reconstructed the frequency attenuated image. The filtered picture enhanced the illusory image, but the experiment did not provide a clue as to how the original pattern features interact to produce the illusion. When the picture was low pass filtered directly, the resulting picture clearly showed the illusory triangle. This result suggests that the low spatial attenuation characteristics of the human visual system do enhance the Kanizsa illusion. Thus, it is possible at least in

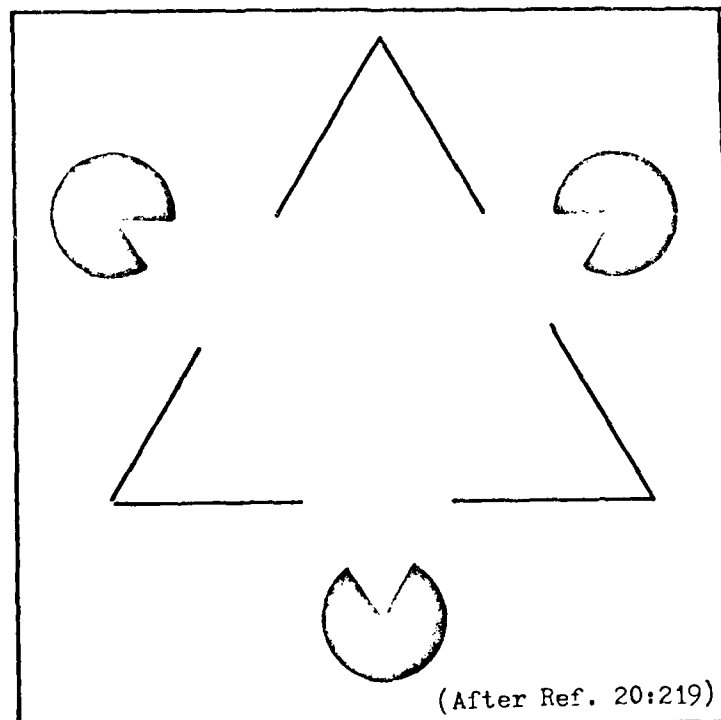


Fig. 6. The Kanizsa Triangle illusion.

specific instances to develop mathematical algorithms that respond to illusions in a manner similar to the human visual system (Ref 20).

Kazumara Ozawa (Ref 22) conducted a similar experiment. Ozawa's research is based on some observations by Koehler (Ref 23). Koehler states that to understand the visual perception of pictures, a field theory of perception must be developed. Thus, the image would be perceived through a field caused by the picture. Ozawa proposes that such a field may be regarded as a Fourier transform corresponding to a spatial filter. He states that such a filter must have the following characteristics common to the visual system:

1. Attenuation of lower frequencies.
2. Cut off characteristics for the higher frequencies.
3. Webster's Law (the minimum separable contrast of the human visual system is proportional to the light intensity).

Ozawa developed a fast Fourier transform algorithm within the constraints listed. By properly selecting the necessary parameters, this algorithm retained the illusory image of the Mueller-Lyer pattern (Fig 7), among others. These results help substantiate Ginsburg's findings.

Lamberto Maffei and his research assistants, conducted an experiment which seems to substantiate the theory that the visual cortex performs a spatial frequency analysis (Ref 24). A spatial square wave contrast grating was generated on an oscilloscope. This square wave grating had the fundamental component removed. Thus, only the third and higher odd harmonics existed in the image. When naive human subjects viewed this image at reading distance, all reported seeing a square wave image at the fundamental frequency. Each subject then retreated to a distance where the image spatial frequency appeared to change. At this moment the

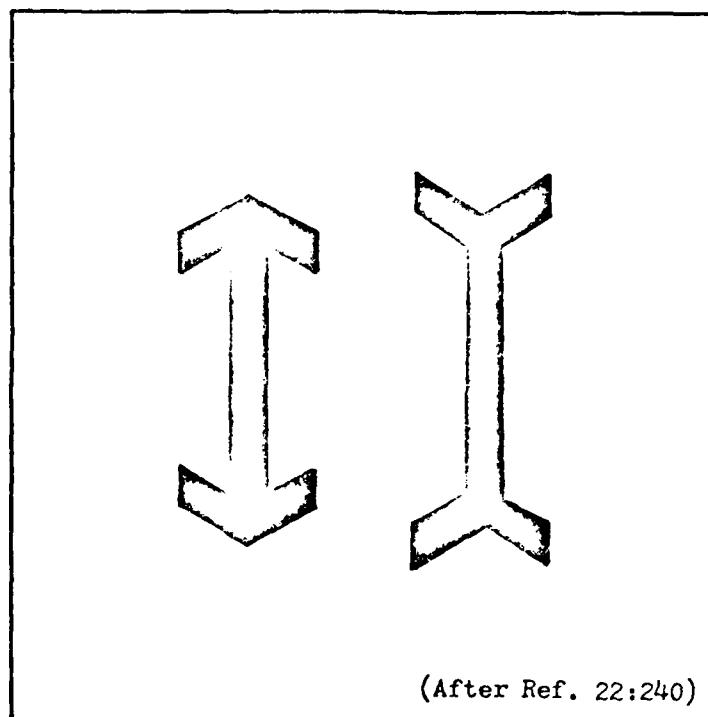


Fig. 7. Mueller-Lyer's illusion.

subject adjusted the spatial frequency of a sinusoidal spatial presentation on another oscilloscope until it matched the first. In every case, the subject adjusted the second image to correspond to the frequency and contrast of the third harmonic of the first image. The distance at which the frequency of the initial image increased corresponded to the distance at which the fifth harmonic of the picture was no longer detectable. These results can be explained by assuming the human visual system processes perceptual images in the spatial frequency domain. Should such processing occur, a modified square wave image consisting of only the third harmonic above threshold would certainly appear to be a sinusoidal contrast grating equivalent to the third harmonic of the original square wave. Although not conclusive, these experiments seem to indicate that the human visual system processes visual information in the frequency domain.

Kabrisky's Theory of Visual Perception

In 1966, Kabrisky proposed that the human visual perception process is accomplished with a two-dimensional Fourier transform (Ref 1:82). He suggests that the dense interconnections between area 17 and 18 of the visual cortex could support such an algorithm. The interconnections can be compared to an optical system that performs two-dimensional Fourier transforms by the interference and reinforcement of various portions of sinusoidal electromagnetic fields propagated along pathways of different lengths with a system of lenses. In a system designed to emulate this process, propagation times in the individual pathways must be controlled so that the proper reinforcement and cancellation can be accomplished. For a neuronal system, Kabrisky suggests that it would be necessary to maintain consistent relative propagation times in axonal pathways to

provide sufficient overall synchronization of activity in order for the possibility to exist that EPSP and IPSP interaction provide the equivalent of the interference found in the optical system. Once the Fourier transform has been accomplished between cortical areas 17 and 18, Kabrisky suggests that the resulting transform is compared to templates which consist of learned data about known shapes. Such a process might be accomplished in cortical areas 19, 20, or beyond. As the previous sections of this chapter indicate, there is considerable evidence to substantiate such a theory.

A Method to Test Kabrisky's Theory

To determine the validity of Kabrisky's theory requires proof that data timing requirements between cortical areas 17 and 18 are met. In addition, if one assumes that the visual perception processing algorithm is some form of frequency domain analysis, then research into this process should include stimulation of the visual system with spatial sine wave gratings. One might compare the research of the visual perception process with the investigation of a frequency sensitive electronic circuit. The circuit characteristics can be fully described by its input-output frequency and phase relationships. Inputs of varying frequencies and amplitudes can be compared to the resulting outputs. Should the device be linear, a plot of amplitude and phase versus input frequency would completely describe its transfer function. Should the device be nonlinear, the problem becomes more difficult, but the same approach is valid. Since the analog to sinusoidal waveforms in an electronic circuit is spatial sine wave gratings in a visual processing system, one might try to determine the transfer function of a portion of the visual system by observing its response to these gratings (Ref 25).

Thus, the problem of determining the transfer function between cortical areas 17 and 18 can be approached from a control theory viewpoint. The input to the visual system is stimulated with a sinusoidal input while a large array of data in cortical area 17 and 18 are simultaneously recorded. The data from area 17 should homeomorphically map the sine wave input while the response at area 18 should be very sparse because only a single frequency mode is excited. As the input sinusoid is varied in frequency, the response in area 18 should remain sparse and move to a new location representing the new single frequency.

To accomplish this experiment, large arrays of data from cortical areas 17 and 18 must be recorded and analyzed. To insure individual BCEs are contacted, the electrode spacing must be at least as small as each individual computing element. The objective of this thesis is to develop and test a prototype multielectrode array that can accomplish this task.

III. Multielectrode Array Design and Fabrication

Introduction

This chapter deals with the design, fabrication and initial evaluation of the multielectrode array (Fig 8). The first section of this chapter will review Tatman's design so that the significance of his work to this thesis can be understood. In addition, this section will describe the design changes made so that the multielectrode array better accommodates this research project. The next two sections discuss the solution of the three major fabrication problems encountered by Tatman and the process schedule which results from these solutions. The last two sections describe the initial evaluation of the multielectrode array and provide suggestions that will improve the device.

Multielectrode Array Design (Ref 11)

Overview. Tatman's primary design criterion was to develop an array of closely spaced electrodes that could record the electrical signals existing over a large surface area of the visual cortex to investigate the possibility that the average membrane potentials over these surfaces, a summation of the EPSP's and IPSP's, perform the reinforcement and cancellation necessary to accomplish a Fourier transform computation. This design goal is consistent with the requirements of this thesis. There are however, some differences between Tatman's specific design requirements and those of this thesis. The following paragraphs describe the significant requirements and differences.

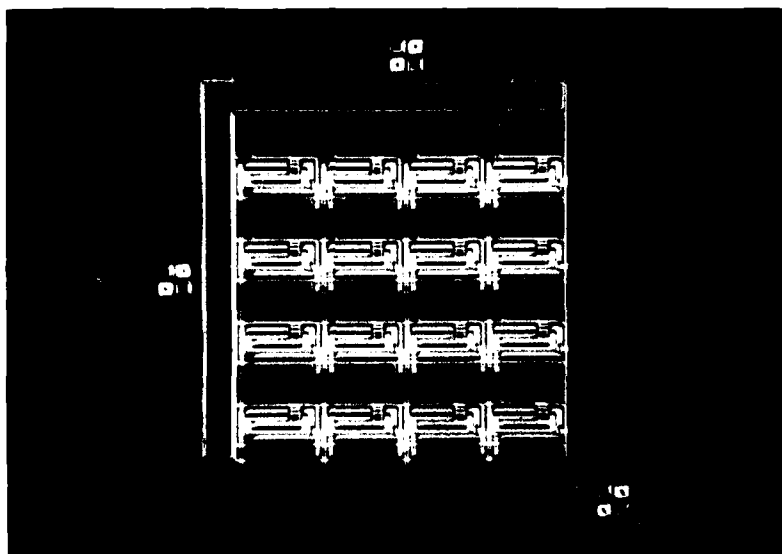


Fig. 8. The Multielectrode Array (X50).

Inter-electrode Spacing. As previously reported, the size of the basic computing elements (BCEs) appear to be between 0.05 and 0.5 millimeters. To assure at least one electrode contacts each BCE, the electrode spacing should be about half the estimated width of the BCE. For the initial experiment it is assumed that the BCEs are 0.5 millimeters apart. Consequently, the electrodes should be arranged on 0.25 millimeter centers. Tatman's multielectrode array meets this requirement.

To accurately determine the size of the BCE the electrode spacing can be reduced until two electrodes contact the same BCE. When this occurs, bioelectric data from adjacent electrodes should be closely correlated. This particular experiment is beyond the scope of this thesis, but should be tried in following research efforts.

Array Size. Tatman limited the size of the array to four by four in order to keep the device simple, yet adequate to test the feasibility of the multiplexing matrix design. For the same reason, the research conducted by this thesis will be limited to a four by four array. If one assumes the BCE size is 0.5 millimeters, the array will contact only four BCEs. It is likely that the data from four BCEs will not be sufficient to provide insight into the transfer function between cortical areas 17 and 18. Fortunately, the prototype array is inherently expandable to several thousand electrodes because of the fact that its physical realization is based on integrated circuit technology. Future research should include experimentation with an expanded version of the multielectrode array.

Contact Resistance. Tatman selected gold as the metal for electrode fabrication. Gold was selected because it can be worked using standard integrated circuit techniques and causes the least tissue damage during

chronic implanting. Histological studies indicate that the extent of tissue damage in chronic implants is a direct function of ionic exchange current densities produced by the metal electrode. Gold has a low exchange current density and its measured value is about 10^{-9} amps per square centimeter. As a comparison, the measured exchange current density for silver is greater than 10^{-5} amps per square centimeter.

Unfortunately, the high contact impedance of the gold electrodes caused noise and multiplexing problems (see chapter 5). Electrode impedance can be approximated as a parallel resistor-capacitor combination whose values vary slightly with frequency (Ref 26:1068). For inert metals such as gold and silver, an electric double layer is produced when an electrode is immersed in an ionic solution such as the saline-rich cerebral spinal fluid (CSF). This double layer, called the Helmholtz layer, is about two to four angstroms thick. The Helmholtz layer creates an electrolytic capacitor whose measured value is about 20 microfarads per square centimeter. Each electrode has an exposed surface area of approximately 0.016 square millimeters. Thus, the calculated capacitance is 3100 picofarads. The parallel resistance value can be calculated based on the exchange current density. For the exchange current densities previously mentioned, gold has a resistance value of about 10^7 ohm-square centimeters and silver has a resistance value of about 2.5×10^3 ohm-square centimeters (Ref 27:214). Thus, the parallel resistor value for the gold electrode is about 6×10^{10} and for silver is about 16×10^6 ohms. Chloriding can further reduce the resistance value of a silver electrode (Ref 28:422). To chloride the silver electrode, it is placed in a solution of sodium chloride and a voltage is applied to cause the chlorine ions to react

with the silver surface. Contact resistances of 12.5 ohm-square centimeters typically result from this process. Thus, the calculated silver-silver chloride electrode resistance value is about 78×10^3 ohms.

In view of the problems associated with the high impedance gold electrode and the fact that acute rather than chronic implants would be done, the electrodes were silver plated and then chlorided. Table I compares the calculated impedance values of the gold electrode and the silver-silver chloride electrode. Note that a significant side benefit obtained from the silver-silver chloride electrode is its relative frequency independence in the desired recording range of 1 to 40 Hertz.

Multiplexing Requirements. To determine the transfer function between the primary and secondary visual cortex requires simultaneous, fine grained bioelectric data from large areas of these cortical regions. Since future research work will extend the prototype four by four array to hundreds or thousands of electrodes, one output lead from each electrode becomes infeasible. These facts led to the idea of a multiplexed array with all signals from a column of electrodes of the array multiplexed onto a single lead. Multiplexing is accomplished with junction field effect transistor (JFET) switches fabricated on the same silicon substrate as the electrodes (Fig 9).

During normal multiplexing operation, an external drive circuit will pinch-off three of the four rows of normally on, n-channel JFET switches. As a result, each column lead receives a bioelectric signal from one of its four electrodes. The drive circuit will scan through the four rows so that every electrode is sampled at a rate sufficient to obtain valid data from the highest frequency component of the bioelectric signal. Thus, the four by four array requires a minimum sampling rate of 320

TABLE I
Calculated Electrode Impedances

Frequency (Hertz)	Impedance (ohms)	
	Gold	Silver- Silver Chloride
0.1	5×10^8	78×10^3
0.2	2.6×10^8	78×10^3
0.5	1×10^8	78×10^3
1.0	5×10^7	78×10^3
2.0	2.6×10^7	78×10^3
5.0	1×10^7	77×10^3
10.0	5×10^6	77×10^3
20.0	2.6×10^6	76×10^3
40.0	1.3×10^6	74×10^3

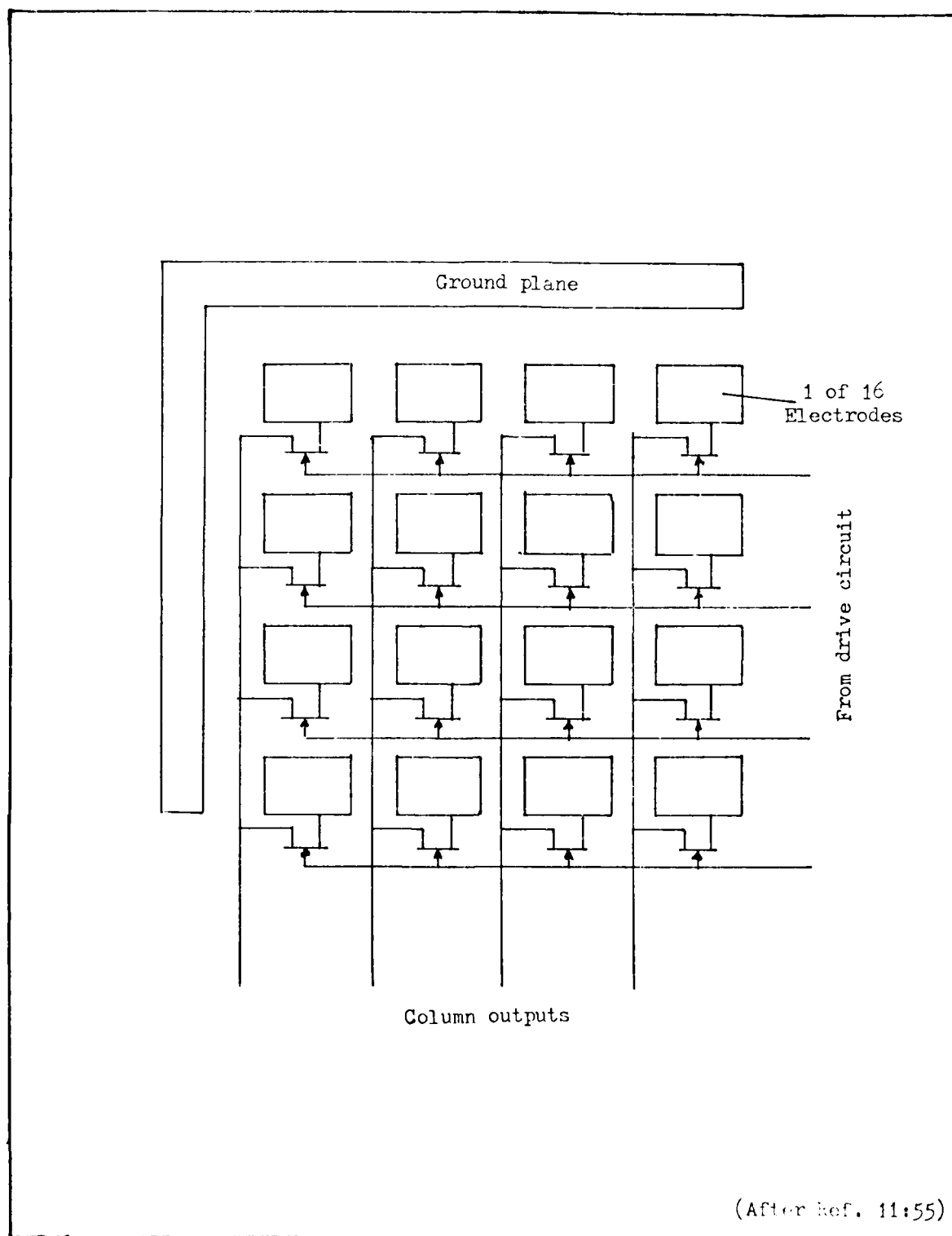


Fig. 9. Multielectrode array circuit diagram.

Hertz to assure the 40 Hertz bioelectric signals are scanned at the 80 Hertz Nyquist sampling rate. In practice the sampling rate should be somewhat higher than the Nyquist rate (Ref 29:696). Consequently, the research conducted for this thesis will use a 1000 Hertz sample rate. The details of the multiplexing drive circuitry are contained in chapter four.

The Insulation Layer. The insulation layer over the silicon substrate must protect the active devices from sodium ion invasion caused by the CSF and be selectively removable by photolithographic methods. Chemical vapor deposited (CVD) silicon dioxide insulated the first nine multielectrode arrays. Device lifetime tests proved it was ineffective in protecting the active devices in a sodium chloride solution environment (details of the lifetime tests are in chapter five). Alternatively, a plasma deposited silicon nitride was used for the insulation layer. The 4000 angstrom silicon nitride layer protected the device for sufficient time to allow an acute implant and about 16 hours of data acquisition.

Solution of the Three Fabrication Problems

Tatman's initial fabrication run resulted in nonfunctional devices. The reasons were poor contacts, leakage paths between the drain, source, and gate, and cracking of the CVD silicon dioxide insulation layer. The following paragraphs describe these problems and their solutions.

The first major problem encountered during the initial fabrication run was lack of ohmic contact between the silicon surface and the chrome-platinum-gold film. Instead of ohmic contact, Schottky diode characteristics were observed across the n-type FET channel connections. Since the FET channel must pass microvolt level electroencephalic signals, such rectifying barriers are unacceptable. Metal-semiconductor rectifying barriers formed

on n-type semiconductors are generally caused by high resistivity semiconductor materials (Ref 30:416). Reduction of the semiconductor surface resistivity usually eliminates the barrier. The design goal was to develop a degenerate semiconductor by increasing the surface impurity concentration to 6×10^{19} per cubic centimeter or greater with an n-type enhancement diffusion. A degenerate semiconductor has the Fermi level within the conduction band which greatly increases the likelihood of ohmic contact with a thin film metal.

The original fabrication run resulted in a surface resistance of about 300 ohms per square (8×10^{17} per cubic centimeter impurity concentration). After diffusion equipment modification, this surface resistance was lowered to 6.8 ohms per square (10^{20} per cubic centimeter impurity concentration). To determine if the resulting concentration would yield ohmic contact, the following test was conducted.

The final enhancement diffusion test was evaluated by metalizing the test wafer surface with 60 mil aluminum dots and measuring the electrical characteristics between two dots spaced approximately 300 mils apart. The metal-semiconductor contacts had a linear and symmetrical voltage-current relationship with a resistance of about 1.7×10^5 ohms. The final enhancement diffusion procedure appears in the revised process schedule.

The second major problem encountered during the initial fabrication run was leakage paths between the gate, source, and drain leads of the JFET switches (Ref 11:85). These leakage paths prevented the turning off of the JFET switches. It was suspected that impurities in the passivation oxide layer created the leakage paths by providing free ion current carriers between the JFET leads. Past research by commercial semiconductor

manufacturers indicates that the sodium ions in the oxide layer causes the large majority of leakage current. To reduce the effects of sodium ions in the oxide, several test oxidation runs were accomplished at various times after purging the oxidation furnace tube with gaseous hydrochloric acid (HCl). The HCl purge diffused negative chlorine ions into the furnace tube which outgassed during the oxidation growth process. Chlorine ions absorbed by the oxide combined with sodium ions producing non-ionic sodium chloride. Capacitor-voltage (C-V) bias-temperature stress measurements were made to determine the effect of the HCl purge on oxide's free ion content.

The C-V bias-temperature stress test consisted of first growing a 1000 to 2000 angstrom oxide layer on a test wafer and metalizing the oxide surface so that a metal-insulator-semiconductor (MIS) structure was created. The structure was then subjected to an initial C-V test which determined its capacitance as a function of a potential difference developed between the semiconductor and metal surface. Following the initial evaluation, the MIS structure was subjected to approximately 10 volts per 1000 angstroms, referenced to the semiconductor substrate. In addition, the MIS structure was heated to 250 degrees centigrade for five minutes. As a result, any cations in the oxide moved away from the metal surface, while anions moved toward the metal. After the bias-temperature stress application, another C-V curve was obtained. Then, a reverse voltage stress was applied, along with another heating cycle. Subsequent to this second bias-temperature stress, a third C-V curve was obtained. The C-V curves indicated the type of ion current carriers because shifts in these curves were caused by mobile ion activity at the silicon-insulator interface. The direction of the C-V curve shift identified the offending ion.

The design goal was to produce a C-V curve shift of less than two volts for a 2000 angstrom thick oxide. A two volt shift in the 2000 angstrom oxide indicates approximately 2×10^{11} charge drifts per square centimeter (Ref 31).

HCl purging the tube immediately before the oxide growth process resulted in C-V stress curves which indicated approximately 7×10^{11} negative ion current drifts per square centimeter. It was suspected that excessive chlorine ions entered the oxide surface during growth. C-V tests of a MIS structure whose oxide was grown eight days after a four hour HCl purge showed approximately 4.2×10^{11} positive ion drifts per square centimeter. Additional testing indicated that oxides grown 24 to 36 hours after an HCl purge would likely yield near zero C-V curve shifts during bias-temperature stress tests. In other words, sufficient chlorine ions would diffuse into the oxide during thermal growth to exactly negate the effects of sodium ions injected during the metalization process. Since the multielectrode array would be subjected to a concentration of 150 millimoles per liter of sodium ions in the cerebral spinal fluid, the passivation oxide layer was grown in a chlorine rich environment. This would extend the lifetime of the device by providing free chlorine ions to combine with the sodium ions entering the passivation layer from the CSF. Thus, the revised process schedule reflects a four hour HCl purge and a fourteen hour nitrogen purge, followed by passivation oxide growth.

Test wafers that accompanied the circuit wafers in the final oxide growth process indicated a drift of 6.8×10^{10} negative charges per square centimeter which was well within the desired limit of 2×10^{11} charges per square centimeter.

The third major problem encountered during the initial fabrication run was cracking of the final passivation layer. The cracks appeared along the gold metalization runs which indicated that the chemical vapor deposition (CVD) silicon dioxide was too brittle to withstand the thermal expansion coefficient differences during cool-down. To preclude cracking, phosphorous was added to the CVD silicon dioxide during deposition. The phosphorous produced a less brittle glass passivation layer. After several test runs, the following CVD schedule was adopted:

1. 10 minute preheat to 435 degrees centigrade.
2. 5 minute deposition of 7000 angstroms of phosphorous silicon dioxide.

The gas flow rates during deposition were as follows:

29 liters/minute of nitrogen

255 cubic centimeters/minute of oxygen

610 cubic centimeters/minute of 4% silane

500 cubic centimeters/minute of 1% phosphorous (PH_3)

The schedule and flow rates are incorporated into the revised fabrication schedule.

Multielectrode Array Fabrication

The following paragraphs review three significant aspects of the fabrication schedule contained in Appendix B. These aspects are: boron glass removal after the isolation diffusion, wire attachment procedures, and silver-silver chloriding the electrodes. For a more complete discussion of the fabrication procedure, the interested reader is referred to Appendix B of this thesis.

After the 110 minute boron isolation diffusion, the boron glass must be removed in preparation for the gate oxidation step. Considerable difficulty was experienced in removing the boron glass. It is believed that two factors contributed to this problem. The first factor is the boron source wafers were new. As a result, the source wafers provided high levels of boron dopant during the diffusion process. The second factor was an insufficient oxygen flow rate during the diffusion.

The original process schedule required 30 cubic centimeters per minute of oxygen mixed with one liter per minute of nitrogen. The boron glass resulting from this diffusion could not be removed with 20 minutes of soak time in a 1:10 hydrofluoric acid:deionized water bath. Results of diffusions with test wafers indicated that 50 cubic centimeters per minute of oxygen improved the removal characteristics of the boron glass. This glass was removed in about 15 minutes of soak time in the dilute hydrofluoric acid.

To assure improved boron glass removal, a hot nitric acid soak step was included in the fabrication schedule. Tests indicate that this modification of the fabrication schedule improved the process, but did not completely remove the boron glass. The electrical tests section describes a problem caused by residual boron glass.

A novel procedure was developed to attach the wire leads to the nine peripheral bonding pads (Fig 10). After photolithographically removing the silicon nitride on the bonding pads, the multielectrode array was placed on a thermal chuck and heated to 200 degrees centigrade. Each pad was tinned with 60/40 tin-lead solder, and the device was cooled to room temperature. Then, 30 gauge insulated wires were individually soldered to



Fig. 10. Lead Attachment to the Array (X8).

the bonding pads with a small soldering iron. After the leads were attached, the soldering flux was removed with a one minute bath in trichloroethylene followed by a 30 second wash in methyl alcohol. The device was then washed in deionized water for five minutes and dried with nitrogen gas.

For extracellular bioelectric potential measurements, frequencies below 40 Hertz are of interest. To reduce the low frequency contact impedance, the gold electrodes were covered by silver chloride. First silver was electrolytically deposited with a 200 microamp current for 40 seconds (Ref 28:422). Electrical contact with the electrodes was accomplished by tying all four column leads together and attaching them to the negative lead of the plating power supply. The positive lead of the power supply was connected to a pure silver anode which was immersed in the silver plating solution. The plating solution consisted of 2 ounces of potassium silver cyanide, 3 ounces of potassium cyanide, and 27 ounces of distilled water. After silver plating the electrodes, they were chlorided. The chloriding process consisted of immersing the array in a sodium chloride solution and passing 320 microamps of current through the electrodes for 10 seconds.

Results of Electrical Tests

The following paragraphs describe the results of curve tracer tests on the JFETs in the multielectrode array. In addition, percent yield is discussed along with the two primary failure modes for the nonworking devices.

To determine the curve tracer characteristics, 40 JFETs from 11 circuits on 2 wafers were tested. Five JFETs from three different

circuits on the same wafer were tested before and after sintering at 435 degrees centigrade. In every case, the following parameters were measured: channel on-resistance (R_c), pinch-off voltage (V_p), channel on-current (I_{dss}), and channel breakdown voltage. Figure 11 shows a typical curve tracer test result.

Pre-sintered R_c of the operational devices varied from 1,600 to 3,500 ohms and was typically 2,200 ohms. Within a particular array, on-channel resistance of the 16 JFETs varied less than 25 percent. After sintering for 10 minutes at 435 degrees centigrade, R_c increased to values ranging from 6,700 to 10,000 ohms. As with the pre-sintered devices, R_c varied less than 25 percent between the JFETs within a particular circuit.

The pinch-off voltage of operational circuits varied from 0.6 to 2.2 volts. The typical V_p was 1.2 volts. Sintering did not significantly affect pinch-off voltage and V_p of the 16 JFETs within any particular device varied less than 10 percent.

The initial design requirements called for R_c to be about 650 ohms with a V_p of 3 volts. Since the JFET switch terminates a 78 kilohm electrode with a 10 megohm input impedance amplifier, R_c is not critical, and can be as high as 100 kilohms without seriously degrading system performance. Thus, even though the devices have R_c values ten times greater than the initial design goal, they are acceptable for use in this research project. The pinch-off voltage is also quite acceptable in that lower V_p values reduce the gating noise created by the multiplexing drive circuitry. It appears that excessive gate diffusion depth increased R_c and reduced V_p .

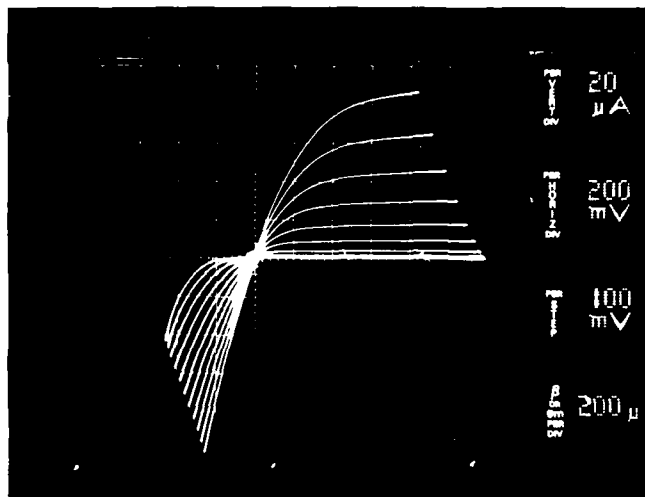


Fig. 11. JFET Curve Tracer Characteristics.

Pre-sintered I_{dss} varied from 80 to 400 microamps with a typical value of 200 microamps. Sintering reduced the I_{dss} values to 20-80 microamps with a typical value of 60 microamps. While not critical, the I_{dss} changes caused by sintering reflect the inherent increase in R_c .

In all cases the channel breakdown voltage exceeds the requirements of this research project. Breakdown voltages ranged from 6 to 50 volts with a typical value of 40 volts. The occasional 6 volt breakdown is probably caused by surface effects. Even 6 volts is an acceptable breakdown limit because the highest applied voltage to the device is the pinch-off voltage, which never exceeds 2.2 volts.

Percent yield was estimated by careful examination of each device with a light microscope. Electrical tests substantiated the findings of the microscopic examination. Of 54 circuits, 37 were considered operational for a 69 percent yield. Electrical tests confirmed that the nonfunctional devices experienced two primary failure modes.

The first failure mode was improper etching of the contact windows through the final oxidation layer. Several nonfunctional JFET devices exhibited electrically open channel pathways. Microscopic examination of these devices confirmed that the metal did not contact the silicon substrate. In every case, the nonfunctional devices were those situated around the periphery of the wafer. It appears that the boron glass removal step contributed to this problem because the residual boron glaze along the edge of the wafer prevented firm impingement of the metalization contact mask with the wafer surface during photolithographic printing.

The second failure mode was a lack of isolation diffusion between JFET devices. Four circuits on one wafer exhibited this characteristic.

This problem was caused by improper etching through the initial oxidation before the isolation diffusion.

Design Improvements

A review of the ultimate objective of this research project and the characteristics of the prototype multielectrode array suggests some improvements to its design. These improvements are beyond the scope of this thesis project, but should be considered for future research work. Some of these suggestions have appeared in previous sections of this thesis and all suggestions will be repeated in the recommendations section. They are placed here to serve as a summary of this chapter.

For simplicity, the prototype array contains only 16 electrodes. It is likely that this four by four array will not provide sufficient coverage of the visual cortex. Future research should include 50 by 50 or larger arrays so that the activity of several thousand basic computing elements can be simultaneously recorded.

The requirement to use silver-silver chloride electrodes highlights the need for a buffer amplifier dedicated to each electrode. This buffer amplifier might be a JFET which could be fabricated directly on the silicon substrate along with the JFET switches. The JFET amplifiers could have input impedances greater than 100 megohms and output impedances less than 500 ohms, virtually eliminating crosstalk and stray noise pickup from the system (Ref 27:212).

Once large arrays with buffer amplifiers are available, they will be able to record bioelectric data from large surface areas of the visual cortex. To reduce the effort associated with implanting these devices in test animals, chronic implants should be considered. To ensure the long

life required for chronic implants however, a new passivation material must be developed. Silicon nitride protected the prototype device for about 16 hours. It is desirable to extend the device lifetime to weeks or months. The problem of protecting active devices in a sodium chloride solution environment is perhaps the most difficult problem for future researchers (Ref 32).

Once the passivation problem is solved and chronic implants become a reality, one should consider developing a hybrid circuit that contains the multielectrode array, buffer amplifiers, multiplexers, multiplexing drive circuitry, and RF data link transmitter. With such a hybrid circuit, a researcher is no longer tied to a surgical operating room for the experimental process, and the visual perception mechanism can be analyzed in its natural environment. The results of such an experiment may provide the data necessary to determine how the mammalian visual perception system works.

IV. Support Electronics

Introduction

This chapter deals with the design, fabrication and operation of the equipment required to support the multielectrode array. The first section contains system descriptions of the equipment used for the data recording and play-back modes. In addition, it discusses the functional requirements for the various components of these systems. The second section contains a detailed diagram of the drive circuitry, which, except for the multielectrode array, is the only fabricated component of the data recording system. The second section also discusses the major design decisions involved in its development.

To facilitate understanding the system descriptions, this paragraph provides an overview of the in vivo test set-up and procedure. Following anesthetization of the test animal, the skull is opened over the visual cortical region of the brain. The dura is incised and two multielectrode arrays are placed on the pia of the cortical surface. The first array rests on the primary visual cortex, or area 17, while the second array is on the secondary visual cortex, or area 18. Each array is connected to a drive circuit that provides both the multiplexing drive signals and the load resistors for the column lead outputs. A master clock will strobe the drive circuits. The experimenter places a projection screen in the visual perception area of the test animal. A projector controlled by an electronic shutter displays spatial sine wave gratings to the test animal. During visual stimulation, the electronic shutter trigger is recorded on one channel of an FM tape recorder. In addition, the clock signals,

frame pulse from the drive circuit, and eight column lead signals are recorded on the FM tape recorder.

System Descriptions

Record Mode. The objective of the multielectrode array and support electronics operation is to simultaneously record bioelectric data from areas 17 and 18 of the cerebral cortex (Fig 4). The stimulus onset event must also be recorded so that future data analysis can identify electroencephalic events as a function of time after visual stimulation. Figure 12 is a block diagram of the multielectrode arrays and support electronics required to accomplish this task. Except for the multielectrode array and the drive circuitry, all equipment is commercially available. This fact simplifies experimental equipment set-up and maintenance. The following paragraph describes the record mode operation and the equipment required for this mode.

There are fifteen pieces of equipment required for recording electroencephalic data: the clock, the drive circuitry for each multielectrode array, two multielectrode arrays, an Ampex 1300 FM tape recorder, eight PAR model 113 low noise preamplifiers, and visual stimulus trigger. The clock provides a one kilohertz, ± 6 volt square wave to the drive circuitry and to channel one of the FM tape recorder. Each drive circuit converts the clock timing signals to the correct voltage levels for sequentially scanning the JFET multiplexing switches in the two multielectrode arrays. The drive circuit also generates a frame pulse that indicates when the first row of JFETs are being scanned. This frame pulse presets the area 18 drive circuit to scan row one so that both array multiplexers remain in synchronization. The frame pulse is also recorded so that demultiplexing operations

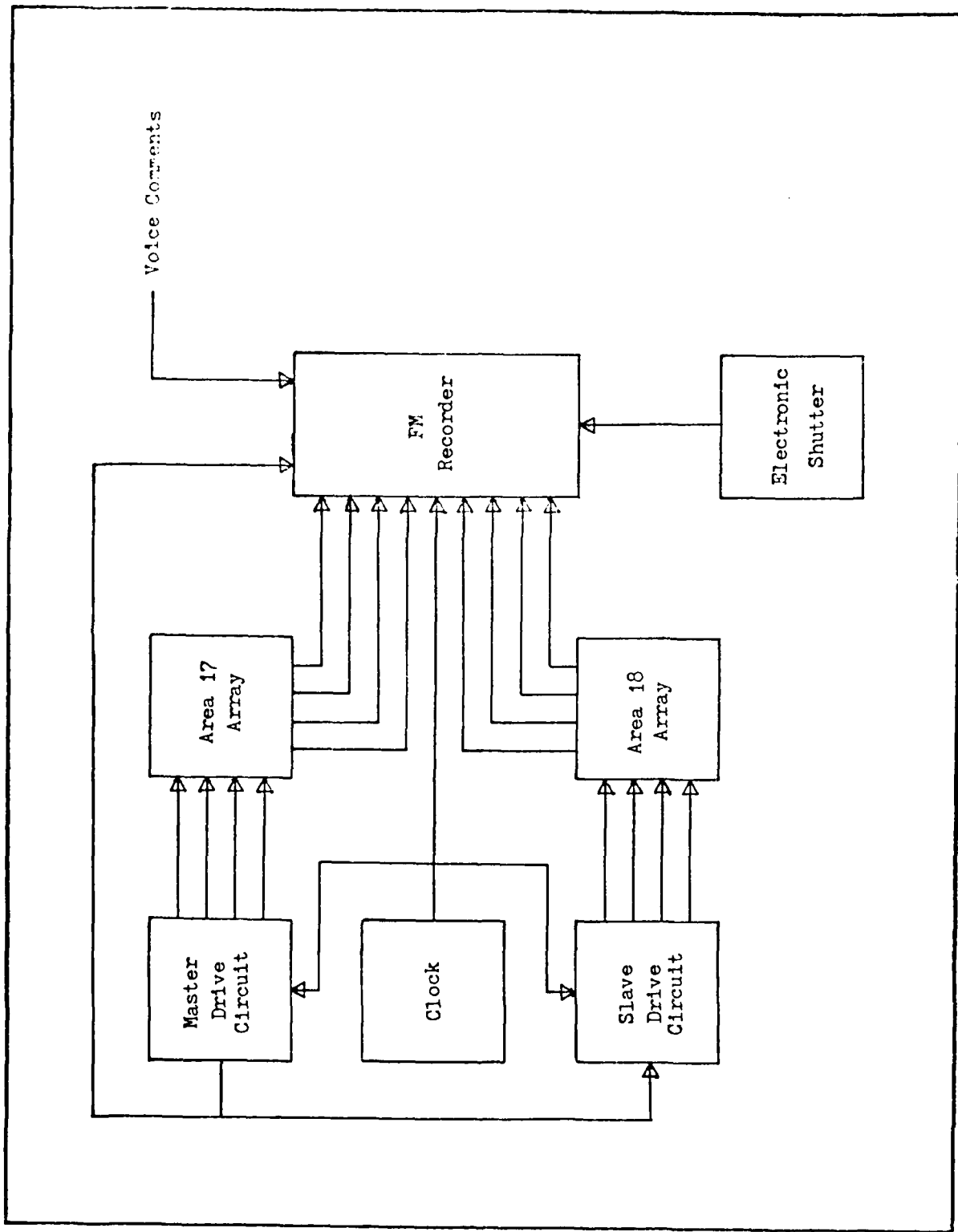


Fig. 12. Record system block diagram.

can be accomplished. Figure 13 is a timing and voltage level diagram which shows the relationship between the master clock signals, each JFET row controller output, and the frame pulse.

The eight preamplifiers band-pass filter and amplify the multiplexed microvolt level electroencephalic signals from each column lead of the two multielectrode arrays. The preamplifiers operate from a self-contained battery pack so that 60 Hertz noise levels are reduced. The PAR 113 preamplifier was chosen because of its low noise, high gain and common mode rejection capabilities. The amplifier has an ambient noise level of approximately 1.0 microvolt, a variable gain from 10 to 25,000, and 120 dB common mode rejection.

The 14 track FM tape recorder receives the amplified, multiplexed bioelectric signals from area 17 and records them on channels two through five. Channels six through nine receive bioelectric signals from area 18. Channel 10 contains voice commentary concerning the experiment and channel 11 receives a stimulus onset signal from an electronic shutter. The electronic shutter controls the output of a slide projector which displays spatial sine wave gratings on a projection screen situated in the visual perception area of the test animal. Channel 12 of the recorder receives the framing pulse from the drive electronics.

To record bioelectric signals, the electronic shutter is triggered and a spatial sine wave grating is presented to the test animal. The recorder receives the stimulus onset pulse along with the appropriate voice commentary. This procedure is repeated for several different spatial frequencies. The clock and framing pulses, and the stimulus onset trigger

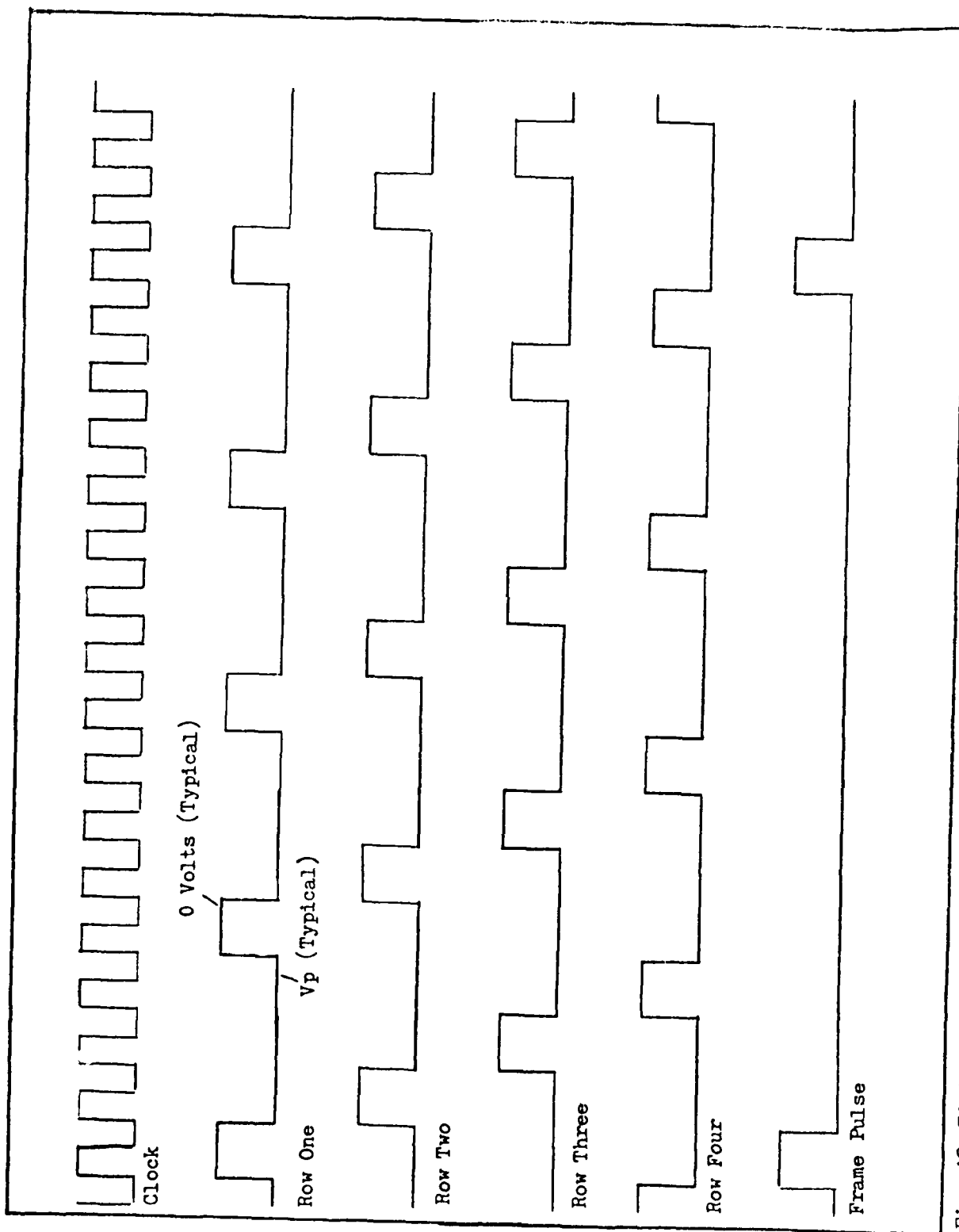


Fig. 13. Timing and voltage level diagram.

allow retrieval of the multiplexed bioelectric signals as a function of time from stimulus onset.

Playback Mode. Data retrieval is accomplished in the playback mode (Fig 14). The FM tape recorder is connected to the input port of an analog-to-digital (A/D) converter. To insure signal synchronization the stimulus onset pulse is used to initiate the A/D conversion process. The process consists of making ten passes through each data block, where a data block is defined as the information recorded after a single stimulus onset. In each pass, a single recorder channel is digitized. Recorder channels one and twelve (clock and frame pulses) are digitized to obtain timing signals required for demultiplexing the bioelectric data. Then, the bioelectric data recorded on channels two through nine are digitized and stored as computer record blocks. The demultiplexing and filtering operations are accomplished with software.

Drive Circuitry

The drive circuitry was designed to convert master clock pulses to properly timed drive voltages for the multielectrode array row leads (Fig 15). These row lead drive pulses are the multielectrode array multiplexing drive signals. In addition, the drive circuit produces a framing pulse that is used for array multiplexing synchronization during the record mode and signal demultiplexing during the playback mode. The drive circuitry also contains the load resistors across which the bioelectric signals are generated for input into the preamplifiers. Battery operation of the preamplifier minimizes 60 Hertz noise on these signals. The drive circuit can be driven by the master clock so that it scans the entire

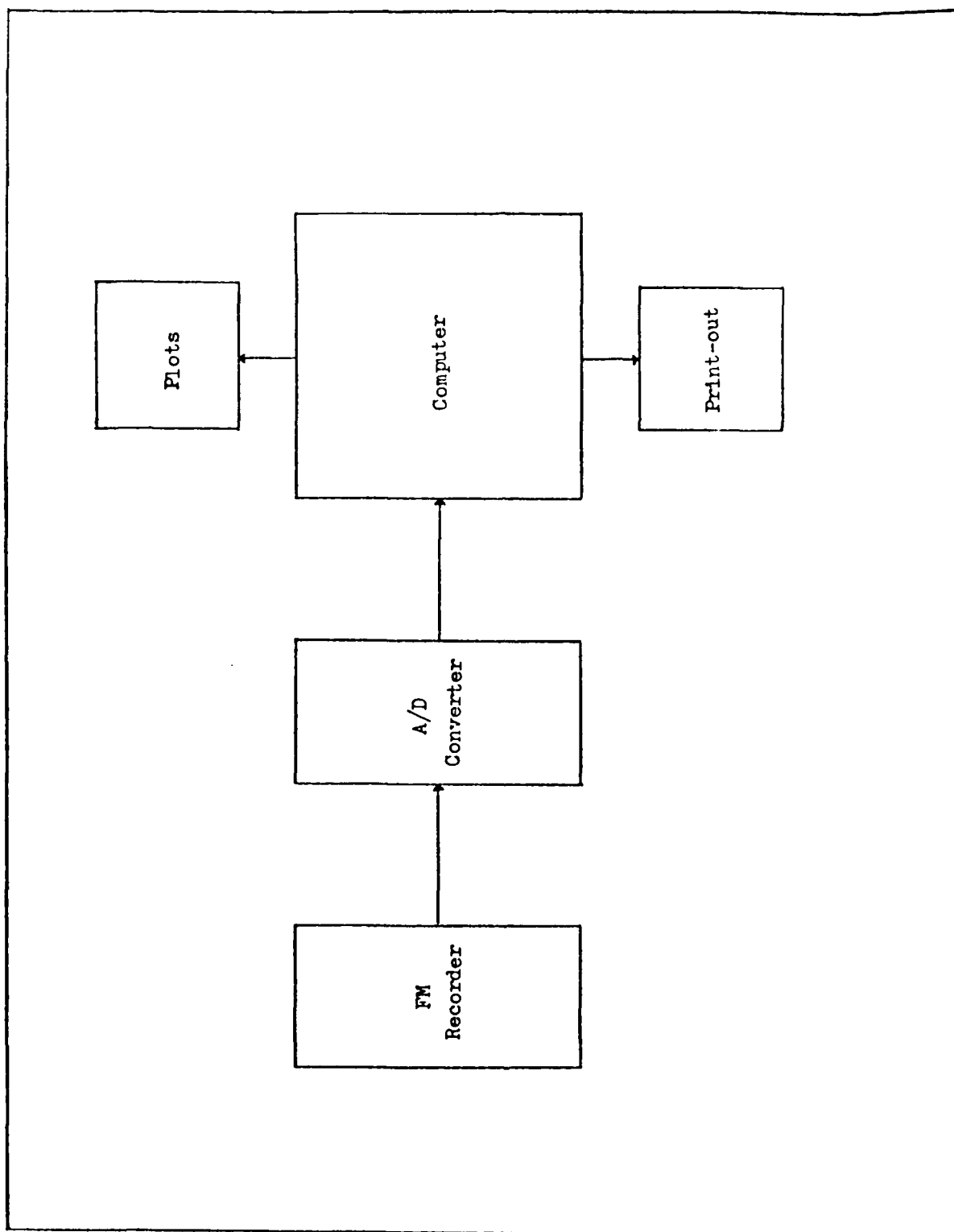


Fig. 14. Playback system block diagram.

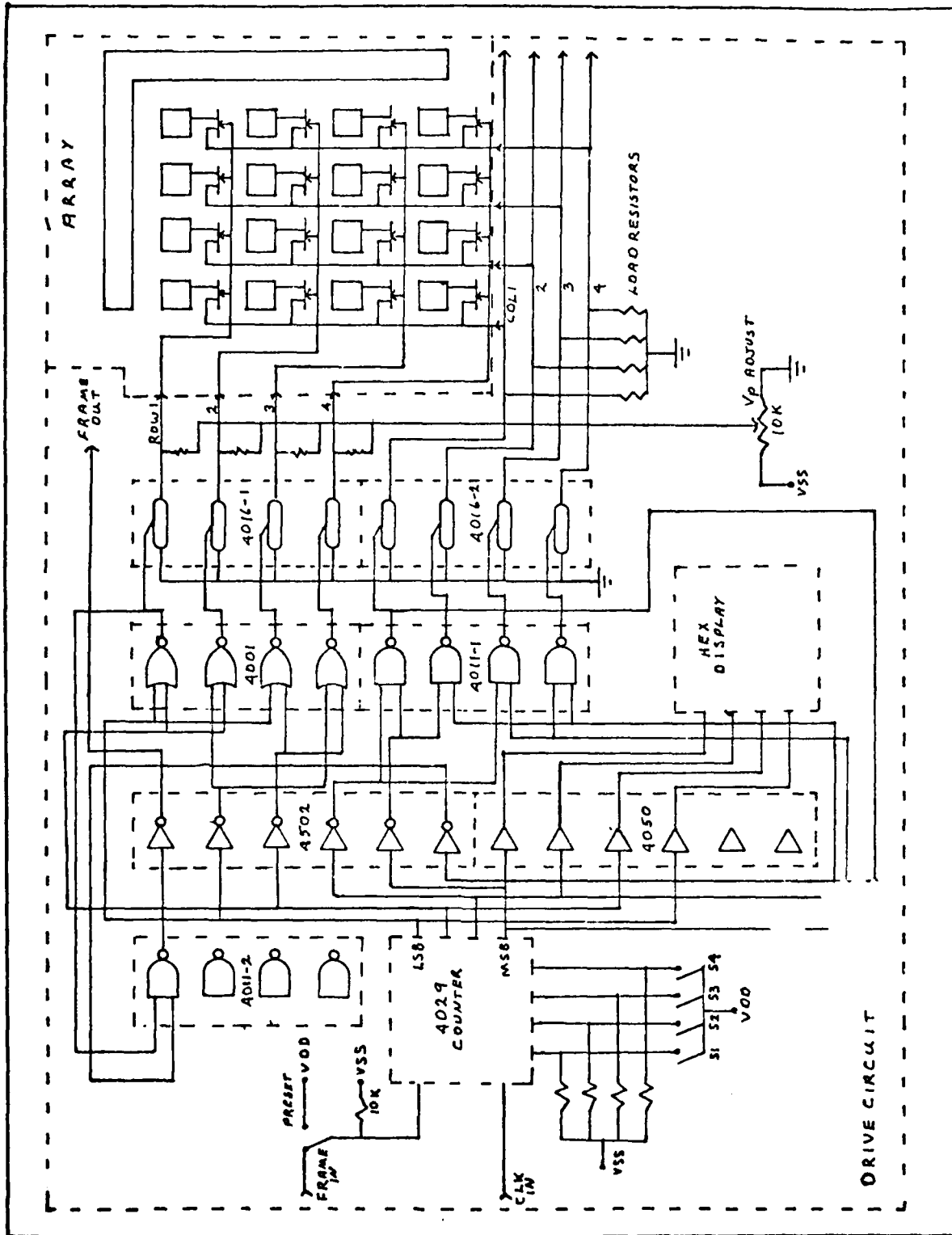


Fig. 15. Drive circuit and array.

multielectrode array, or be preset to monitor a desired row of electrodes. Since the pinch-off voltage of the multielectrode arrays can vary from 0.6 to 2.2 volts (see Chapter 3), the drive circuit was designed to provide a pinch-off voltage level which is adjustable between 0.0 and 6.0 volts. CMOS logic devices were used for the drive circuitry design. CMOS was chosen to reduce noise and power supply current requirements. The following paragraphs describe the logic circuitry operation and the major design requirements.

The 4029 presettable up/down counter is used to produce the four bit code required to drive the display and switching circuitry. The 4029 is used in its preset mode when the experimenter wants to look at a particular electrode output. The preset value is controlled by switches one through four. When multiplexing is desired, the 4029 is driven by the master clock and operates in the binary count-up mode. The 4502 strobed hex inverter, the 4001 quad nor gate, and the two 4011 quad nand gate circuits produce the logic levels required to control the two 4016 quad bilateral switches and to generate the frame pulse. The area 17 drive circuit generates the frame pulse which is sent to the area 18 drive circuit. The area 18 drive circuit receives the frame pulse at the 4029 preset line. With all preset data switches set to zero, each frame pulse forces the drive circuit to scan the first row. This slave operation of the area 18 drive circuit guarantees synchronous multiplexing by both multielectrode arrays. Synchronous operation is necessary to allow correct demultiplexing during the playback mode operation.

The 4016-1 package controls the pinch-off voltage levels to the row leads of the multielectrode array, while the 4016-2 package scans the column leads during multiplexing. It should be noted that the results of in vitro testing determined that strobing the column leads is unnecessary. As a result, the 4016-2 package is removed from the drive circuit during in vitro tests.

The 4016-1 quad bilateral switch routes the pinch-off voltages to the row leads during multiplexing. In the off mode, the switch impedance is approximately 10^9 ohms. When turned on, the switch behaves as a nearly linear 300 ohm resistor. To provide the proper pinch-off voltage, a variable voltage power supply is connected to each switch output lead through a 22 kilohm resistor. All switch input leads are tied to ground. When the switch is on, the corresponding row of JFETs in the multielectrode array are turned on because the gate leads are forced to ground potential. With the switch turned off, the pinch-off voltage is supplied to the corresponding row of JFETs through the 22 kilohm resistors. Note that a return path for gate leakage current is supplied by the 10 megohm load resistor on each column lead. Measured gate leakage current is approximately five nanoamps which means that the resulting voltage drop across the load resistor is about 50 millivolts. This voltage drop creates an offset voltage to the input of the preamplifier. To preclude amplifier saturation, the preamplifier is AC coupled to the column lead. AC coupling does not degrade low frequency response of the amplifier because the three dB rolloff point is 0.03 Hertz, which is below the desired signal bandwidth of 1 to 40 Hertz.

There were two conflicting design constraints for selecting the column lead's 10 megohm load resistor value. First, the load resistor must be much larger in value than the electrode source impedance to minimize bioelectric signal voltage loss. Second, it must be much smaller in value than the off-resistance of the JFET switch so that the bioelectric signal on-off voltage ratio is high (Fig 16). The calculated silver-silver chloride electrode impedance is 78 kilohms resistive (approximately 10^4 ohms), and the measured characteristics of the JFET switch indicate 10^4 ohms on-resistance and 10^9 ohms off-resistance. Since the preamplifier input impedance is 10^9 ohms, one can assume it is infinite because the load resistor value is several orders of magnitude smaller. The first design constraint was to require at least 99 percent of the bioelectric signal voltage to be developed across the load resistor. Using the voltage divider equation,

$$V_1/V_s = R_1/(R_e + R_1 + R_m) \quad (1)$$

where

V_1 = voltage across the load resistor
 V_s = bioelectric signal voltage
 R_1 = load resistor value
 R_e = electrode resistance
 R_m = JFET multiplexing switch on-resistance

The requirement for the V_1/V_s ratio to be greater than 0.99 results in a load resistance value which must be greater than 10.9 megohms. The second design constraint was to require that less than one percent of the bioelectric signal be developed across the load resistor when the JFET multiplexing switch was off. A similar calculation with the voltage divider equation indicated that the load resistor must be less than 10.1 megohms. Both constraints could not be simultaneously met, but 10 megohms

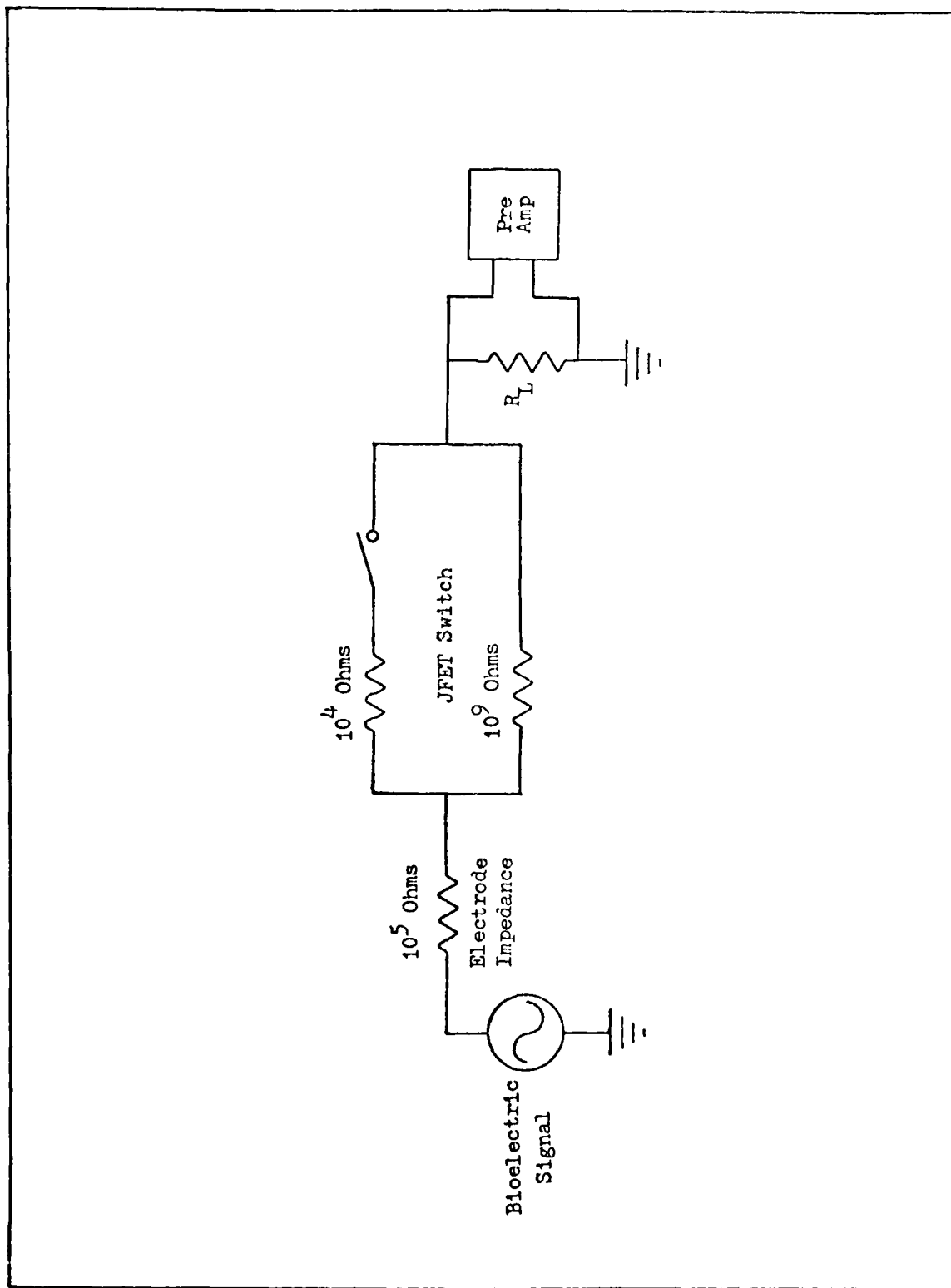


Fig. 16. JFET switch equivalent circuit.

is sufficiently close to allow successful operation of the multielectrode array. In fact, signal voltage on-off ratio resulting from the 10 megohm load resistor is about 40 dB.

The 4050 hex buffer provided drive current to the TTL hexadecimal indicator. This indicator showed the electrode that was being interrogated in the preset mode. Since the TTL display consumed considerably more current than the CMOS devices, a switch was added to turn off the display during clocked multiplexing operation.

V. In Vitro Multielectrode Array Evaluation

Introduction

A series of in vitro tests were conducted to determine how well the multielectrode array performed in obtaining and multiplexing pseudo-bioelectric data. The primary motivation for this evaluation was to identify any operational anomalies before a live animal was used for testing. An in vitro evaluation procedure was established that tested both the multielectrode array and the support electronics. This chapter contains an explanation of the evaluation procedures, success criteria, and the results of these tests.

For all in vitro tests except those conducted in a saline bath environment, the multielectrode array was placed on a vacuum chuck in a probe station of the type commonly found in the microelectronics industry. A microscope was used to observe needle probe placement on the electrodes. The multielectrode array on test had all wire leads attached and terminated to the support electronics or test equipment required for evaluation. The microscope light was turned off to minimize test artifacts due to photoelectric effects.

The first section describes the static FET pinch-off tests and compares the test results to previous curve tracer data. The second section describes the column lead crosstalk evaluation, defines the predetermined crosstalk limits, and reports the results of the crosstalk evaluation. The third section explains the ambient noise tests, and the results of lifetime tests are covered in the fourth section. Some interesting observations concerning multiplexing speed as a function of electrode

impedance are presented in section five. In addition, this section describes the effects of the pinch-off voltage on device lifetime in a saline bath environment. Section six covers frequency response tests with both gold and silver-silver chloride electrodes. This section also presents the rationale for silver plating the gold electrodes.

Static Pinch-off Tests

Test Set-up. In preparation for the static pinch-off tests, the electrode associated with the JFET on test was contacted with a needle probe. An audio oscillator was connected to the JFET drain lead through the needle probe. The audio oscillator signal ground was connected to the preamplifier signal ground and the JFET source lead was terminated across a 10 megohm load resistor to signal ground. The resulting voltages developed across the load resistor were input to a PAR 113 preamplifier. The preamplifier gain was set at 100 and the 3 dB rolloff points for the low pass and high pass filters were set at 0.03 and 3000 Hertz respectively. The preamplifier output was monitored with an oscilloscope. Signal source input impedance to the JFET switch was varied from 600 ohms to 1 megohm resistive, and data were also recorded with a 3300 picofarad capacitor coupling the signal generator to the drain lead. Pinch-off voltage was provided by a drive circuit (see Chapter 4 for details of the drive circuit).

Test Procedure. The test procedure consisted of injecting a 100 millivolt, peak-to-peak sinusoid, varying from 500 to 1 Hertz, into the electrode through a signal source resistor (or in one case, a 3300 picofarad capacitor). The output voltage was recorded with the JFET on (the gate lead grounded by the drive circuit) and with the JFET pinched off. The test

frequencies were 500, 200, 100, 50, 40, 30, 25, 20, 15, 10, 5, 2, and 1 Hertz. The test source resistances were 600 ohms, 10.6, 56.6, 100.6 kilohms, and 1 megohm. In addition, one test was conducted using a capacitively coupled input signal through a 3300 picofarad capacitor. A total of 63 tests at different combinations of signal input impedance and frequency were conducted on one JFET. The JFET output on-off voltage ratio and off-resistance were calculated.

Test Results. Initially, data for the pinched off test condition was obtained while applying the predetermined 1.2 volt value for V_p . Calculated channel resistance for the pinched off device varied between 718 megohms at 500 Hertz and 105 megohms at 5 Hertz, as compared to the design goal channel off-resistance of 10^9 ohms. There was no significant channel resistance change as a function of input impedance. These test results indicated that the off-resistance of the channel was unacceptably low. It was discovered, however, that the predetermined pinch-off voltage was not completely turning off the JFET. With approximately 1.5 volts applied to the JFET gate, channel off-resistance increased asymptotically to approximately 1290 megohms. The off-resistance did not vary as a function of frequency once complete pinch-off occurred.

Pinch-off voltage did vary, however, as a function of input impedance. As the input impedance increased, a larger pinch-off voltage was required. For the capacitively coupled case, the pinch-off voltage increased to 1.75 volts compared to 1.5 volts in the resistive input cases. It is believed that this phenomenon is associated with the resistance of the gate leakage current pathway. When relatively low input impedances exist, the

gate leakage current can travel from the drain lead through the audio amplifier to signal ground. Thus, the voltage drop associated with the leakage current is low and the JFET "sees" almost all of the gate pinch-off voltage. When the input is capacitively coupled, all gate leakage current must travel through the source lead and across the 10 megohm load resistor. As a result, some of the pinch-off voltage is dropped across the load resistor and the JFET requires a higher applied V_p for pinch-off to occur. The results of this test indicate that, to assure pinch-off when the 78 kilohm silver-silver chloride electrodes are used, the multielectrode array must be driven with a V_p set about 0.3 volts higher than the curve tracer indicated pinch-off voltage.

To determine on-off voltage output characteristics of the gold electrode and the silver-silver chloride electrode, static pinch-off tests were conducted with input impedances set to the values calculated for the two metals. Based on these tests, the on-off ratio for a gold electrode terminated with a 10 megohm load resistor is about 7 dB while the silver-silver chloride electrode yields about 60 dB. The design goal for the signal to noise and crosstalk ratio was 10 dB. The gold electrode does not meet this requirement. Thus, the silver-silver chloride electrode must be used to meet the design constraint.

Crosstalk Tests

Test Set-up. To determine the amount of crosstalk between column leads, the multielectrode array on test was placed on a vacuum chuck and connected to the drive circuitry. An audio oscillator was connected to column four and columns one through three were connected one at a time to

a preamplifier. The preamplifier gain was set at 100 and the 3 dB bandpass frequency rolloff values were set at 0.03 and 3000 Hertz. The preamplifier output was connected to an oscilloscope.

Test Procedure. A 100 millivolt sinusoid varying from 5000 to 5 Hertz was injected into column four of the multielectrode array on test. The crosstalk signals on column leads one through three were recorded at each of twelve frequencies. The tested multielectrode array was not driven with multiplexing signals. Thus, all JFET switches were on. Two different multielectrode arrays were tested.

Test Results. As expected, the column lead closest to the one receiving the signal had the largest amount of crosstalk. At 5000 Hertz, crosstalk was -42, -40, and -28 dB on columns one, two, and three respectively. Crosstalk decreased with frequency and was approximately -60 to -54 dB between 5 and 50 Hertz on column three. These results indicate that interlead coupling is primarily capacitive and the interlead capacitance is less than one picofarad. Thus, for the bioelectric signal bandwidth of 1 to 40 Hertz, the signal-to-crosstalk ratio is at least 33 dB, which exceeds the 10 dB design goal.

Ambient Noise Tests

Test Set-up. Ambient noise levels were evaluated in two different environments. The first environment was an isotonic sodium chloride solution and the second environment was in free air.

The test set-up for the saline bath test consisted of immersing a multielectrode array into a saline bath and connecting the leads to the drive circuitry. The column lead outputs were connected one at a time to a preamplifier. The preamplifier gain was set at 1000 and the bandwidth was set at 1 to 100 Hertz. The preamplifier output was connected

to an oscilloscope. For the free air test, the test set-up was identical to the saline bath evaluation except the preamplifier gain was reduced to 100 and the multielectrode array was attached to a vacuum chuck. The electrodes were not electrically terminated.

Test Procedure. Ambient noise levels on each column lead were recorded while the drive circuitry provided pinch-off voltages varying between zero and V_p plus 0.5 volts. For the saline bath evaluation, the coaxial leads between the multielectrode array and the drive circuitry were physically moved about until a minimum ambient noise level was obtained.

Test Results. The saline bath test resulted in minimum ambient noise levels of about 30 microvolts. When the multielectrode array row leads were strobed with a voltage level equivalent to the JFET's V_p , 4 millivolt spikes were observed at the multiplex switching times. When the array was scanned with V_p plus 0.5 volts, the spikes increased to 80 millivolts. These tests indicate that it is important to drive the multielectrode array with a pinch-off voltage no greater than V_p so that the switching spikes do not saturate the preamplifier. Fortunately, the spikes occur at the leading and trailing edge of the sample times. As a result, the bioelectric data is not vitiated since subsequent circuitry can be used to gate the true data in the interval between the spikes. This test demonstrates the importance of using data samples in the center 50 percent of sample time so that the switching transients do not color the bioelectric data.

Tests in free air resulted in approximately 100 millivolts peak-to-peak, 60 Hertz noise. Such noise levels will saturate the preamplifier.

The noise source was isolated to the multielectrode array. It is believed that when the electrodes experience a virtual open circuit, the omnipresent 60 Hertz electric field impresses a large voltage gradient across the 10 megohm load resistor. For the in vivo test, the electrodes must remain in electrical contact with the cerebral spinal fluid so that this problem does not occur. These test results suggest that saturating the multielectrode array with saline solution prior to implanting may be required.

Lifetime Tests

Test Set-up. The set-up for the lifetime tests required the use of the drive circuitry, preamplifier, oscilloscope, curve tracer, and probe station. The multielectrode array on test was attached to a microscope slide and held by the vacuum chuck in the probe station. For the JFET characteristics tests, a needle probe provided electrical contact between the drain lead and the curve tracer. For the crosstalk tests, the drive circuitry provided the load resistor termination and the connections to the preamplifier input. The oscilloscope was connected to the preamplifier output.

Test Procedure. The multielectrode array on test was first evaluated to determine its JFET characteristics and crosstalk values. After this initial evaluation, it was immersed in an isotonic saline solution. After immersion for a prescribed time, the device was washed in deionized water, and JFET operating characteristics and crosstalk levels were again tested. This procedure was repeated until the device on test failed to operate.

Crosstalk tests were conducted by injecting a 100 millivolt peak-to-peak sine wave into the column one lead while crosstalk on column two

was recorded. The input sinusoid test frequencies were 5000, 500, and 25 Hertz. JFET operating characteristics were evaluated with a curve tracer. In every test case, the following data were recorded or calculated: pinch-off voltage, channel on-current, channel breakdown voltage, gate pinch-off current, channel on-resistance, and channel off-resistance. This procedure was used to test a chemical vapor deposited (CVD) silicon dioxide passivated device and a plasma deposited silicon nitride passivated device.

Test Results. The multielectrode array insulated with CVD silicon dioxide showed serious degradation after only ten minutes immersion in the isotonic saline bath. The pinch-off voltage increased from 3 to 4 volts and pinch-off gate current increased from 25 nanoamps to 90 microamps. In addition, the JFETs in row two, three, or four could be pinched off with a voltage applied to row one. Channel on-resistance increased from 17 kilohms to 20 kilohms and channel on-current decreased from 70 to 55 microamps. Crosstalk noise increased and interlead leakage path characteristics became frequency independent (Fig 17). This change indicates that sodium ions permeating the passivation layer provided a current path between the column leads. The ions also provided a current path between the row leads. The results of these tests prove that CVD silicon dioxide is unfit for use as insulation on an implantable multielectrode array.

Tests with a plasma silicon nitride insulated multielectrode array were more promising. Crosstalk remained well within design limits after 28 hours of total saline bath immersion time. The JFETs on test survived 16 hours of total immersion time before failure occurred. The failure

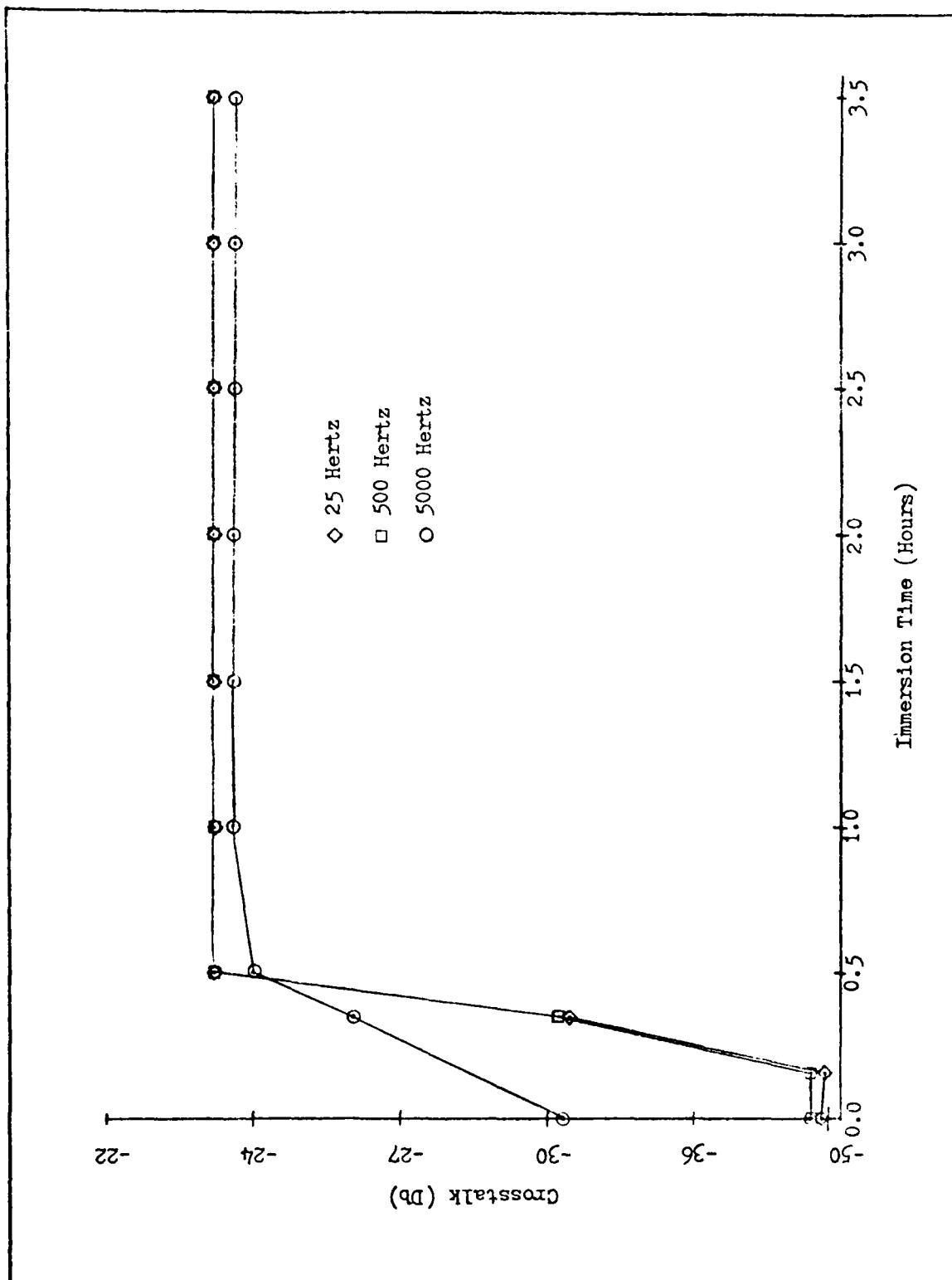


Fig. 17. Crosstalk in CVD passivated device.

mode was two-fold. First, the contacts to the JFET channel exhibited Schottky junction characteristics. Additional immersion time caused the JFET channel to become open. Even though 16 hours is sufficient time for acute implant testing, future research should include work to identify an insulating material that can survive several weeks or perhaps indefinitely in a saline bath environment.

The multiplexing tests identified a problem with the nitride passivation layer. The results of these tests are contained in the next section.

Multiplexing Tests

Test Set-up. As with the ambient noise evaluation, this test was conducted both in a saline bath and in free air. The set-up for the free air test will be discussed first.

The multielectrode array on test was attached to a microscope slide and placed on the vacuum chuck in the probe station. Needle probes contacted electrodes one and five in column one. An audio oscillator was attached to each needle probe so that signals could be injected into the drain lead of the JFETs to be tested. The drive circuitry provided pinch-off voltages to the row leads and terminated the column leads with ten megohm load resistors. Column lead one was attached to a preamplifier and the preamplifier output was monitored on an oscilloscope.

The saline bath multiplexing test set-up was identical to the free air test except the multielectrode array was immersed in isotonic saline and a signal generator used to create input sinusoids was terminated to a pair of wires immersed in the saline bath.

Test Procedure. For the free air test, the electrode was subjected to a 100 millivolt peak-to-peak input sinusoid while varying the input impedance and multiplexing frequency. The objective of this test procedure was to determine multiplexing frequency limits as a function of input impedance. The second free air multiplexing test consisted of impressing two different sinusoids on two electrodes in the same column. The column lead was monitored with an oscilloscope to determine how well the multi-electrode array could multiplex two different signals.

The saline bath test consisted of injecting a sinusoid into the saline bath while monitoring the column lead output. The objective of this test was to assure the multielectrode array could pinch-off the signals in the saline bath.

Test Results. The free air multiplexing tests show a direct correlation between the multiplexing frequency limit and electrode input impedance. The multiplexing frequency limit was defined as the frequency at which ten percent of the sample time was required for the JFET to switch. With a 600 ohm input impedance, the multiplexing frequency limit was about 20 kilohertz while an input impedance of 100 kilohms reduced the maximum multiplexing rate to about 1 kilohertz. A 3300 picofarad coupling capacitor further reduced the maximum multiplexing speed to 300 Hertz. It is for this reason that the gold electrodes were silver-silver chloride plated. By changing the equivalent 3300 picofarad capacitive signal coupling to a 78 kilohm resistive coupling, the multiplexing frequency limit was increased from 300 Hertz to more than one kilohertz. The one kilohertz multiplexing rate was the design goal.

Multiplexing two different signals onto one column lead proved possible. With a one kilohertz sampling rate and a 100 kilohm input impedance, two phase shifted 20 Hertz input signals were successfully time multiplexed. In actual operation, each column lead will carry four time multiplexed signals instead of two. The test with two time multiplexed signals, however, indicates that multiplexing four signals is feasible.

The results of the saline bath tests were inconclusive. Immediately after immersion in the isotonic saline solution, the test sinusoid was picked up by the electrodes and displayed on an oscilloscope. When the drive circuit output voltage was adjusted to the pinch-off value of the device on test, the amplitude of the sinusoid decreased significantly, indicating pinch-off was occurring. Unfortunately, precise measurements of the output signal at pinch-off could not be made because in less than 30 seconds, the sinusoid returned to the same amplitude that was observed before pinch-off. Careful electrical examination of the device on test revealed that a leakage path had developed between the row three lead and column leads one and four. A two hour immersion in isotonic saline solution caused the leakage path resistance value to decrease from approximately 5 megohms to less than 100 kilohms. Microscopic examination of the device showed several pinholes in the nitride coating over the gold leads. Subsequent evaluation of the nitride coating indicated a pinhole density exceeding 50 per square centimeter. It is believed that these pinholes allowed sodium ions to enter the silicon dioxide insulation layer. In addition, the device failure appears to be greatly accelerated when pinch-off voltages are applied during saline solution immersion. Where static lifetime was approximately 16 hours, active lifetime was less than 30 seconds. It

appears that pinch-off voltage application accelerates failure by greatly increasing the sodium ion absorption rate. This mechanism is not well understood, but the writer hypothesizes that the electric field developed by the pinch-off voltage attracts sodium ions through the pinholes over the gate leads. As a result, the silicon dioxide insulating layer beneath the metal is compromised and leakage paths occur between the metal leads. The following facts support this hypothesis. Calculations based on circuit geometry show that pinch-off voltages between one and two volts generate an electric field strength of 50,000 to 100,000 volts per centimeter across the silicon dioxide insulating layer at the row-gate lead crossunder resistor. Capacitor-voltage (C-V) bias-temperature stress measurements conducted during the fabrication process showed that a 100,000 volt per centimeter electric field easily transported sodium ions through the silicon dioxide passivation layer. The pinch-off voltage creates a positive to negative electric potential gradient between the silicon dioxide layer's outer surface and the silicon-silicon dioxide interface. Thus, sodium ions will be attracted through the silicon dioxide to the surface of the crossunder resistor.

The fact that pinch-off actually occurred, however, indicates that the fundamental circuit design is sound. With a high quality nitride coating, the device should function properly. Unfortunately, a high quality nitriding process was not available for additional testing during the immediate course of this investigation. If future lifetime tests with a low pinhole density nitride do not result in sufficient device lifetime, parylene may be used as an alternative passivation material (Ref 33:7).

AD-A100 763 AIR FORCE INST OF TECH WRIGHT-PATTERSON AFB OH SCHOO--ETC F/S 6/5
THE DEVELOPMENT OF A TWO-DIMENSIONAL MULTIELECTRODE ARRAY FOR V--ETC (1)
DEC 80 S H FITZGERALD
UNCLASSIFIED AFIT/GE/BE/80D-21

AIR FORCE INST OF TECH WRIGHT-PATTERSON AFB OH SCHOO--ETC F/S 6/5
THE DEVELOPMENT OF A TWO-DIMENSIONAL MULTIELECTRODE ARRAY FOR V--ETC(1)
DEC 80 6 M FITZGERALD
AFIT/EE/EE/80D-21

UNCLASSIFIED

ML

2 OF 2
AD
A/00763

END
DATE
FILMED
7-81
DTIC

Electrode Impedance Tests

Test Set-up. The electrode impedance tests required a multielectrode array, a signal generator, a preamplifier, and an oscilloscope. The multielectrode array on test was immersed in an isotonic sodium chloride solution. The signal generator output lead was connected to a two square centimeter silver-silver chloride electrode which was also immersed in the saline bath. Column one output lead of the multielectrode array on test was connected across a load resistor and the load resistor was connected across the input leads of the preamplifier. The signal generator ground lead was connected to the preamplifier ground. The oscilloscope vertical input was connected to the preamplifier output leads (Fig 18).

Test Procedure. A 100 millivolt peak-to-peak sine wave was injected into the saline solution through the large silver-silver chloride electrode. The resulting voltage across the load resistor was measured and the impedance of the four column one electrodes was calculated and recorded. It was assumed that the impedance of the large electrode was negligible when compared to the load resistor and the electrode impedance. This procedure was repeated at signal frequencies from 0.1 to 200,000 Hertz. The multielectrode array on test was evaluated before and after silver plating and silver chloride treatment.

Test Results. Figure 19 shows the measured impedance of a single gold, silver, and silver-silver chloride electrode. Silver electrode impedance is typically one-fourth the gold electrode impedance in the 1 to 40 Hertz bioelectric signal bandwidth. The silver-silver chloride impedance is about two orders of magnitude less than the gold electrode. The 20 to 80 kilohm impedance for the silver-silver chloride electrode fits well with

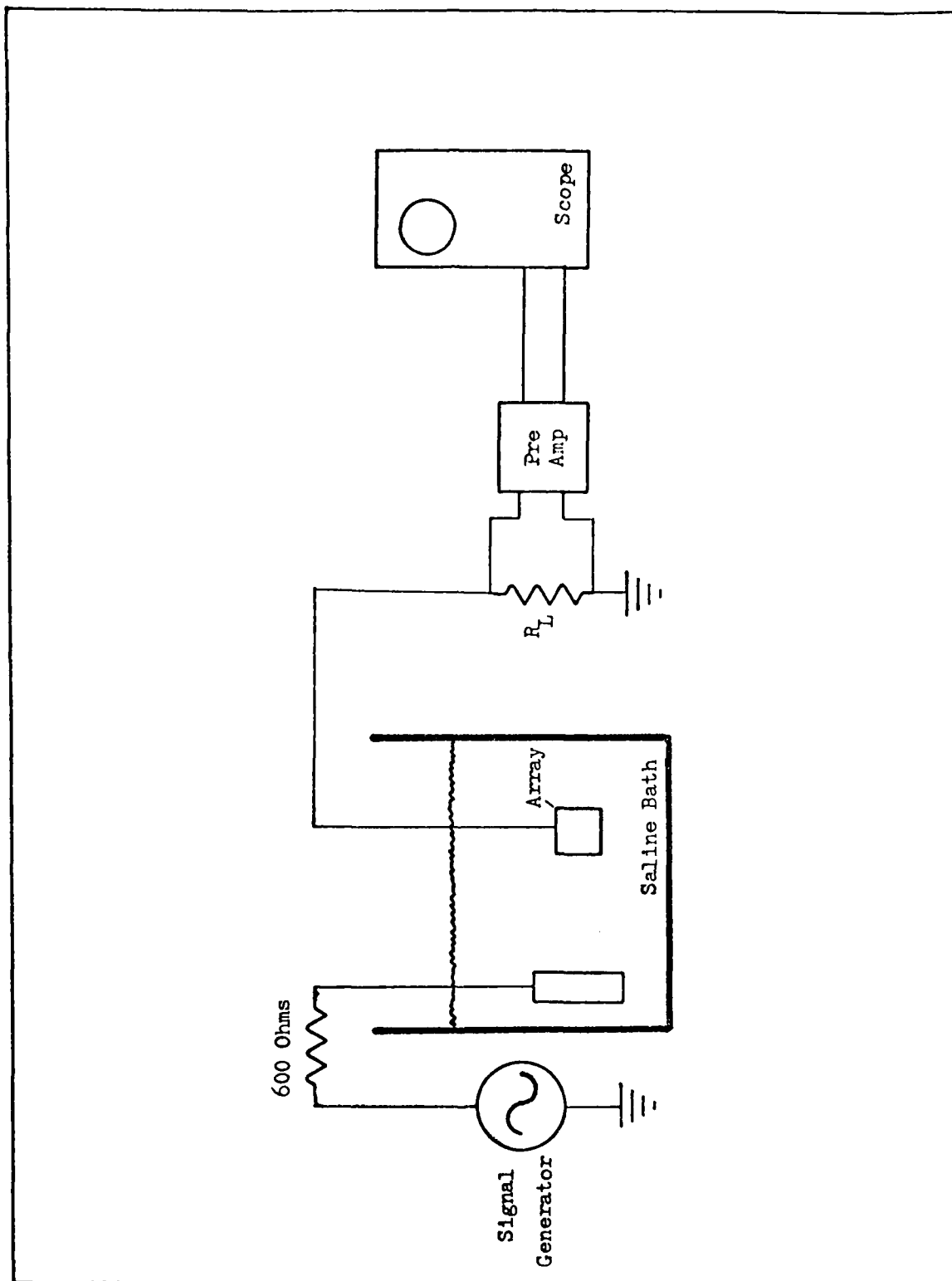


Fig. 18. Electrode impedance test set-up.

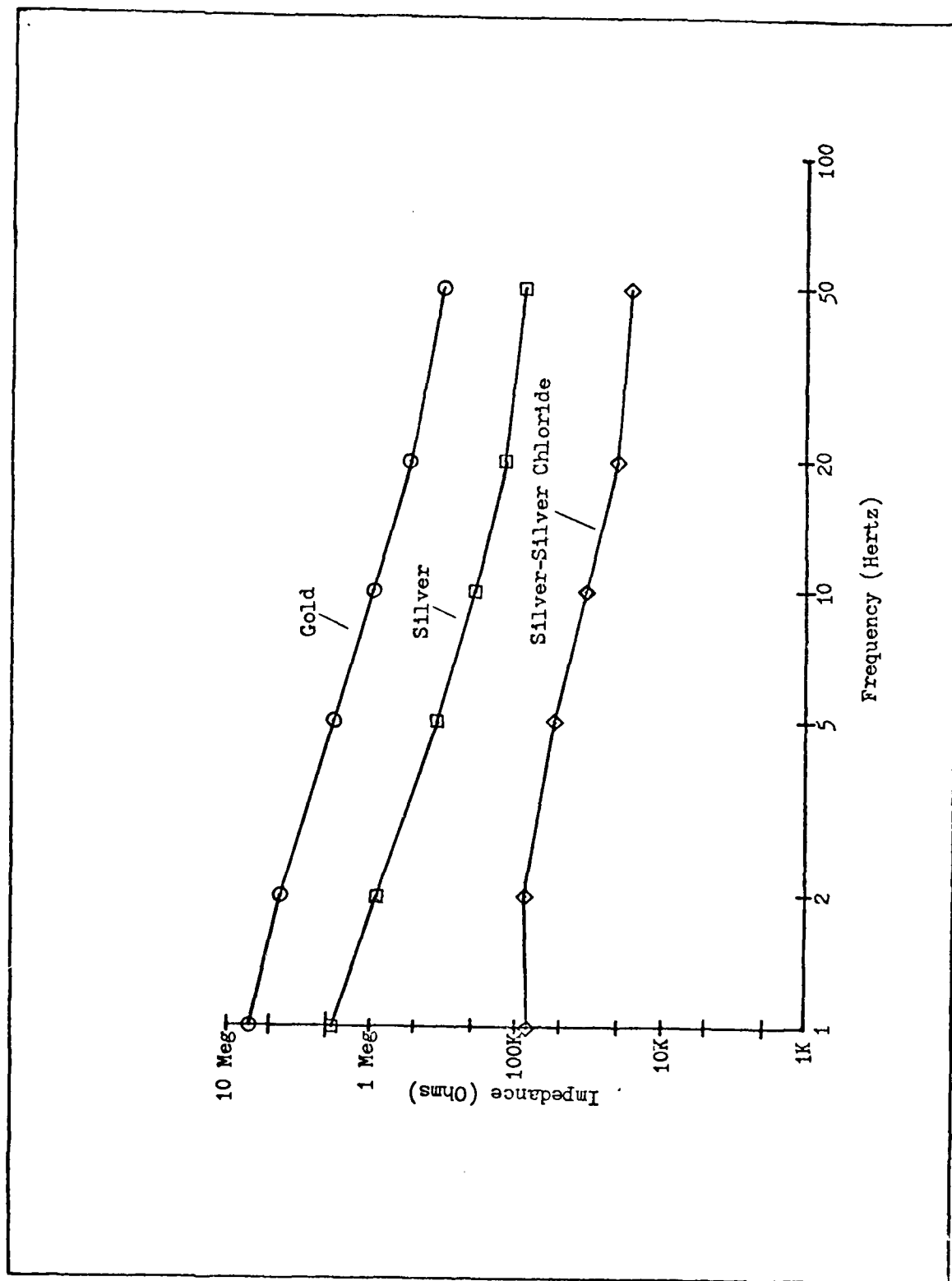


Fig. 19. Electrode impedance.

the predicted 78 kilohm value. A cursory examination of phase angle associated with the silver-silver chloride electrode indicates that it is essentially resistive. The reduction of electrode impedance by the silver-silver chloride plating reduces noise and increases multiplexing speed capability.

VI. In Vivo Multielectrode Array Evaluation

Introduction

Problems associated with the nitride passivation layer (see Chapter 5) precluded conducting the in vivo test. To provide assistance to future researchers, this chapter describes the suggested procedure for this important test.

The objective of the in vivo evaluation is three-fold. First the implant procedures must be evaluated to determine their feasibility and to identify any problem areas that require additional research. Second, the multielectrode array and all support electronics must be evaluated to determine if they can receive and multiplex electroencephalic signals from the visual cortex. Third, the bioelectric data must be examined to determine some operating characteristics of the visual system.

The first section of this chapter contains the details of the support equipment set-up. It should be noted that only one multielectrode array is proposed for this test. Other experiments that will obtain data for more detailed evaluation of the visual processing mechanism will require two multielectrode arrays. One array must be implanted on the surface of area 17 and the other on area 18 of the visual cortex. The use of two arrays will enable the simultaneous collection of data from both the input visual cortex (area 17: presumably a homeomorphic mapping of the retinal pattern) and the secondary visual cortex (area 18: by which time some analysis and evaluation of the visual data have occurred). The second section of this chapter describes the proposed implant protocol which includes subject preparation and surgical implant procedures. The third

section summarizes the baseline tests, the fourth section describes the data acquisition procedures, and the final section outlines the suggested data processing and analysis methods.

Test Equipment Set-up (Fig 20)

The equipment for the in vivo test should consist of the multielectrode array, four PAR 113 preamplifiers, an Ampex 1300 FM tape recorder, an oscilloscope, the drive circuitry, a square wave generator, an electronic shutter, a slide projector with the appropriate visual stimulus slides, and a projection screen.

Before the surgical implant procedure, the proposed setting of the PAR 113 preamplifiers includes a gain of 2000 and a bandwidth of 0.03 to 3000 Hertz. The gain of 2000 provides a 200 to 1000 millivolt output level when the anticipated 200 to 500 microvolt electroencephalic signals are received (Ref 8). This output level is compatible with the FM recorder input level requirements. The 3000 Hertz bandwidth ensures that the multiplexed bioelectric data can be recorded. After the preamplifiers are adjusted as above, the inputs to each must be connected to the four column lead outputs of the drive circuitry. The preamplifier output leads will be connected to channels five through eight of the FM tape recorder.

The recorder input modules for channels five through eight will be adjusted so that a 100 millivolt input sinusoid develops a 100 millivolt output signal at the reproduce module. This one-to-one correspondence between recorder input and output amplitude simplifies the process of maintaining faithful reproductions of the electroencephalic data. The recorder input

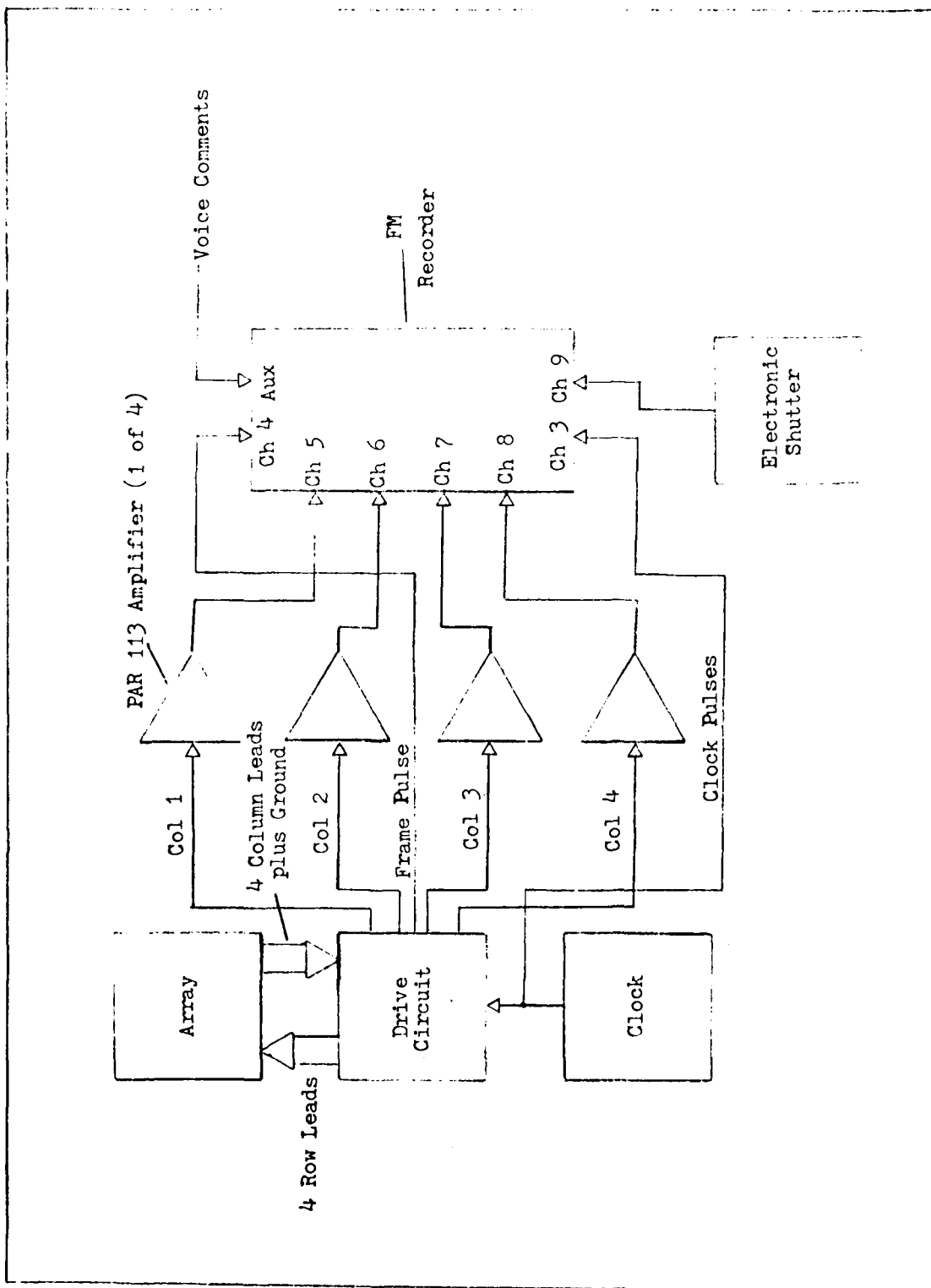


Fig. 20. In Vivo Test Set-up.

modules for tracks three and four will be adjusted so that the twelve volt peak-to-peak clock and frame signals generate a two volt peak-to-peak reproduce module output signal. This attenuation adjustment will prevent saturation of the input and output modules of the FM tape recorder.

The four row lead multiplexing lines, the four column input leads, and the ground for the drive circuit will be connected to a 14 pin dual inline package (DIP) socket which interfaces with the 14 pin DIP connector attached to the multielectrode array wires. The square wave generator output will be adjusted to 12 volts peak-to-peak, and connected to the drive circuit clock input and channel three of the FM tape recorder. The frame output from the drive circuit will be connected to channel four of the FM tape recorder.

The electronic shutter drive signal output will be connected to channel nine of the FM tape recorder, and the input module will be adjusted to prevent saturation. The slide projector and screen must be arranged so that a large portion of the test animal's visual area will be stimulated by the projected image. To maximize the probability that the projected image stimulates a portion of the visual cortex that the multielectrode array is monitoring, the projected image should cover at least ten degrees of the central visual area of the test animal. To ensure that the visual cortex is receiving fine grained images (high spatial frequency data), the projected slides should consist of sine wave gratings with a frequency range of 5 to 15 cycles per degree. In addition, preliminary analysis should include a slide which depicts a two-dimensional square wave grating (checkerboard) with the fundamental frequency at about five cycles per degree.

This pattern is selected because the spatial step functions generated by the square wave grating should be highly observable in the electro-encephalic data recorded from area 17 of the visual cortex.

Once the slide projector and screen are arranged, the projected image brightness must be measured with a photometer so that the level of visual stimulus intensity is known.

Implant Protocol

Since the visual cortex of mammals with good visual acuity possess characteristics similar to those of the human visual cortex, many species of test animals are potential test subjects. The primates, cats, or dogs are all possible choices. The primate, of course, is preferable, if available, because of the great similarity of its visual system with that of man. Once an animal is selected, the following implant procedure is advised.

Under a general anesthetic such as halothane, the skin and muscle tissue over the posterior portion of the cranium, just left of the lateral midline, must be incised and retracted. Once an area approximately three centimeters by three centimeters of the posterior skull is exposed, a two centimeter diameter craniostomy must be performed. In many animals, such as the baboon, there exists a cranial crest directly over the occipital lobe of the cerebrum. In this case, the craniostomy can be performed just superior to this crest to reduce the difficulty of the surgery and the trauma to the test animal.

Once the cranium is open, the dura must be incised and retracted. If the cranial opening is above the occipital pole, the brain must be

depressed away from the cranium so the multielectrode array can be slipped downward between the cortex and the dura until it rests on the surface of the pole of the left occipital lobe. The brain can then be released and the pressure exerted by the brain on the multielectrode array should hold it in place as long as the animal remains sessile. If the cranial opening can be made over the occipital pole, the multielectrode array can be placed directly on the cortex. The second procedure is preferable to the first because the array can be more easily moved about on the cortex until satisfactory electroencephalic signals are obtained. In both cases, the multielectrode array must be perfused with isotonic saline solution before implanting so that good electrical contact is made with the surface of the cortex.

Once the multielectrode array is in place, the animal must be physically situated so that the projection screen is located slightly to the right of the center of its visual field. The array leads are then to be connected to the drive circuitry. At this point, the incisions must be locally anesthetized and the animal allowed to completely recover from the general anesthetic. To maintain sessility, the test animal should be either firmly restrained, or treated with a drug that creates muscular relaxation. Curare, or curarine type alkaloids can be used as long as vital functions are mechanically maintained. The drug used must not depress the central nervous system.

Baseline Test Procedures

Data acquisition should begin with a series of baseline tests that will ensure integrity of the multielectrode array and the support

equipment. These tests will consist of two parts: non-multiplexed electrode evaluation, and multiplexed system evaluation. The following paragraphs describe these procedures.

For the non-multiplexed baseline tests, the drive circuit shall be set in the preset mode, and the preset switches set to select electrodes 1, 5, 9, and 13. The oscilloscope will be attached to the reproduce modules for the FM tape recorder channels five through eight, one at a time. With the oscilloscope first attached to channel five, the FM recorder will be set to record and the oscilloscope trace will be monitored for cortical electrical activity. This same test will be accomplished with recorder channels six, seven, and eight. This test will ensure that the electrodes on the multielectrode array are being stimulated by electrical cortical signals. In addition, the test will verify that the bioelectric data are passing through the drive circuitry and being recorded.

The next baseline test will check for proper operation of the multiplexing drive circuitry and clock. This test will begin by setting the drive circuit to run, and adjusting the clock frequency to one kilohertz. The oscilloscope should be triggered with the frame pulse, and channel two of the oscilloscope should be adjusted to display sixteen clock pulses. Channel one of the oscilloscope will be connected to the FM recorder reproduce modules for channels five through eight, one at a time. The oscilloscope trace should depict the four multiplexed signals from each of the four electrodes of the column being monitored. Pinch-off voltage to the multielectrode array must be adjusted to minimize spikes at the leading and trailing edge of each electrode interrogation time, while still ensuring that the electrode JFETs are being completely

pinched off. Once these adjustments are made, the experimental system can be considered ready for data acquisition.

Data Acquisition Procedures

The data acquisition procedures will consist of stimulating the animal with five different projected images while recording at three different multiplexing frequencies. The three frequencies are 240 Hertz, 320 Hertz, and 1000 Hertz. Two reasons suggest the need for using these three frequencies. First, the exact maximum frequency of the electroencephalic data is not known. It is thought to be about 30 to 40 Hertz. By multiplexing at Nyquist rates for 30, 40, and 125 Hertz, any aliasing or distortion that might occur should be evident. Thus, an approximate maximum frequency of the electroencephalic data should be observed. The second reason for the various multiplexing speeds is to establish the multiplexing rate limit for the array. If the array cannot multiplex at the 1000 Hertz rate, the recorded data should show improper pinch-off of the multiplexing JFETs. If the array successfully multiplexes at the 1000 Hertz rate, future tests should increase the multiplexing speed until the maximum limit is established. The maximum multiplexing speed is important for future work because larger arrays will require faster multiplexing speeds.

The first data acquisition test will consist of visual stimulation by a light flash of 25 milliseconds duration. This test will be repeated 30 times at each multiplexing frequency. By accomplishing the test 30 times, visual evoked response signal averaging can later be accomplished (if necessary) to increase signal to noise ratio.

The next four tests involve stimulation with projected images. Each image will be projected for 25 milliseconds and the test will be repeated 30 times at each multiplexing speed. The four images are: a two-dimensional square wave grating with a fundamental spatial frequency of approximately five cycles per degree, and three sine wave gratings with spatial frequencies of approximately 5, 10, and 15 cycles per degree. The sine wave gratings should be projected both in the horizontal and the vertical direction.

It would be useful to improve the system so that in the future, the various test conditions could be established by digitally controlling and generating the visual stimuli on a television or oscilloscope screen. Such a stimulus generator could be used to spatially move the gratings while electroencephalic data are recorded. By comparing the location of the grating pattern with the bioelectric data, information concerning the spatial resolution of the primary visual cortex could be determined. In other words, as a single cycle of the sine wave grating passes across the visual field associated with the visual cortical area being monitored, one would expect to see variations in the electroencephalic data. Correlation of these data variations with the movement rate of the stimulus would determine the number of degrees of visual area serviced by the visual cortical area being monitored.

Another method to improve the data quality of future tests would be to impress an electrical stimulus directly onto the primary visual cortex. The multielectrode array developed by this thesis is capable of transmitting as well as receiving electrical signals. If the researcher desires better control over visual stimulus, he can deliver an electrical signal to the

primary visual cortex with the multielectrode array. The effects of this stimulus can then be monitored in area 18 with a recording multielectrode array. Thus, the ambiguity associated with assumptions concerning the precise location of visual stimulation of the retina are eliminated. Once the support electronics for this test are developed, the data acquisition process would be greatly simplified because the experimenter no longer needs to arrange the test animal so that the visual stimulus can excite the retina. This procedure should prove to be a very powerful research tool, but it should be conducted only after the previous experimental techniques have well described the typical signals found on the primary visual cortex. In fact, previously recorded signals from the primary visual cortex should be used as the model for electrical stimulus. This procedure raises the question as to whether a signal recorded from the primary visual cortex during the time that the test animal is observing, say, a checkerboard, can elicit the image of that same checkerboard when used as a stimulus to the primary visual cortex. The same question may be asked about signals from the secondary visual cortex. Future tests with animals trained to respond to particular visual stimuli might answer these questions.

Data Processing and Analysis

After the time multiplexed electroencephalic information and its associated timing signals are recorded in an analog format on the FM tape recorder, data processing and analysis must be accomplished. The analysis must concern both test equipment operation and function of the visual system. To accomplish this goal, data processing must consist

of analog to digital (A/D) conversion, demultiplexing, filtering, and presentation of the data in a form amenable to careful scrutiny by the researcher. Data analysis will then consist of determining signal to noise ratios, effects of multiplexing on data quality, bandwidth of the bioelectric signals, time delays between the retina and primary visual cortex and between the primary and secondary visual cortex, and ultimately, the transfer function(s) between the primary and secondary visual cortex. The following paragraphs describe the various steps in the data processing and analysis phases.

As previously mentioned, the first step in data processing is A/D conversion. The conversion process can be accomplished on each FM recorder channel containing electroencephalic data, one at a time. To ensure timing integrity between channels of the FM recorder, care must be taken to maintain a constant tape speed for all passes through the tape. This can be accomplished by observing the FM recorder phase indicator. For each pass, the phase indicator should be centered. This guarantees that the capstan drive motor speed is synchronized to the 60 Hertz line frequency. Fortunately, data framing periods are relatively short (16 clock pulses) so that for small variations in tape speed, the accumulated amount of timing error between frame pulses should be small. If one desires to maintain the total error less than fifteen percent of a multiplexing sample period, some straightforward calculations show that the total timing error must not exceed 0.93 percent of a 16 bit frame period. The FM recorder specification states that short term tape speed drift (low frequency flutter) does not exceed 0.6 percent and long term tape speed variations are less than 0.25 percent.

Thus, worst case timing errors (a combination of flutter and long term variations) are 0.85 percent of a sample period which is adequate for the present research. Future tests may require much smaller tolerances in timing errors because larger multiplexing arrays will have relatively longer frame periods. To preclude significant timing errors in these tests may require parallel digitizing of the electroencephalic signal and the clock pulses so that data synchrony can be maintained.

To guarantee start-time integrity between A/D conversion passes, the conversion process can be initiated with the stimulus onset pulse (channel nine of the FM tape recorder). Thus, each of the four A/D conversion passes for one experiment will start at the same time.

Once all electroencephalic, frame pulse, and clock pulse records are digitized, demultiplexing must be accomplished. The demultiplexing operation will be primarily a synchronous sampling and prefiltering task. sampling will be accomplished by first determining the number of A/D samples per clock period and identifying the total number of samples in each frame. This can be easily accomplished with a software routine that counts the number of data points that exist in each clock period. The clock period start-stop times can be identified by observing the low to high voltage transition. Once a record of A/D samples per clock period are identified, the same procedure can be used to identify the number of samples in each frame period. With these two pieces of information, the sample periods for each electrode in the multielectrode array can be identified. For example, assume that the A/D converter sampled each clock period 10 times and the associated frame period had 160 samples.

By reviewing the samples of bioelectric data from the FM recorder track five, the experimenter would know that the first ten samples occurred during the on-time for the JFET associated with electrode one. The second ten samples were from electrode five, the third ten samples from electrode nine, and the fourth ten samples from electrode thirteen. This sequence would repeat three more times until a new frame began. It is important to restart the A/D sample counting process at each new frame pulse so that long term tape speed errors do not cause asynchronous demultiplexing.

Once A/D samples are identified with a particular electrode, these samples along with timing information would be placed in a separate file. This process must be repeated for each channel of bioelectric data. Channel six is associated with electrodes two, six, ten, and fourteen. Channel seven and eight contain data for electrodes three, seven, eleven and fifteen, and four, eight, twelve, and sixteen respectively.

After sampling is complete and each electrode's data are stored in a separate file, prefiltering should be accomplished. Prefiltering will consist of ignoring the A/D samples from the leading and trailing 25 percent of each sample period. This process should reduce the effects of the multiplexing spikes and ensures that tape speed errors do not cause erroneous sampling. Next, the center 50 percent of the samples will be averaged to eliminate the high frequency noise components. This prefiltering process will yield one averaged sample for each electrode sample period. It is believed that a multiplexing rate of one kilohertz coupled with these prefiltering techniques will provide an accurate

representation of the electroencephalic data. This belief is based on the assumption that the data bandwidth does not exceed forty Hertz. Should future evaluations show that wave front propagation or data bandwidth exceeds the limits of the nominal one kilohertz multiplexing speed, the sampling and prefiltering techniques remain valid, but multiplexing and A/D conversion rates must be increased.

One copy of the demultiplexed data generated by the process previously described must be retained in its original form so that future data analysis can be conducted to determine the effects of multiplexing (if any) and the bandwidth of the electroencephalic data. A second copy of these data can be processed with the filtering algorithm described below so that the low frequency bioelectric signal to noise ratio will be increased.

The filtering operation to increase the signal to noise ratio may not be required. If, however, the bioelectric data are vitiated, the Wiener filtering technique solved by the Bode-Shannon method should improve signal to noise ratio (Ref 34:267). The assumptions required for this filtering method are: stationary signal and noise, and knowledge of the power spectral densities for the signal and noise input. The Wiener filter's disadvantage is that it must be discretized before use in a digital machine. A discrete time Kalman filter can also be used to enhance signal quality by assuming the wanted signal is the output of a linear system driven by white Gaussian noise and the corruptive noise is the sum of time correlated and white noises (Ref 34:275). By varying the noise and signal parameters, one could observe the condition at which electroencephalic data quality is maximized. At this time, the parameters

in the Kalman filter would also convey information about the noise and signal statistics.

To prepare for the analysis procedures, the demultiplexed and filtered data must be displayed in a spatially correct form. It is recommended that the data from each electrode be printed so that the first row of values represent electrode numbers one through four and the subsequent three rows of values represent the next three sets of four electrodes. In this manner, the experimenter can glance over this matrix of numbers and identify the spatial characteristics of the electroencephalic signals. To simplify analysis, contour line mappings or three-dimensional plots may be used. Initially, the data should be printed out every four clock periods so that the maximum sample rate for each multiplexing frequency will be maintained.

Now that the data are in a form that can be easily scrutinized, data analysis must begin. The two objectives of the analysis procedures are: to evaluate the ability of the multielectrode array and support electronics to obtain electroencephalic data, and to determine some operating characteristics of the visual processing system. The following paragraphs suggest some methods to accomplish these tasks.

To determine if the multielectrode array and its support equipment operates properly, the data must be reviewed for multiplexing effects, bandwidth, and reproducibility. To reduce artifacts introduced by the filtering operation, the following analysis procedure must be accomplished with the unfiltered data.

To determine multiplexing effects, the researcher should observe the data for spikes and step changes during the "no visual stimulus" acquisition periods. If spikes are present, they are likely caused by

JFET on-off transitions. Step changes in the data may be caused by asynchronous demultiplexing. After multiplexing effects are determined, the data bandwidth should be evaluated.

The bandwidth tests should also be accomplished with unfiltered data. These tests should consist of first comparing the 30 data segments recorded during identical multiplexing frequency and stimulus periods. If these data appear reproducible, then electroencephalic bandwidth can be evaluated by observing signals recorded at different multiplexing frequencies. If any of the multiplexing frequencies are below the Nyquist sampling rate, the data at the slower multiplexing frequency will differ from data recorded at a higher multiplexing frequency. If data at all multiplexing frequencies are comparable, then the original hypothesis that the electroencephalic data bandwidth is less than 30 Hertz will be supported.

The next data analysis procedure will involve identifying some characteristics of the visual system. The first characteristic to be analyzed is the data transfer time from the retina to the primary visual cortex. This information can be obtained by measuring the time delay between stimulus onset and the visual cortical response. The second characteristic to be analyzed is the approximate size of the basic computing elements (BCEs) in the cortex. Highly time correlated data from adjacent electrodes might suggest that the electrodes are recording data from the same BCE. Uncorrelated data suggest the opposite. Additional characteristics such as wave front propagation (if any) may also be investigated.

The data analysis procedures previously described are not inclusive, but should provide a strong basis for additional research. The initial procedures described maintain conformity with past research by initially duplicating their results. The writer feels that a primary consideration is that future research should build on past analysis so that this continuity is maintained.

VII. Conclusions and Recommendations

Introduction

An investigation of past research and theories of the function of the mammalian visual perception system was conducted. This investigation suggests that fine grained electroencephalic data recorded from the surface of the visual cortex will enhance understanding of the visual perception process. To obtain these data, a multiplexing multielectrode array was developed and tested. This chapter contains the conclusions and recommendations resulting from the investigation of past research, and the development and test of the multielectrode array.

Conclusions

The mammalian primary visual cortex contains a homeomorphic mapping of the visual image. Due to the lack of lateral data transfer in this area, the visual field interaction necessary for spatial pattern analysis cannot occur in the primary visual cortex. Thus, visual perception occurs elsewhere. Each point on the primary visual cortex connects to many points on the secondary visual cortex. These complex connections allow, for the first time in the processing of visual information, interaction between elements in the two-dimensional visual field. It is likely that the perception process begins here. Thus, knowledge of the nature of the connections between the primary and secondary visual cortex should enhance the knowledge of the visual perception process.

The complexity and number of cortico-cortical interconnects between the primary and secondary visual areas preclude a detailed anatomical

mapping. An alternate research method is to map the data flow instead of the anatomical structure. This mapping could be accomplished by simultaneously recording electrical signals from large areas of the primary and secondary visual cortex so that a transfer function could be determined.

The primary and secondary visual cortex regions appear to consist of blocks of neural tissue, called basic computing elements, that accomplish similar tasks. Their size is estimated to be between 0.05 and 0.5 millimeters in diameter. Simultaneously recording electroencephalic data from many of these small blocks might yield sufficiently fine grained data to determine the transfer function between the primary and secondary visual cortex.

The multielectrode array developed by this research project can record these data. In vitro tests of the multielectrode array reveal that gold electrodes plated with silver-silver chloride provide a 60 dB on-off ratio during multiplexing operations. Worst case column lead crosstalk is -54 dB between adjacent leads. Thus, for the electroencephalic signal bandwidth of 1 to 40 Hertz, the signal to crosstalk ratio exceeds 33 dB. The design goal was 10 dB. Ambient noise levels are approximately 30 microvolts which allow at least a 16.5 dB signal to noise ratio with the anticipated 200 to 500 microvolt electroencephalic signals. Lifetime tests indicate that a silicon nitride passivation layer can protect the device for approximately 16 hours in an isotonic saline environment. High pinhole density nitrides, however, caused failure of the device in less than 30 seconds when pinch-off voltages were applied. It is believed that the electric field developed by the pinch-off voltage attracts

sodium ions through the pinholes over the gate leads. As a result, the silicon dioxide insulating layer beneath the metal is compromised and leakage paths occur between metal leads. A high quality nitriding process was not available, but low pinhole density silicon nitride should solve this problem. Tests indicate that the multielectrode can successfully time multiplex electroencephalic signals. The maximum multiplexing rate for this device appears to be about one kilohertz, which is sufficient for the four by four array. This multiplexing rate is about four times the Nyquist sampling rate for thirty Hertz bandwidth electroencephalic signals.

Recommendations

Future researchers must obtain and evaluate a high quality silicon nitride passivation layer to ensure that device lifetime is sufficient for in vivo tests (about two hours should be sufficient). If the silicon nitride coating is inadequate, an organic polymer such as parylene may be used. Tantalum as a metalization may also improve lifetime characteristics because of its ability to develop an organic oxide that has excellent insulative properties. Device lifetime research should continue until a chronic implant is feasible. Such an implant would reduce in vivo test complexity and allow acquisition of electroencephalic data while the test animal functions in its natural environment.

After solving the passivation problem, numerous in vivo tests must be conducted to evaluate the multielectrode array and its support electronics. In addition, the electroencephalic data must be reviewed to obtain information about the visual system's operating characteristics.

The multielectrode array developed by this thesis is inherently expandable to a larger array. The device should be expanded to a 50 by 50 or larger array so that the activity of several thousand basic computing elements can be simultaneously recorded. If multiplexing speeds limit the size of the array, several arrays simultaneously implanted could serve the same purpose.

The requirement to use silver-silver chloride electrodes highlights the need for a buffer amplifier dedicated to each electrode. This buffer amplifier might be a JFET which could be fabricated directly on the silicon substrate along with the JFET multiplexing switches. The JFET amplifiers could have input impedances greater than 100 megohms and output impedances less than 500 ohms, virtually eliminating crosstalk, stray noise pickup, and multiplexing speed problems.

A hybrid circuit that contains the multielectrode array(s) buffer amplifiers, multiplexers, multiplexing drive circuitry and RF data link should be developed. With such a hybrid circuit, a researcher is no longer tied to a surgical operating room for the data acquisition process, and the visual perception mechanism can be analyzed in its natural environment.

Bibliography

1. Kabrisky, M. A Proposed Model for Visual Processing in the Human Brain. Urbana: University of Illinois Press, 1966.
2. Brindley, G. S. and W. S. Lewin. "The Sensations Produced by Electrical Stimulation of the Visual Cortex," Journal of Physiology, 196: 479-493 (1968).
3. Donaldson, P. E. K. "Experimental Visual Prosthesis," IEE Proceedings of Control and Science, 120 (2): 125-132 (February 1973).
4. Dobelle, W. H., et al. "Artificial Vision for the Blind: Electrical Stimulation of Visual Cortex Offers Hope for a Functional Prosthesis," Science, 183 (4123): 440-444 (February 1974).
5. Hubel, D. H. and T. N. Wiesel. "Brain Mechanisms of Vision," Scientific American, 241 (3): 150-162 (September 1979).
6. -----"Receptive Fields, Binocular Interaction and Functional Architecture in the Cat's Visual Cortex," Journal of Physiology, 160: 106-154 (1962).
7. Jeffreys, D. A. and J. G. Axford. "Source Locations of Pattern-Specific Components of Human Visual Evoked Potentials," Experimental Brain Research, 16: 1-21 (1972).
8. DeMott, D. W. "Cortical Microtopscopy," Medical Research Engineering, 4: 23-29 (1966).
9. Mercer, H. D. and R. L. White. "Photolithographic Fabrication and Physiological Performance of Microelectrode Arrays for Neural Stimulation," IEEE Transactions on Biomedical Engineering, BME-25 (6): 494-500 (November 1978).
10. Wise, K. D., et al. "An Integrated Circuit Approach to Extracellular Microelectrodes," IEEE Transactions on Biomedical Engineering, BME-17 (4): 238-247 (July 1970).
11. Tatman, J. A. A Two-Dimensional Multielectrode Microprobe for the Visual Cortex. MS Thesis. Wright Patterson AFB Ohio: School of Engineering, Air Force Institute of Technology, December 1979. (AD A080378).
12. Animals and DoD Research and Training. Air Force Regulation, AFR 169-2. 12 August 1977.
13. Guyton, A. C. Textbook of Medical Physiology. Philadelphia: W. B. Saunders Company, 1976.

14. Iverson, L. L. "The Chemistry of the Brain," Scientific American, 241 (3): 134-149 (September 1979).
15. Geschwind, N. "Specializations of the Human Brain," Scientific American, 241 (3): 180-199 (September 1979).
16. Penfield, W. The Excitable Cortex in Conscious Man. Springfield: Charles C. Thomas, 1958.
17. Netter, F. H. The Nervous System. New York: Ciba, 1958.
18. Mountcastle, V. B. "Modality and Topographic Properties of Single Neurons of Cat's Somatic Sensory Cortex," Journal of Neurophysiology, 20: 408-434 (1957).
19. Robinson, J. O. The Psychology of Visual Illusion. London: Hutchinson, 1972.
20. Ginsburg, A. P. "Is the Illusory Triangle Physical or Imaginary?" Nature, 257: 219-220 (September 1975).
21. Kabrisky, M., et al. "A Theory of Pattern Perception Based on Human Physiology," Contemporary Problems in Perception, A. T. Welford, Editor (129-147). London: Taylor and Francis Ltd., 1970.
22. Ozawa, K. "Simulation of the Optical Illusions Using a Spatial Filter," Pattern Recognition, 10: 237-242 (1978).
23. Koehler, W. Dynamics in Psychology, Liveright Publishing Co., 1939.
24. Maffei, L., et al. "A Perceptual Phenomenon and its Neuro-physiological Correlate," Perception, 5: 43-46 (1979).
25. Campbell, F. W., et al. "A Comparison of Threshold and Supra-threshold Appearance of Gratings with Components in the Low and High Spatial Frequency Range," Journal of Physiology, 284: 193-201 (1978).
26. Robinson, D. A. "The Electrical Properties of Metal Microelectrodes," Proceedings of the IEEE, 56 (6): 1065-1071 (June 1968).
27. Wise, K. D. and J. B. Angell. "A Low Capacitance Multielectrode Probe for use in Extracellular Neurophysiology," IEEE Transactions on Biomedical Engineering, BME-22 (3): 212-219 (May 1975).
28. Prohaska, F., et al. "A Multielectrode for Intracortical Recordings Produced by Thin-Film Technology," Electroencephalography and Clinical Neurology, 42: 421-422 (1977).

29. Ary, J. P., et al. "A Multiplexing System for Multichannel Signal Averaging of the Visual Evoked Response," IEEE Transactions on Biomedical Engineering, BME-26 (6): 696-699 (December 1979).
30. Sze, S. M. Physics of Semiconductor Devices. New York: John Wiley and Sons, 1969.
31. Zaininger, K. H. and F. P. Heiman. "The C-V Techniques as an Analytical Tool," Solid State Technology, 13: 5-6 (May-June 1970).
32. Donaldson, P. E. K. "The Encapsulation of Microelectronic Devices for Long-Term Implantation," IEEE Transactions on Biomedical Engineering, BME-23 (4): 281-285 (July 1976).
33. White, R. L. "The Stanford Artificial Ear Project," The Stanford Engineer, 3 (1): 3-10 (Spring/Summer 1980).
34. Maybeck, P. S. Stochastic Models, Estimation, and Control Volume 1. New York: Academic Press, 1979.

A. Initial Fabrication Procedure

This appendix contains the initial fabrication process schedule which was derived from research by Tatman (Ref 11). The research of this thesis revised the process schedule. The revised process schedule is contained in appendix B of this thesis.

Initial Process Schedule

1. Starting material: substrate: p-type (100), 20-60 ohm-cm.
Epitaxial layer: n-type, 0.91 ohm-cm.
2. Initial clean:
 - A. Schedule: 10 min. in TCE, 10 min. in acetone, 10 min. in methanol, DIW rinse (10 min. above 14 megohms).
3. Initial oxidation:
 - A. Standard clean, CL1.
 - B. Oxidation: 1050 degrees C.
 - C. Cycle: 10 min. dry O_2 , 60 min. H_2O , 10 min. anneal in N_2 .
 - D. Nominal thickness: 5000 angstroms.
4. Mask: Apply mask 1 (isolation diffusion): back side protection unnecessary.
5. Isolation Diffusion:
 - A. Standard clean CL3.
 - B. Diffusion: 1100 degrees C.: boron⁺ sources.
 - C. Cycle: 110 min. in 1 liter/min. N_2 + 30 cc/min. O_2 , 10 min. in 500 cc/min. O_2 .
 - D. Strip all oxide in 10:1 DIW:HF.
 - E. Standard clean CL3.

- F. Oxidation: 1000 degrees C.
 - G. Cycle: 5 min. in dry O_2 , 10 min. in H_2O , 5 min. in N_2 .
 - H. Nominal parameters: depth is 3.5 microns, oxide is 1400 angstroms.
6. Mask: Apply mask 2 (gate diffusion); back side protection unnecessary.
7. Gate diffusion:
- A. Standard clean CL3.
 - B. Diffusion: 1050 degrees C.; boron⁺ sources.
 - C. Cycle: 25 min. in 1 liter/min. N_2 + 30 cc/min. O_2 , 5 min. in 500 cc/min. O_2 .
 - D. Strip all oxide in 10:1 DIW:HF.
 - E. Standard clean CL3.
 - F. Oxidation: 950 degrees C.
 - G. Cycle: 5 min. in dry O_2 , 25 min. in H_2O , 5 min. in N_2 .
 - H. Nominal parameters: depth is 0.9 micron, oxide thickness is 1500 angstroms.
8. Mask: apply mask 3 (enhancement diffusion); back side protection unnecessary.
9. Enhancement diffusion:
- A. Standard clean CL3.
 - B. Diffusion: 1000 degrees C.; $POCl_3$ source.
 - C. Cycle: 5 min. soak, 10 min. diffusion, 5 min. purge.
 - D. Flow rates: N_2 source 70 cc/min., N_2 bypass 500 cc/min., O_2 150 cc/min.
 - E. Nominal parameters: resistivity is 10 ohms/square, depth is 0.4 micron.

10. Final oxidation:

- A. HCl flush of oxide tube (overnight or about 8 hours).
- B. Strip all oxide in 10:1 DIW:HF.
- C. Standard Clean CL3.
- D. Oxidation: 950 degrees C.
- E. Cycle: 5 min. dry O_2 , 25 min. H_2O , 5 min. N_2 .
- F. C-V measurement of oxide impurity content.
- G. Nominal parameters: oxide thickness, 2000 angstroms, gate

depth, 1.0 micron, adequate C-V measure to be determined.

11. Mask: apply mask 4 (contacts); back side protection unnecessary.

12. Mask: apply mask 5 (metal liftoff); back side protection unnecessary.

13. Metallization:

A. Evaporate 500 angstroms of chromium, 700 angstroms of platinum and 2000 angstroms of gold.

B. Liftoff.

C. Alloy at 500 degrees C. for 5 min.

14. Insulating oxidation:

A. CVD oxidation (add approximately 2 percent phosphorous).

B. Nominal thickness: 1 micron.

15. Mask: apply mask 6 (exposure windows); protect back side.

16. Packaging: hand solder wires to bonding pads.

Standard Procedures

CL1:

- 1. 3:2, $H_2SO_4:H_2O_2$ (self heating) for 15 min.

2. DIW rinse for 10 min. above 14 meg.
3. 10:1 DIW:HF for 15 sec.
4. DIW rinse for 10 min. above 14 meg.
5. Spin dry for 2 min.

CL3:

Same as CL1 except 100:1 DIW:HF for 20 sec.

PR1:

All mask steps except for liftoff

1. 2 hour bake, 220 degrees C., N₂ flow.
2. Waycoat (-), spin on at 4000 rpm.
3. Prebake, 70 degrees C., 20 min., N₂ flow.
4. Exposure appr 4 sec., 0.6 mw/cm².
5. Develop, butyl acetate, then xylene.
6. Postbake at 150 degrees C., 30 min., N₂ flow.
7. Etch in buffered HF:NH₄F, 1:6.
8. Photoresist strip (O₂ plasma), 10 min.

PR2:

For liftoff mask

1. 2 hour bake, 220 degrees C., N₂ flow.
2. KTI + 2, 30 cs, spin on at 3000 rpm.
3. Prebake at 90 degrees C., 30 min., N₂ flow.
4. Exposure, 10 sec., 0.6 mw/cm².
5. Develop, KTI developer:DIW, 1:1.
6. Postbake at 90 degrees C., 30 min., N₂ flow.
7. Liftoff, boiling acetone 55 degrees C.

B. Revised Process Schedule

Introduction

This appendix describes the fabrication process for the multielectrode array concomitant to this research project. It is a modified form of the process schedule information found in reference 11. The major steps in the process will be stated, followed by a more detailed description of the process. The original detailed process schedule is found in appendix A. The last section of this appendix contains the process schedule arrived at through the research of this thesis.

Fabrication Process

The major steps of the fabrication process are listed below.

1. Formation of the initial oxide layer on the substrate.
2. Three photolithographic masking and diffusion steps to construct the junction field effect transistor (JFET) devices.
3. Formation of the final thermal oxide insulating layer over the probe surface.
4. Contact windows opened through the final thermal oxide layer.
5. Metallization and liftoff.
6. Overcoating with a silicon nitride insulation layer.
7. Exposure windows opened to the bonding pads and electrodes.
8. Lead attachment and final insulation.
9. Silver-silver chloride plating the electrodes.

The starting material is a p-type silicon substrate, 13 mils thick with a (100) orientation, and a 2 micron n-type epitaxial layer grown onto it. Substrate resistivity is 20 to 60 ohm-cm. Epitaxial wafers

were chosen to simplify the fabrication of the JFET devices. the n-type epitaxial layer provides n-channel JFETs which have a lower on-resistance.

The major steps of the fabrication sequence are shown in figure A-1. Standard photoresist procedures are used throughout the diffusion steps to selectively etch windows through the silicon dioxide through which the dopants will diffuse. In this fashion, the geometries of the diffusions are controlled. These same photoresist-etching steps are used to define geometries in the contact windows, metallization, and exposure windows processes. For ease of fabrication and for yield considerations, five micron design rules have been used throughout the design of the device. This means no feature of the probe can be closer together than five microns.

The first step of the fabrication sequence is to thermally grow 0.5 micron of silicon dioxide onto the surface in wet oxygen at 1050 degrees centigrade. This oxide is then selectively etched using photolithographic techniques with photoresist to open windows in the oxide over the areas where the dopant is to diffuse into the wafer. A p-type dopant, boron, is then diffused at 1100 degrees centigrade through the epitaxial layer to a depth of 3.5 microns, to join with the p-type substrate. This forms isolated pockets across the wafer. Each of these pockets will contain a single JFET device. Through these isolation regions, each JFET is electrically isolated from the rest of the probe by two back to back p-n junctions. Following the isolation diffusion, the remaining oxide layer is completely removed through another etching step and a new 1400 angstrom thermal oxide layer is grown to prepare the surface for the gate diffusion.

The above steps result in the structure shown in figure A-1e. Steps C and D, shown in figure A-1 and discussed in the above paragraph are

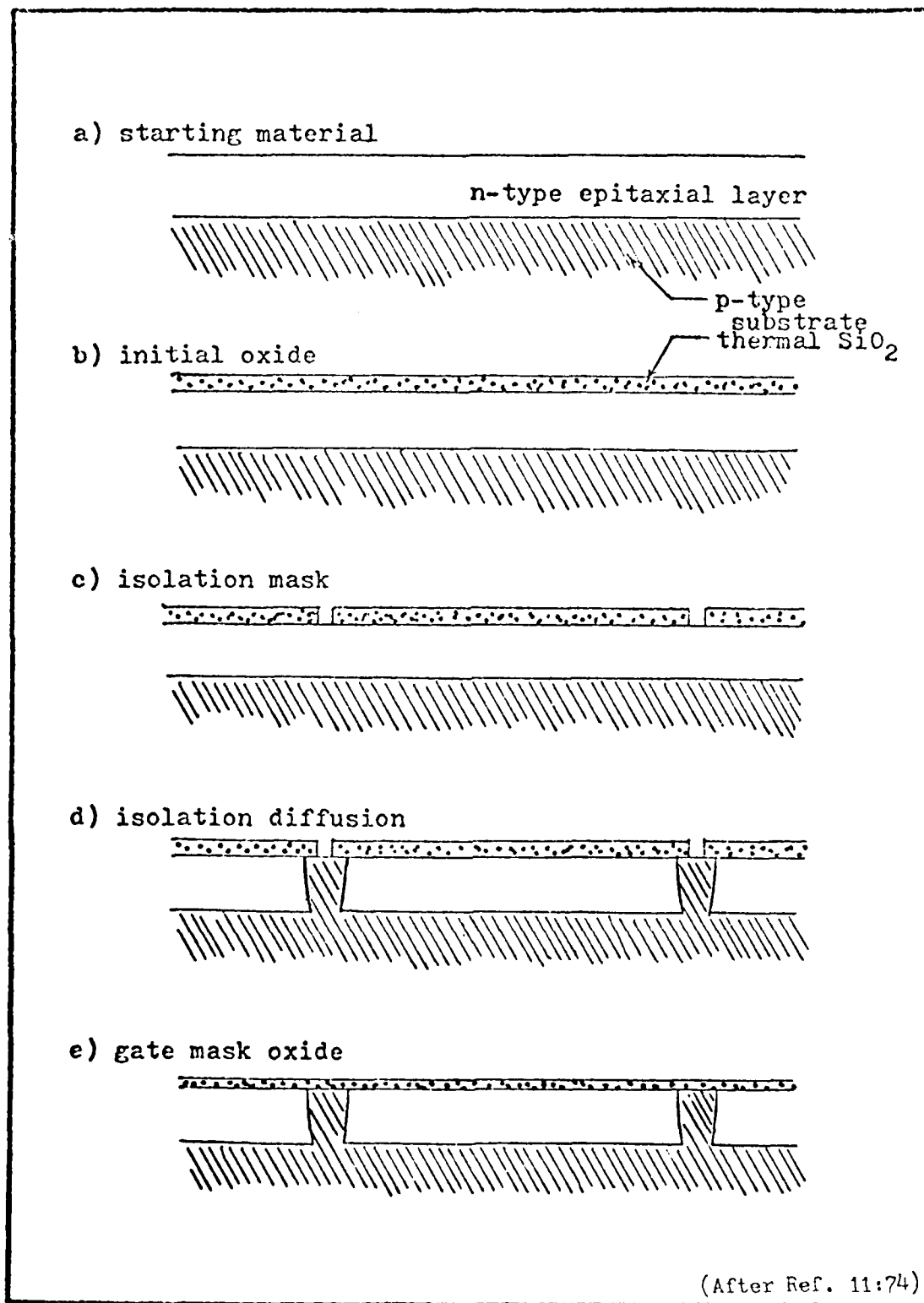


Fig. A-1. The Fabrication Process Sequence.

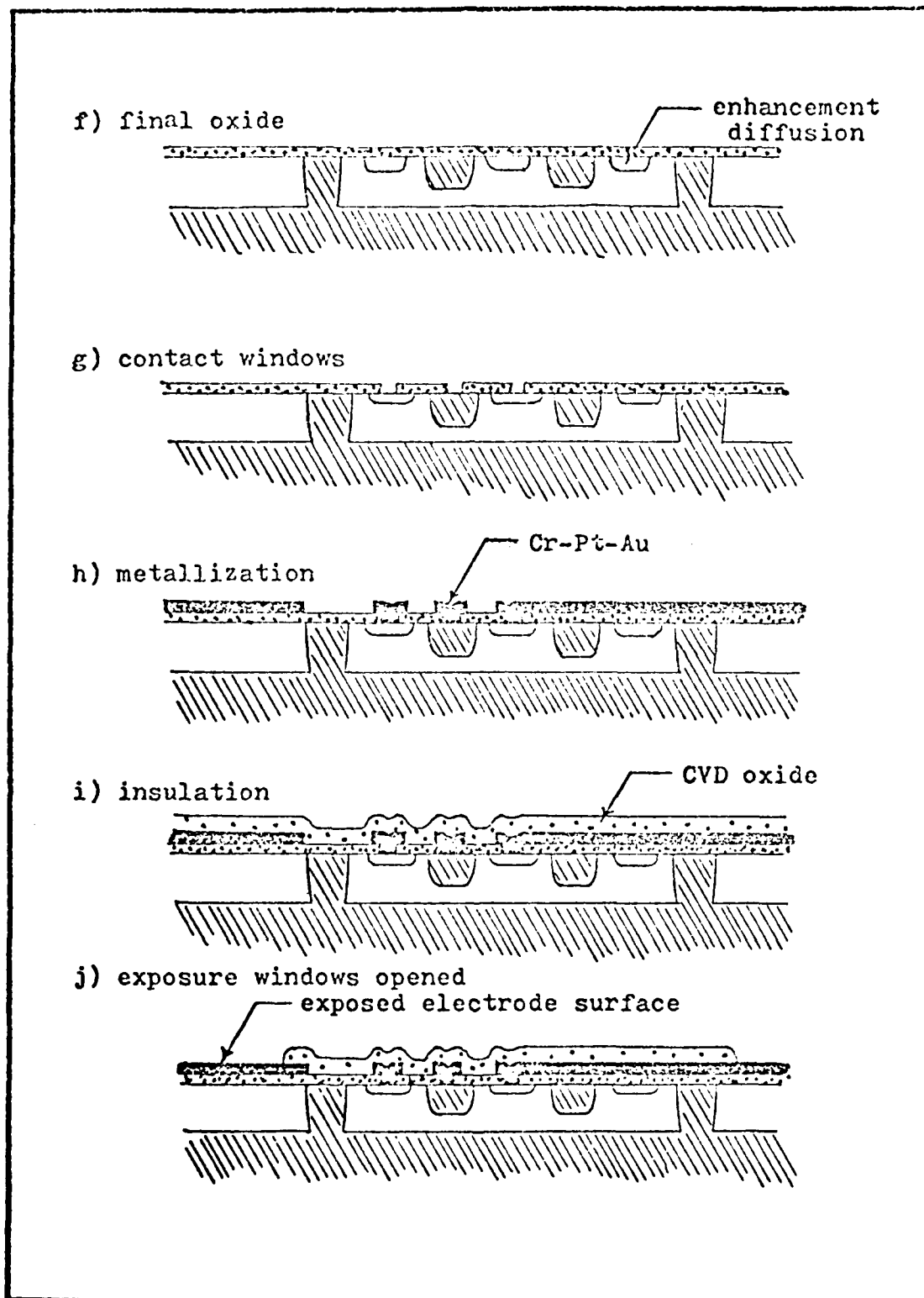


Fig. A-1(continued).

now repeated for the gate diffusion and then for the enhancement diffusion. A final 1500 angstrom thermal oxide layer is grown in wet oxygen to produce the JFET structure shown in figure A-1f.

The gate diffusion is another p-type, boron diffusion. It is diffused to a junction depth of 1.0 micron. The resulting n-type layer sandwiched between the p-type gate diffusion and the substrate forms the channel of the field effect transistor. The gate diffusion also forms the 10 ohms per square crossover structures. The shallow n-type enhancement diffusion, using a POCl_3 source, increases the surface impurity concentration of the n-type source and drain regions to ensure ohmic contacts of the metal leads to these regions. Since the high surface impurity concentrations resulting from the isolation, gate, and enhancement diffusions do not degrade device performance, and are actually desirable in the enhancement and crossover regions, drive-in diffusions are not necessary in the fabrication of this device.

The contact windows are next etched through the final silicon dioxide layer. These windows expose areas of the source, drain, gate, and crossover regions to allow the metallic leads to make contact to these active regions.

A liftoff technique is used to define the device metal pattern. A positive photoresist is spun onto the wafer and the metal mask applied. The metal evaporation is then performed followed by the liftoff of the photoresist and the unwanted metal.

The metallization involves a three step chromium, platinum, and gold vacuum evaporation process. An initial base layer of 250 angstroms of chromium is first applied to the surface. The chromium acts as a

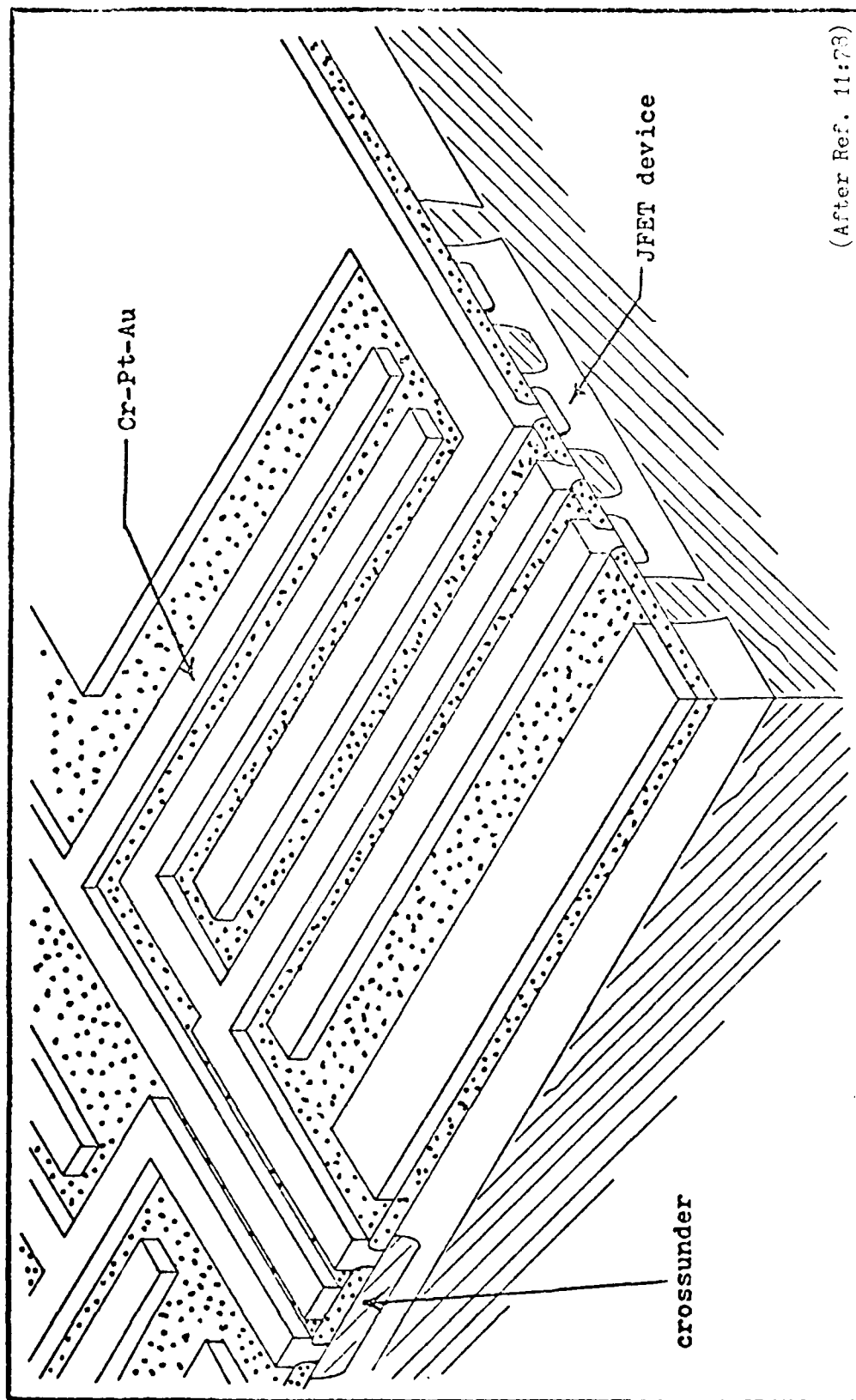
"glue" as the gold does not adhere well to silicon or silicon dioxide. A layer of platinum, sandwiched between the chromium and the gold, prevents the gold from diffusing through the chromium to the silicon. This would defeat the adhesive effect of the chromium. A layer of gold, 2000 angstroms thick, is then vacuum evaporated onto the platinum. The liftoff is now performed by placing the wafer in an acetone solution. After this step, a cross section of one of the JFET-electrode cells is as shown in figure A-2.

The final silicon nitride layer is now plasma deposited over the entire multielectrode array. This layer insulates the array structure from the cerebral spinal fluid. Windows are etched through the layer to expose the metal electrode sites, the ground plane, and the bonding pads.

The lead wires, which will attach the multielectrode array to the support electronics, are hand soldered to the bonding pads. These wires must be hand soldered to give the bonds and lead wires sufficient strength for handling during surgical implantation and testing. Thermocompression bonds would not provide this strength.

To insulate the bonding areas from the saline bath of the cerebral spinal fluid, the entire structure, except the center area containing the electrodes, is coated with moisture-proof epoxy.

Once the epoxy layer had hardened, the electrodes are silver-silver chloride plated. This process consists of immersing the entire multielectrode array into a silver plating bath. All column leads and the ground plane connection are tied together and attached to the plating power supply. Thus, all electrodes and the ground plane are simultaneously



(After Ref. 11:73)

Fig. A-2. Cross Section of the JFET Structure.

silver plated. Once silver plating is complete, the array is washed in deionized water and then immersed in a saline solution for the chloriding process. An electric current is passed through all electrodes and the ground plane until the surface of the silver plating is converted to silver chloride. The device is again washed in deionized water and placed in a dry nitrogen environment to await the surgical implant procedure.

Revised Process Schedule

1. Starting material:

- A. Substrate: p-type, (100), 20-60 ohm-cm.
- B. Epitaxial layer: n-type 0.91 ohm-cm.

2. Initial clean:

- A. Xylene, 120 degrees C. for 10 min.
- B. 1:1 TCE:acetone for 5 min.
- C. Methanol for 5 min.
- D. Spin dry.
- E. Standard clean, CL1.
- F. Solution A, 80 degrees C. for 15 min. (6:2:1 of DIW:H₂O₂:NH₄OH).
- G. Solution B, 80 degrees C. for 15 min. (7:2:1 of DIW:H₂O₂:HCl).
- H. DIW rinse for 10 min.
- I. Spin dry.

3. Pre-oxidation furnace preparation:

- A. HCl purge at 1050 degrees C.
- B. Cycle: 480 min. in 10:1 O₂:HCl, 480 min. in N₂.
- C. C-V test on pilot wafer, require voltage shift be less than 5 volts for 2000 angstrom oxide.

4. Isolation oxidation:

- A. Include one test wafer.
- B. Standard clean, CL1.
- C. 1050 degrees C. pyrolytic steam.
- D. Push-pull at 2 inches per min.
- E. Cycle: 10 min. in O₂, 60 min. in H₂O, 10 min. in N₂.
- F. Measure thickness on test wafer, must be 5000 \pm 1000 angstroms.

5. Mask 1 - isolation diffusion:

- A. Standard photoresist, PR1.
- B. Back side protection for isolation diffusion unnecessary.

6. Isolation diffusion:

- A. Include one test wafer.
- B. Standard clean, CL3.
- C. Boron⁺ source at 1100 degrees C.
- D. Push-pull at 2 inches per min.
- E. Cycle: 110 min. in 1 liter/min. N₂ + 40 cc/min. O₂, 10 min.

in 500 cc/min. O₂.

- F. Measure surface resistivity and junction depth on test wafer.

Surface resistivity should be less than 15 ohms per square. Junction depth should be 3.5 \pm 0.5 microns.

7. Gate oxidation:

- A. Nitric acid, 80 degrees C. for 15 min.
- B. DIW wash for 10 min.
- C. 10:1 DIW:HF until wafers are hydrophobic.
- D. Standard clean, CL1.
- E. 1000 degrees C. pyrolytic steam.

- F. Push-pull at 2 inches per min.
 - G. Cycle: 5 min. in O_2 , 15 min. in H_2O , 10 min. in N_2 .
 - H. Measure oxide thickness: should be 1400 ± 300 angstroms.
 - I. Measure surface resistivity: must be less than 230 ohms per square.
8. Mask 2 - gate diffusion:
- A. Standard photoresist, PR1.
 - B. Back side protection unnecessary.
9. A. Include two test wafers.
- B. Standard clean, CL3.
 - C. Boron⁺ source at 1050 degrees C.
 - D. Cycle: 20 min. in 1 liter/min. N_2 + 40 cc/min. O_2 , 5 min. in 500 cc/min. O_2 .
 - E. Push-pull at 3.2 inches per min.
 - F. Measure surface resistivity: must be less than 25 ohms per square.
10. Enhancement oxidation:
- A. Include one test wafer from step 8.
 - B. 10:1 DIW:HF until wafer is hydrophobic.
 - C. Standard clean, CL1.
 - D. 950 degrees C. in pyrolytic steam.
 - E. Push-pull at 2 inches per min.
 - F. Cycle: 5 min. in O_2 , 30 min. in H_2O , 10 min. in N_2 .
 - G. Measure oxide thickness: must be 1500 ± 200 angstroms.
 - H. Measure surface resistance: must be less than 100 ohms per square.

- I. Measure gate depth: should be 1 ± 0.2 micron.
- 11. Mask 3 - enhancement diffusion:
 - A. Standard photoresist, PR1.
 - B. Back side protection is necessary.
- 12. Enhancement diffusion:
 - A. Include two test wafers.
 - B. Standard clean, CL3.
 - C. POCl_3 source at 1000 degrees C.
 - D. Cycle: 5 min. Soak, 4 min. Diffuse.
 - E. Flow rates: 70 cc/min. N_2 source, 500 cc/min. N_2 bypass, 150 cc/min. O_2 .
 - F. Measure surface resistivity: must be 10 ± 5 ohms per square.
- 13. Pre-oxidation furnace preparation:
 - A. HCl purge at 950 degrees C.
 - B. Cycle: 240 min. in 10:1 O_2 :HCl, 14 hours in N_2 .
 - C. C-V test on pilot wafer: voltage shift less than 2 volts for 2000 angstrom oxide.
- 14. Final oxidation:
 - A. Include two test wafers: one from step 12 and one unused.
 - B. 10:1 DIW:HF until phosphorous glass is removed.
 - C. Standard clean, CL1.
 - D. 950 degrees pyrolytic steam.
 - E. Push-pull at 2 inches per min.
 - F. Cycle: 5 min. O_2 , 30 min. H_2O , 10 min N_2 .
 - G. Measure diffusion depth: must be 0.4 ± 0.2 microns.
 - H. C-V test: voltage shift less than 2 volts for 2000 angstroms.

- I. Measure oxide thickness: should be 2000 ± 200 angstroms.
15. Mask 4 - contacts:
- A. Standard photoresist, PR1.
 - B. Back side protection unnecessary.
16. Mask 5 - liftoff:
- A. Standard photoresist, PR2.
 - B. Back side protection is necessary.
17. Metallization:
- A. Evaporate 500 angstroms chromium, 700 angstroms platinum, 2000 angstroms gold.
 - B. Liftoff.
18. Electrical check:
- Check for ohmic contacts, pinchoff voltage, on-resistance, and leakage paths between column leads and gate leads. Nominal pinchoff voltage is 3 volts. Nominal on-resistance is 1000 ohms.
19. Insulating nitride:
- A. Standard clean, CL3.
 - B. Plasma deposition parameters: preheat to 300 degrees C.
 - C. Set Rf output to 35 watts, evacuate to 0.45 torr.
 - D. Flow 20 cc per min. 2 percent silane in argon and 20 cc/min.
- N₂. Deposition time is one hour.
20. Mask 6 - electrode exposure:
- A. Standard photoresist, PR1.
 - B. Back side protection is necessary.

21. Wire lead connection:

- A. Preheat device to 200 degrees C.
- B. Melt 60/40 solder on each bonding pad and cool device to room temperature.
- C. With small soldering iron, hand solder each wire to pad.

22. Insulation of bonding pads:

- A. TCE wash for 10 min.
- B. Acetone wash for 10 min.
- C. Methyl alcohol wash for 10 min.
- D. DIW wash for 10 min.
- E. Blow dry with nitrogen.
- F. Visually inspect to insure soldering resin is removed.
- G. Apply moisture-proof epoxy to bonding pads and back of device.

23. Silver-silver chloride plating:

- A. Connect all column leads and ground plane lead together.
- B. Immerse in silver plating solution.
- C. Plate for 40 seconds with 200 microamps of current.
- D. DIW wash for 10 min.
- E. Immerse in saline solution.
- F. Chloride by applying 320 microamps of current for 10 seconds.
- G. DIW wash for 10 min.
- H. Blow dry with nitrogen.

Standard Procedures

CL1:

- 1. 3:2 $\text{H}_2\text{SO}_4:\text{H}_2\text{O}_2$ (self heating) for 15 min.

2. DIW rinse (start time when resistivity above 14 megohms) 10 min.
3. 10:1 DIW:HF for 15 sec.
4. DIW rinse (start time when resistivity above 14 megohms) for 10 min.
5. Spin dry for 2 min.

CL3:

Same as CL1 except 100:1 DIW:HF for 20 sec.

PR1:

All mask steps except for liftoff

1. 2 hour bake, 220 degrees C.
2. Waycoat (-) 43 cs, spin on at 4000 rpm.
3. Prebake, 70 degrees C., 20 min.
4. Expose for 4 seconds, 0.6 mw/cm^2 .
5. Develop, xylene, then butyl acetate, 40 sec. each.
6. Postbake at 150 degrees C. 30 min.
7. Etch in buffered HF:NH₄F, 1:6.
8. Photoresist strip O₂ plasma, 10 min.

PR2:

For liftoff mask

1. 2 hour bake, 220 degrees C.
2. KTI + 2, 30 cs, spin on at 3000 rpm.
3. Prebake at 90 degrees C., 30 min.
4. Expose, 10 sec., 0.6 mw/cm^2 .
5. Develop, KTI developer:DIW, 1:1.
6. Postbake at 90 degrees C., 30 min.
7. Liftoff, boiling acetone.

Vita

Gary Howard Fitzgerald was born on January 25, 1946 in Oklahoma City, Oklahoma. He graduated from Harrah High School, Harrah, Oklahoma in May of 1964. He enlisted in the United States Air Force in June of 1964 and received technical training at Lackland AFB, Texas, to perform duties as a Cryptographic Electronics Communication Systems Repairman. Subsequent duty stations include Carswell AFB, Texas; Sunnyvale Satellite Test Center, Sunnyvale, California; Korat Royal Thai Air Force Base, Korat, Thailand; and Elmendorf AFB, Alaska. He was accepted into the Airman Education and Commissioning Program in December of 1971 and received a Bachelor of Science degree from Oklahoma State University in May of 1975. He was commissioned a Second Lieutenant via Officer Training School in August 1975 and assigned to Edwards AFB, California, as a flight test engineer. He was assigned to the Air Force Institute of Technology in June 1979.

Permanent address: Route 3, Box 128
Harrah, Oklahoma 73045

UNCLASSIFIED

SECURITY CLASSIFICATION OF THIS PAGE (When Data Entered)

REPORT DOCUMENTATION PAGE		READ INSTRUCTIONS BEFORE COMPLETING FORM
1. REPORT NUMBER AFIT/GE/BE/80D-21	2. GOVT ACCESSION NO. AD-A100 763	3. RECIPIENT'S CATALOG NUMBER
4. TITLE (and Subtitle) THE DEVELOPMENT OF A TWO-DIMENSIONAL MULTIELECTRODE ARRAY FOR VISUAL PERCEPTION RESEARCH IN THE MAMMALIAN BRAIN		5. TYPE OF REPORT & PERIOD COVERED MS Thesis
		6. PERFORMING ORG. REPORT NUMBER
7. AUTHOR(s) Gary H. Fitzgerald Capt		8. CONTRACT OR GRANT NUMBER(s)
9. PERFORMING ORGANIZATION NAME AND ADDRESS Air Force Institute of Technology (AFIT-EN)		10. PROGRAM ELEMENT, PROJECT, TASK AREA & WORK UNIT NUMBERS
11. CONTROLLING OFFICE NAME AND ADDRESS Aerospace Medical Research Laboratory AFWAL/HEG Wright-Patterson AFB, Ohio 45433		12. REPORT DATE December 1980
		13. NUMBER OF PAGES 141
14. MONITORING AGENCY NAME & ADDRESS (if different from Controlling Office) Aerospace Medical Research Laboratory AFWAL/HEG Wright-Patterson AFB, Ohio 45433		15. SECURITY CLASS. (of this report) Unclassified
		15a. DECLASSIFICATION/DOWNGRADING SCHEDULE
16. DISTRIBUTION STATEMENT (of this Report) Approved for public release; distribution unlimited		
17. DISTRIBUTION STATEMENT (of the abstract entered in Block 20, if different from Report)		
18. SUPPLEMENTARY NOTES 16 JUN 1981 Fredric C. Lynch Approved for public release IAW AFR 190-17 Fredric C. Lynch, Major, USAF Director, Public Affairs		
19. KEY WORDS (Continue on reverse side if necessary and identify by block number) Bioelectrode array, multiplexed multielectrode array, implantable electronics microprobe, visual perception system, biomedical integrated electronics.		
20. ABSTRACT (Continue on reverse side if necessary and identify by block number) A review of previous mammalian visual system neurological and psychological research is presented. Results of previous research motivated the development of a device that would record fine grained electroencephalic data from the surface of a living mammalian cortex. A multiplexing multielectrode array has been developed and tested for this purpose. The device consists of a four by four array of electrodes and sixteen junction field effect transistors fabricated on a silicon substrate using		

DD FORM 1473

1 JAN 73

EDITION OF 1 NOV 65 IS OBSOLETE

UNCLASSIFIED

SECURITY CLASSIFICATION OF THIS PAGE (When Data Entered)

UNCLASSIFIED

SECURITY CLASSIFICATION OF THIS PAGE(When Data Entered)

integrated circuit manufacturing techniques. In vitro tests indicated the device is capable of detecting and multiplexing fine grained cortical signals. Technical problems with the passivation material precluded in vitro evaluation. A solution to this problem is presented and an in vivo test procedure recommended.

UNCLASSIFIED

SECURITY CLASSIFICATION OF THIS PAGE(When Data Entered)

END

DATE
FILMED

7-81

DTIC